(2)

AD-A234 768

The Pennsylvania State University
APPLIED RESEARCH LABORATORY
P.O. Box 30
State College, PA 16804

THE WAVENUMBER-FREQUENCY FILTERING CHARACTERISTICS OF COMPLIANT LAYERS

by

J. E. Phillips, C. B. Burroughs, W. J. Hughes

Technical Report No. TR 91-004
April 1991

Supported by:
Space and Naval Warfare Systems Command

L.R. Hettche, Director
Applied Research Laboratory

Approved for public release; distribution unlimited

REPORT DOCUMENTATION PAGE

Form Approved
OMB No. 0704-0188

1. AGENCY USE ONLY (Leave blank)	2. REPORT DATE	3. REPORT TYPE AND DATES COVERED
	April 1991	

4. TITLE AND SUBTITLE

THE WAVENUMBER-FREQUENCY FILTERING CHARACTERISTICS OF COMPLIANT LAYERS

5. FUNDING NUMBERS

N00039-88-C-0051

6. AUTHOR(S)

J. E. Phillips, C. B. Burroughs, W. J. Hughes

7. PERFORMING ORGANIZATION NAME(S) AND ADDRESS(ES)

Applied Research Laboratory
Penn State University
P.O. Box 30
State College, PA 16804

8. PERFORMING ORGANIZATION REPORT NUMBER

TR 91-004

9. SPONSORING/MONITORING AGENCY NAME(S) AND ADDRESS(ES)

Space and Naval Warfare Systems Command
Department of the Navy
Washington, DC 20363-5100

10. SPONSORING/MONITORING AGENCY REPORT NUMBER

11. SUPPLEMENTARY NOTES

12a. DISTRIBUTION/AVAILABILITY STATEMENT

Approved for public release, distribution unlimited.

12b. DISTRIBUTION CODE

13. ABSTRACT *(Maximum 200 words)*

Techniques for the measurement of the wavenumber-frequency filtering characteristics of compliant layers mounted on an elastic structure and subject to unsteady pressures are developed and demonstrated. In order to measure the performance of the layer at arbitrary wavenumbers and frequencies, an array of shakers was fabricated and used to generate a standing wavepattern of force where the maximum spectrum levels of the input forces could be concentrated at selected wavenumbers independent of the selected frequency. Arrays of thin film transducers were designed, fabricated, and used to measure the wavenumber-frequency pressure spectra above and below compliant layers. The wavenumber-frequency admittances of a coated and uncoated beam were used to determine the effectiveness of compliant layers in reducing the vibration response of the beam as a function of wavenumber and frequency.

14. SUBJECT TERMS

wavenumber-frequency filtering, compliant layers, elastic structure, unsteady pressure, thin film transducers, beam

15. NUMBER OF PAGES

120

16. PRICE CODE

17. SECURITY CLASSIFICATION OF REPORT	18. SECURITY CLASSIFICATION OF THIS PAGE	19. SECURITY CLASSIFICATION OF ABSTRACT	20. LIMITATION OF ABSTRACT
U nclassified	Unclassified	Unclassified	Unlimited

13. Abstract (cont'd.)

The development of the shakers, transducers, and data processing algorithms is described. Measurement results of the effectiveness and pressure transmission loss are presented as functions of frequency at different drive wavenumbers for several compliant layers with different properties. The pressure spectra above and below the layers, velocity spectra of the beam response, and admittances of the coated and uncoated beam are presented and analyzed as functions of wavenumber and frequency.

Abstract

Techniques for the measurement of the wavenumber-frequency filtering characteristics of compliant layers mounted on an elastic structure and subject to unsteady pressures are developed and demonstrated. In order to measure the performance of the layer at arbitrary wavenumbers and frequencies, an array of shakers was fabricated and used to generate a standing wavepattern of force where the maximum spectrum levels of the input forces could be concentrated at selected wavenumbers independent of the selected frequency. Arrays of thin film transducers were designed, fabricated, and used to measure the wavenumber-frequency pressure spectra above and below compliant layers. The wavenumber-frequency admittances of a coated and uncoated beam were used to determine the effectiveness of compliant layers in reducing the vibration response of the beam as a function of wavenumber and frequency.

The development of the shakers, transducers, and data processing algorithms is described. Measurement results of the effectiveness and pressure transmission loss are presented as functions of frequency at different drive wavenumbers for several compliant layers with different properties. The pressure spectra above and below the layers, velocity spectra of the beam response, and admittances of the coated and uncoated beam are presented and analyzed as functions of wavenumber and frequency.

Table of Contents

List of Figures

List of Tables

Chapter 1

INTRODUCTION

Pressure fluctuations in a turbulent boundary layer (TBL) excite underlying structures which is often a source of unwanted vibration or radiated noise. A compliant layer placed between the TBL and the structure may reduce the response of the structure to excitation by TBL wall pressure fluctuations. Because TBL wall pressure spectra are continuous functions of both wavenumber and frequency (see, for example, references [1,2,3]) the effectiveness of a compliant layer depends not only on the physical properties of the layer and structure, but also on the spectra of the TBL wall pressures, admittance of the structure, and the transfer function of the layer as a function of wavenumber and frequency. Methods for measuring the transfer function of compliant layers as a function of both wavenumber and frequency are developed in this thesis and applied to measure the effectiveness and transmission loss of several compliant layers.

Partly because of the difficulty in generating pure wavenumber drives, little experimental data are available in the open literature on the response of compliant layers to wall pressures as a function of wavenumber and frequency. Many of the theoretical studies on boundary layer interaction with compliant layers have concentrated on flow instabilities introduced in the boundary layer flow by deformation of the compliant layer [4,5,6] and the modification of TBL wall pressures by compliant layers [7,8]. Maidanik et al. [9] considered the effect of compliant layers on reducing

acoustic radiation from vibrating panels. By treating the layer as a liquid layer, Maidanik and Reader [10] investigated the wavenumber/frequency filtering action of a layer. Ko and Schloemer [11] included the elastic properties of a compliant layer in computing the transfer of TBL wall pressures into the layer to pressure sensors embedded inside the layer.

This thesis is a continuation of work done by two previous students. Hutto [12] laid the initial ground work for this project. In his thesis, the response of a Timoshenko beam to multiple point drives was examined experimentally and theoretically. His thesis lead to the method of using an array of accelerometers to measure the wavenumber-frequency velocity response of the beam to multiple point drives. He also conducted a theoretical study on the response of the beam to an array of force drives weighted to a particular wavenumber.

Hutto's work formed some of the basis of the work done by Grosh [13] who developed the experimental system for measuring the response of a Timoshenko beam to an array of force drives weighted (steered) to a particular wavenumber. The shakers used in this present study were developed by Grosh. The data reduction method for obtaining the wavenumber-frequency transfer admittance of the beam was also developed largely by Grosh. This thesis extends and refines the techniques used by Grosh and applies them to beams with compliant layers attached.

1.1 Experimental method

It is proposed that the filtering characteristics of an elastic layer can be determined using the techniques described in this thesis. These techniques are

based largely upon the developments of Hutto and Grosh. As stated above, these developments were based on research using the Timoshenko beam theory, thereby reducing the problem to one dimension. The present study continues their work with the addition of an elastic layer mounted onto the beam. Techniques developed by Hutto [12] and Grosh [13] are employed to measure two distinct quantities of compliant layers. The first of these quantities is the effectiveness of the layer in the reduction of the vibration response of the beam. This is determined by comparing the wavenumber-frequency (spectral) transfer admittance of the coated beam to the spectral transfer admittance of the bare (uncoated) beam. The second quantity is the wavenumber-frequency transmission loss. This is equal to the ratio of the wavenumber-frequency spectrum of the force at the bottom of the layer to the wavenumber-frequency spectrum of the force at the top of the layer. A negative value of the transmission loss in dB is obtained if the force at the bottom of the layer is less than the force at the top. The spatial force spectra at the top and bottom of the layer were measured using an array of transducers developed in this thesis.

1.2 Outline of the thesis

Chapter 2 presents a study of a single isolated section of the coated beam. This involved a small piece of steel, a sample of elastomer (compliant layer), and a single shaker mounted on the layer to simulate the excitation of a section of the coated beam. The results of this study will become useful for explaining some of the phenomena observed in the measurements on the coated beam.

Chapter 3 will describe the measurement system used in this thesis. This includes a discussion on spatial Fourier transforms, the effects of transducer arrays on the measurements, and the use of an array of shakers for concentrating the force spectrum to a desired wavenumber. This is then concluded with sections defining and describing the spectral quantities that were measured.

A description of the measurements is presented in Chapter 4. The instrumentation, procedures, and data processing used in the measurements are discussed. An important section of this chapter is the description of the construction and use of transducer arrays to measure the force spectra above and below the compliant layer on the beam.

Chapter 5 presents the results obtained from the measurements described in Chapter 4. Some of the results from the bare beam are compared to those obtained by Grosh [13]. The effects of using different materials for the compliant layer are examined. Finally, conclusions and recommendations for furthur study are presented in Chapter 6.

Chapter 2

ISOLATED SECTIONS OF COATED BEAMS

Isolated sections of the coated beam consisting of block sections of the beam covered by sections of compliant layers were driven by single shakers. Results from measurements conducted on the isolated sections will be used to assist in the analysis of the results obtained from the measurements conducted on the coated beams. The transfer admittance and the transmission loss were measured over a range of frequency for several sections with different samples of compliant layers.

2.1 Description of the samples and experiment

A schematic of a sample and shaker is given in Figure 2.1. The small sample (2 cm in length) represents a section of the coated beam driven by one of the shakers in the wavenumber drive array discussed in Chapter 3. The sample consists of a steel mass representing the beam, a section of elastomer for the layer, and pieces of piezo film used as force gauges. The parts of the sample unit were bonded together using Devcon 5-minute epoxy. Table 2.1 lists the dimensions of the individual pieces.

The steel mass was cut from the same stock as the full beam and therefore has the same material properties. Three masses were made which were within one gram of each other. The average weight of the masses was 38.6 grams. It should also be noted that this mass roughly equaled with the mass of a single shaker which was approximately 38 grams.

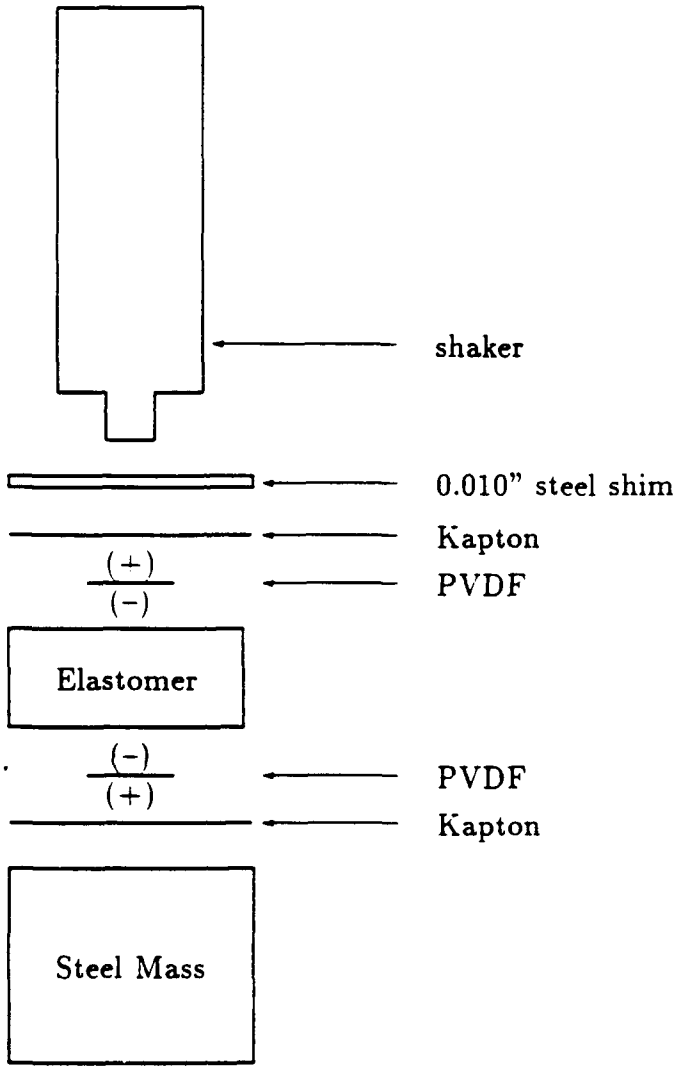

Figure 2.1: Schematic of a sample unit.

Table 2.1: Sample dimensions.

Description	*Size*
steel mass	2cm x 1.27cm x 1.92cm
Kapton	2cm x 1.27cm x 0.003cm
piezo film	2.54cm x 0.5cm x 52μm
elastomer	2cm x 1.27cm x 0.635cm
steel shim	2cm x 1.27cm x 0.025cm

The materials used in the samples were natural rubber (Shure A hardness of 65 durometer), neoprene (50 durometer), and polyurethane (90 durometer). These materials represent those which are commonly used for vibration isolation and provide a good distribution of properties for comparison. Natural rubber and neoprene have approximately the same stiffness; however, neoprene has a much greater loss factor than the natural rubber. The polyurethane is much stiffer than either natural rubber or neoprene, yet it has approximately the same loss factor as the natural rubber.

The two pieces of piezo film were used as force gauges to measure the forces present on both sides of the elastomer. The piezo films are made of a piezoelectric polymer with nickel-aluminum electrode coatings on both sides of the film. After cutting the film to size, an area of the electroding (across the full width of the film and 0.635 cm long) was scraped off one side at one of the ends. This step was repeated on the other side, but at the opposite end, leaving an active area 1.27 cm in length and 0.5 cm wide with the 0.635 cm scraped end sections acting as the positive and negative leads. The film pieces were mounted in the sample units with

the ends exposed so that the signal and grounding leads could be attached. Care was taken to keep track of the polarities of the film pieces. The negative sides of the film pieces were mounted facing the elastomer while the positive sides were mounted facing the Kapton pieces. Kapton, an insulating polymer that is commonly used in electrical printed circuit (pc) boards, was chosen because it was thin and available. The Kapton pieces used in the sample sections insulated the positive electrodes from the steel shim above and the steel mass below the compliant layer sample. Clip leads were used to ground the negative leads of the film while probes with electrical buffers were used to obtain the signals from the positive leads. The steel shim and mass were grounded to provide electrical shielding for the piezoelectric film pieces. The steel shim provided a good surface for mounting the shaker and prevented localized deformation around the contact area. The shim also allowed the shaker to be detached and reattached without damaging the piezo film on top of the elastomer.

The procedure for taking the measurements was straightforward. For each experiment, an IBM Personal Computer (PC) AT was used to operate an HP 4192A as a network analyzer via a General Process-Interface Bus (GP-IB). Programs run on the PC caused the network analyzer to vary the frequency and take the ratios of the signals from the piezo films. To obtain the transfer admittance of the unit, an accelerometer was mounted onto the steel mass on the side opposite the elastomer. The output from the accelerometer was divided by the angular frequency and shifted by 90 degrees to compute velocity. The velocity was then divided by the force measured by the force gauge in the shaker to yield the transfer admittance. To

obtain the transmission loss, the output of the bottom piezo film force gauge (the one between the elastomer and the steel mass) was divided by the output of the top force gauge. There was no need to include the sensitivities of either force gauge since they were similar. Measurements of the transfer admittance and transmission loss were made for all three elastomer materials.

2.2 Results and conclusions

The experimental transfer admittances of polyurethane, natural rubber, and neoprene are given in Figure 2.2. The peaks in the transfer admittances of polyurethane and natural rubber indicate the natural frequencies for those samples. For the neoprene, the stiffness is low enough so that the natural frequency appears below 2 kHz which is below the measurement frequency band. The Shure A hardness of the polyurethane is 90 durometer, the natural rubber is 65 durometer, and the neoprene is 50 durometer. These hardnesses are reflected in the stiffnesses, so that the highest natural frequency occurs with polyurethane and the lowest occurs with neoprene. Also, above the natural frequency for the polyurethane (3.8 kHz), the transfer admittances are highest for the hard polyurethane and lowest for the soft neoprene.

The measured transmission losses for the three samples are plotted in Figure 2.3. The greatest transmission losses were measured with the neoprene which has the greatest density (1.44 gm/cm^3). The densities of the polyurethane (1.0 gm/cm^3) and natural rubber (1.01 gm/cm^3) are nearly equal which may be why the transmission losses measured for these two samples are nearly equal.

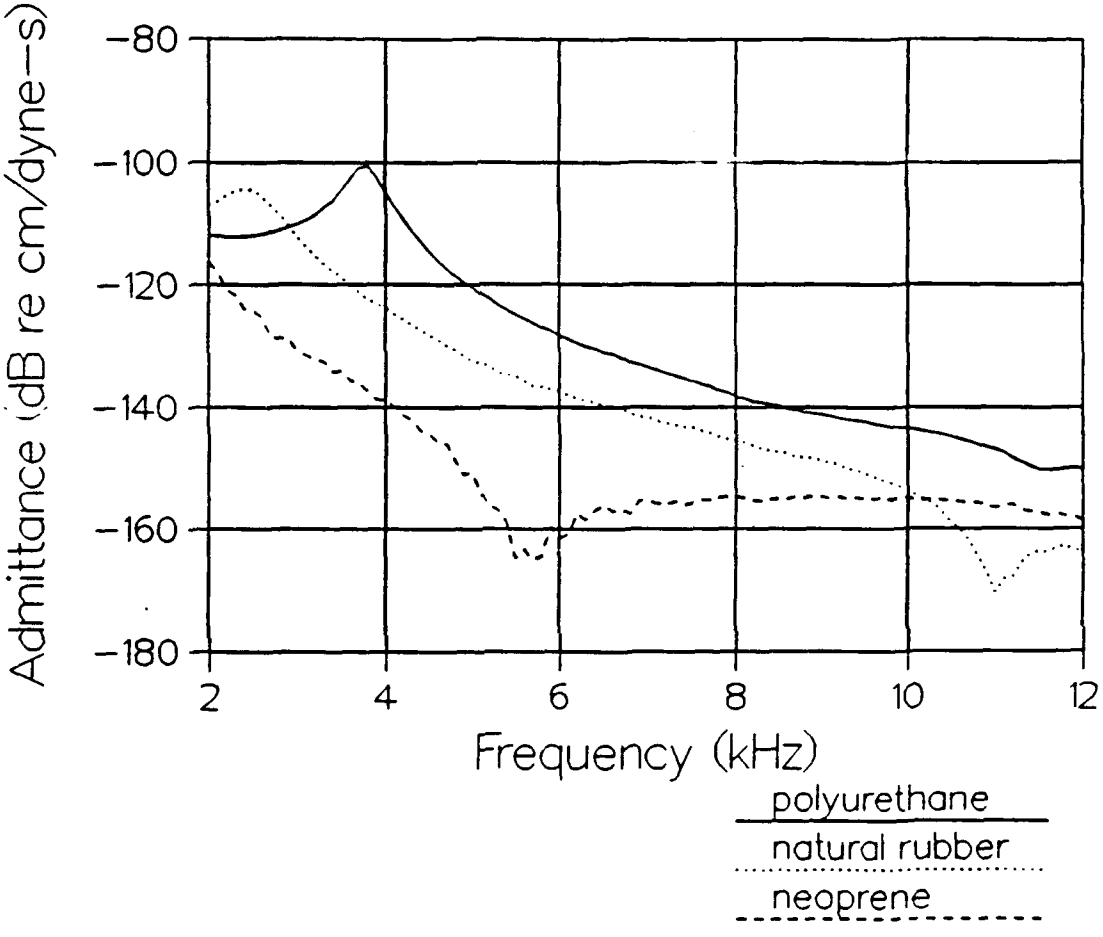

Figure 2.2: Measured transfer admittances of the samples.

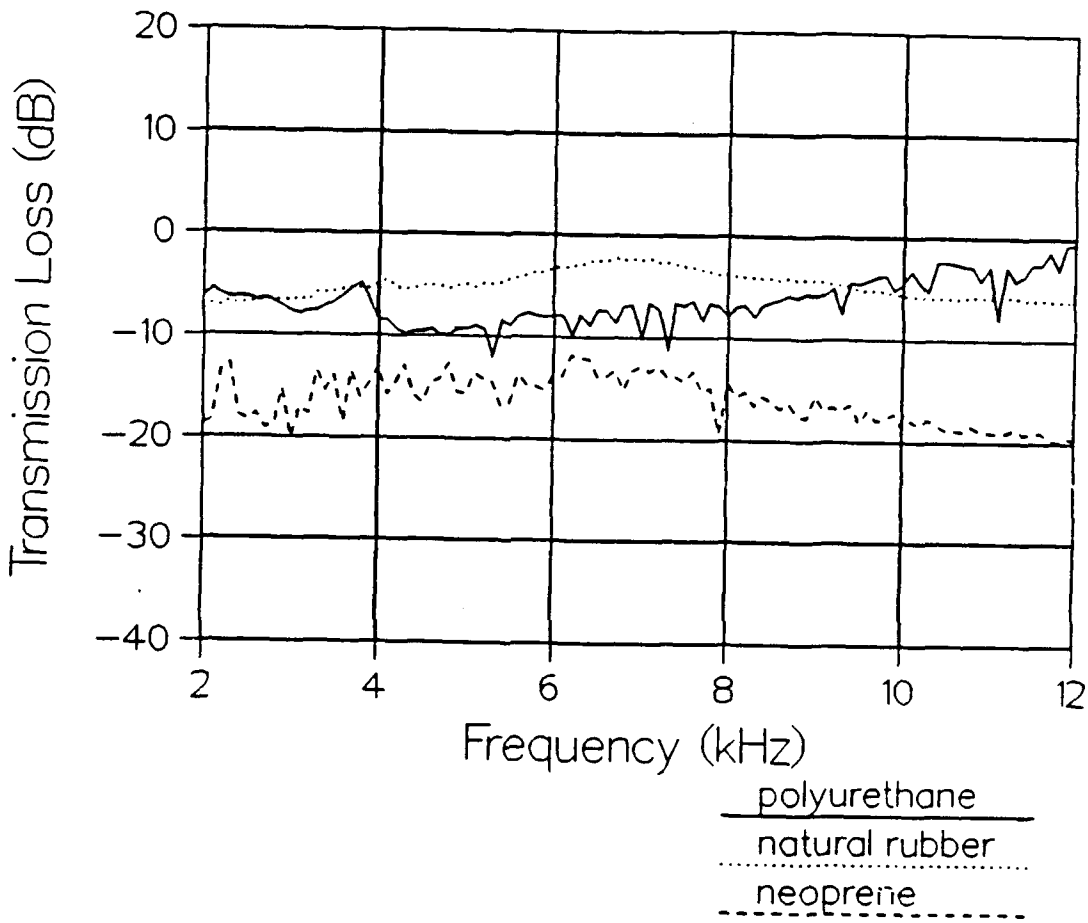

Figure 2.3: Measured transmission losses of the samples.

Chapter 3

EXPERIMENTAL APPROACH

The experimental approach, transducer requirements and limitations are described. The first section defines the transforms that were used throughout the thesis. The requirements for the transducer arrays and how the physical size of the individual transducers and the distance between them affected the results are outlined in the next section. The technique used to adjust the force drive array inputs so that the beam would respond to the driven wavenumber is described. Finally, the measured spectral beam admittance and the measured spectral transmission loss are defined.

3.1 Fourier transforms

A function $f(x)$ in the spatial domain transforms to $F(k_x)$ in the wavenumber domain through the spatial Fourier transform defined as

$$F(k_x) = \int_{-\infty}^{\infty} f(x) e^{-jk_x x} dx \tag{3.1}$$

where x is the spatial coordinate and k_x is the wavenumber in the x direction. The discrete Fourier transform which is fundamental to the data reduction in this thesis is given by

$$F(k_x) = \Delta x \sum_{n=0}^{N-1} f(n\Delta x) e^{-jn\Delta x k_x} \tag{3.2}$$

where Δx, the spacial distance between N points of data, is the proper normalization factor for the transform [14].

3.2 Transducer array considerations

3.2.1 The effect of transducer spacing

In order to drive the beam at a certain wavenumber, there must be at least two shakers per wavelength. In time sampled signals, this requirement is often referred to as the Nyquist rate. Thus, for a definite number of shakers with a constant spacing, there is a maximum wavenumber at which they can drive the beam. The size of the shakers requires that the distance between the shakers of this system be at least 2 cm. The smallest wavelength that can be driven by these shakers is equal to twice the length of the spacing between them, or 4 cm. Since $k = 2\pi/\lambda$, the largest wavenumber that can be driven by this array is $\pi/2$ cm^{-1}.

The spacing between the measurement points of the accelerometer array was 1 cm. The highest free bending wavenumber of the beam in the measurement frequency range of 2 to 12 kHz was about 0.6 cm^{-1}. Since the admittance of a finite beam falls off as a sinc function that is centered about the free bending wavenumber, the response of the beam should be down 30 dB at three wavenumber octaves above the free bending wavenumber or at $k_x = 2.4$ cm^{-1} [13]. A spacing of 1 cm yielded a Nyquist rate of 3.14 cm^{-1} (or π cm^{-1}) therefore, an array spacing of 1 cm will cover the wavenumber range of at least three octaves above the highest free bending wavenumber of the beam. Grosh also found that the spacing of 1 cm caused the aliasing lobes to lie outside the measured range of π cm^{-1}, thus reducing the effects

of aliasing on the transform of the data. This spacing was also applied to the PVDF force gauge array located between the layer and the beam for the same reasons that applied to the accelerometer array.

3.2.2 The effect of transducer size

If the size of the active area or "contact" surface of the transducer is on the order of the wavelength in the medium, some attenuation of the signal will begin to occur. This is caused by a spatial averaging of the signal over the area of the transducer. The spatial response of the transducer appears as a low pass wavenumber filter. In the case of an accelerometer, if the contact area is nearly equal to or larger than the wavelength on the beam, the signal will be attenuated so that the true response will not be measured. This error would occur likewise for the PVDF force gauges. Blake and Chase [15] analyzed this effect and found that if

$$\lambda > 4.2R \tag{3.3}$$

where R is the radius of the transducer surface, the sensitivity will not be attenuated by more than 3 dB.

3.3 Steering the drive array to a desired wavenumber

An important aspect used in measuring the wavenumber characteristics of compliant layers is the amplitude weighting of the drive array to concentrate the energy at the measurement wavenumber. All of the measurements were conducted on the same beam. At certain frequencies, this beam has a strong natural response

at its resonance or free bending wavenumber. For a Bernoulli-Euler beam, the free bending wavenumber is related to frequency [16] by

$$k_{BE}^4 = \frac{\rho A \omega^2}{EI} \tag{3.4}$$

where ρ is the density, A is the cross-sectional area, E is Young's modulus, and I is the moment of inertia. A single point source has a flat wavenumber spectrum, that is, all of the wavenumbers would be excited. However, most of the observed beam response would be transmitted into the beam at or near the free bending wavenumber for each frequency. This would create a ridge in the wavenumber-frequency response of the beam at the free bending wavenumber for each frequency. Because the turbulent boundary layer wall pressures excite structures at all wavenumbers, the admittance of the beam should be measured at all wavenumbers. To do this, it is necessary to drive the beam at regions in wavenumber and frequency that are away from the free bending wavenumber ridge. Therefore, energy must be concentrated at a single wavenumber to measure the admittance of the beam at wavenumbers other than the free bending wavenumber.

Consider an array of M equally spaced shakers of amplitudes q_m, the forcing function on the beam can then be represented as a summation of delta functions in space given by

$$q(x) = \sum_{m=1}^{M} q_m \delta(x - m\Delta x) \tag{3.5}$$

where Δx is the spacing between the shakers. The Fourier transform can be calcu-

lated directly:

$$Q(k_x) = \sum_{m=1}^{M} q_m e^{-jk_x m\Delta x} \quad . \tag{3.6}$$

This transform is the wavenumber spectrum of the array of point forces.

The spectrum of the force array is steered to the desired wavenumber by letting

$$q_m = \cos(k_d(m\Delta x - L/2)) \tag{3.7}$$

where k_d is the driven or steered wavenumber and L is the length of the beam. Equation (3.7) centers the force distribution about the middle o the beam. The spectrum of this distribution will have peaks at $k_x = \pm k_d$ as long as the Nyquist criterion is met or $k_d < \pi/\Delta x$. In other words, as mentioned before, there must be at least two shakers per wavelength.

Besides the peaks at $\pm k_d$, there will be additional peaks in the spectrum at $k_x = \pm(2\pi/\Delta x - k_d)$. The locations of these peaks can be found by examining the convolution of the Fourier transforms of the cosine function and the array of M point forces [13]. The wavenumbers at which these peaks occur correspond to wavelengths that also "fit" the force distribution as illustrated in Figure 3.1. These additional peaks, which have the same amplitude as the main lobes at $\pm k_d$, are called grating lobes. The main and grating lobes are collectively referred to as the major lobes. Between the major lobes, there will exist peaks with smaller amplitudes referred to as sidelobes.

The amplitudes of the side lobes are dependent upon the type of window that is applied to the force function. A rectangular window will produce the best

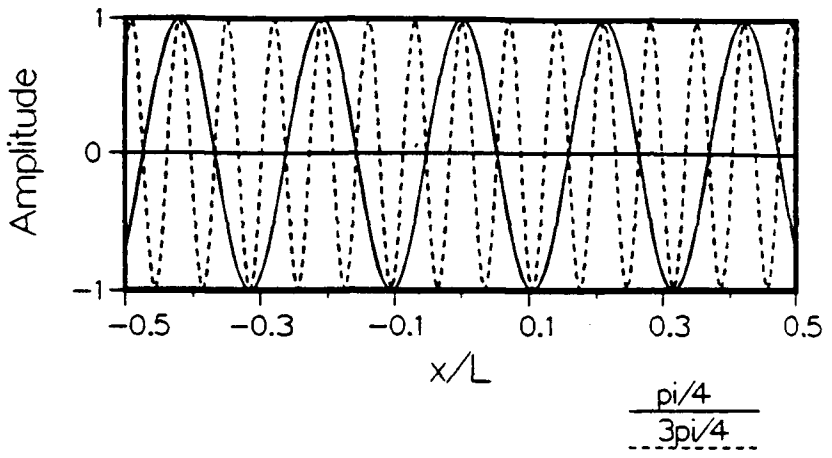

Figure 3.1: Illustration of grating lobe effects.

wavenumber resolution, yet the first side lobe will only be 13.8 dB down from the main lobe. These high side lobes are caused by the "discontinuities" (or sharp edges) of the distribution at the ends of the beam. The "discontinuities" are avoided by adjusting the voltage inputs such that

$$q_m = W(x_m)\cos(k_d(x_m - L/2)) \tag{3.8}$$

where $W(x_m)$ is a selected window function. The window used throughout this thesis was a Kaiser-Bessel window with the variable parameter α set to 1.5. This window is described in reference [17]. The amplitudes given by equation (3.8) are used for the voltage inputs to the shakers. By using this window, the sidelobes of the spectrum were decreased to a level where the first sidelobe was 36 dB down from the main lobe. However, this reduction in the sidelobe structure was achieved

at the expense of reducing the wavenumber resolution of the array.

A sample of the calculated wavenumber-frequency spectrum for seventeen shakers is given in Figure 3.2. The drive wavenumber k_d is $\pi/4$ cm^{-1} and the data were expanded over the frequency range 2–12 kHz to simulate the experiment. The grating lobe (at $k_x = 3/4\ \pi$ cm^{-1}) can be easily seen as well as the sidelobes. Ideally, this is what the spectrum of the force gauge outputs should look like if the applied forces on the beam are directly proportional to the applied voltages. How well the ideal wavenumber spectrum is duplicated will be discussed later when the results from the force gauges are presented.

3.4 Beam admittance

Consider a beam with an infinite length. Given the transform $Q(k_x)$ of the force on the infinite beam and the transform of the response, $Y(k_x)$, Grosh [13] defined the admittance of the infinite beam, $H_\infty(k_x)$, as

$$H_\infty(k_x) = j\omega \frac{Y(k_x)}{Q(k_x)} \tag{3.9}$$

where the multiplicative $j\omega$ comes from the conversion of the displacement to velocity.

Using the non-dimensional Timoshenko beam equations for finite beams, Grosh [13] derived the expression for the admittance of the finite beam $H_f(k_\ell)$ as

$$H_f(k_\ell) = \frac{j\omega Y_f(k_\ell)}{Q_f(k_\ell)}$$

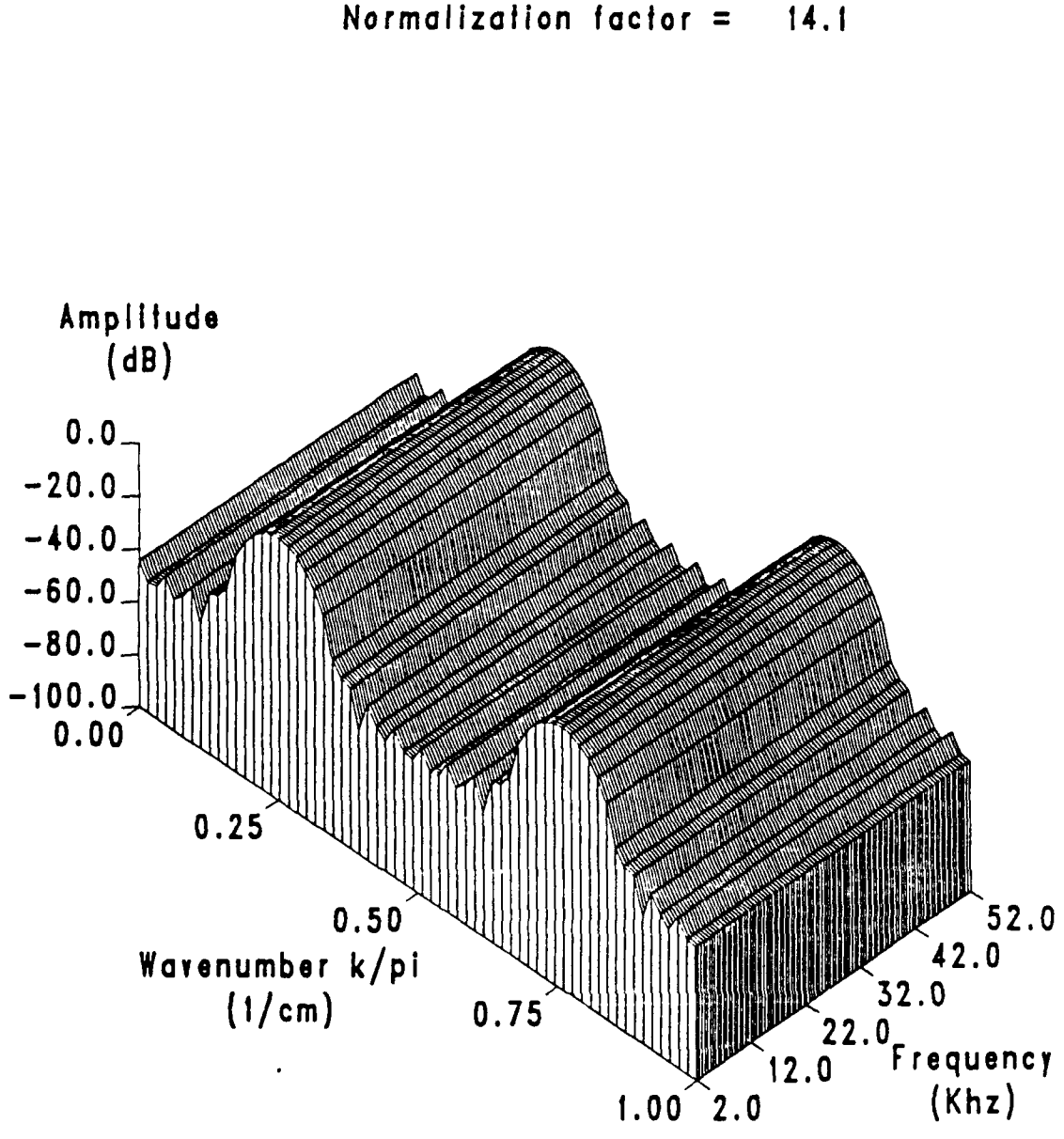

Figure 3.2: Wavenumber-frequency spectrum of force generated by an array of 17 shakers.

$$= H_\infty(k_\xi/L)\left\{1 + \frac{1}{Q_f(k_\xi)}\left[\mathcal{B}_1(k_\xi) + \frac{\mathcal{B}_2(k_\xi)}{\frac{E^* I}{L\nu} j k_\xi + \frac{L}{j k_\xi \nu}(\Theta - \nu)}\right]\right\} \quad (3.10)$$

where k_ξ is the transform variable for the non-dimensional spatial variable ξ used in the non-dimensional beam equations and Y_f and Q_f are the displacement and force spectra of the finite beam. The physical properties of the beam are given by E^* (the complex Young's modulus), I (the moment of inertia of the cross-section), ν (Poisson's ratio), and Θ which is given by the expression

$$\Theta = \rho I \omega^2 \quad (3.11)$$

where ρ is the density of the beam. The terms $\mathcal{B}_1(k_\xi)$ and $\mathcal{B}_2(k_\xi)$ contain the values of the displacement and bending slope at the ends of the beam.

If the amplitude of the forcing function spectrum $Q_f(k_\xi)$ is high, the measured admittance of the finite beam approximates the admittance of the infinite beam. That is,

$$H_f(k_\xi) \approx H_\infty(k_\xi/L) \quad . \quad (3.12)$$

Using the scaling rule for Fourier transforms [18] the nondimensional admittance of the infinite beam is related to the dimensional admittance by

$$H_\infty(k_\xi/L) = H_\infty(k_x) \quad . \quad (3.13)$$

Because the admittance of the finite beam at or near resonances is large, the above approximation (3.12) fails when the drive wavenumber is at or near resonance.

3.5 Wavenumber-frequency admittance and transmission loss

To measure the wavenumber frequency admittance of the beam, the spatial distributions of the force input on the beam and the velocity response were determined using the arrays of force gauges and accelerometers. The output from each transducer in each array was referenced to a common signal required for computing the Discrete Fourier Transforms.

The output signal from the force gauge in the center shaker was used as this reference throughout all of the admittance measurements. This signal was chosen since the voltage input to the center shaker was the reference for the other voltages inputs. Therefore, the force measurements were actually measurements of the force ratio of the output from each shaker force gauge to the force measured at the center shaker. Corrections were made for the differences in the sensitivities of the force gauges.

Because the measurements of the beam velocity were referenced to the force measured at the center shaker, the velocity measurements are expressed in terms of transfer admittances. A single accelerometer was used to measure the velocity at each measurement point along the beam relative to the force at the center. Using the sensitivities of the accelerometer and the center force gauge along with dividing the output by $j\omega$ yielded units of velocity over force.

Spatial Fourier transforms were taken of the force and velocity measurements. The wavenumber-frequency admittance was obtained by taking the ratio of the transformed velocity response to the transform of the force response. The dependence on the central force gauge is eliminated in the ratio calculation. Results

for the admittance will be presented only at the drive wavenumbers, where the force spectra are high. Although the data are valid at all wavenumbers, low signal levels at wavenumbers other than the driven wavenumber could introduce errors into the results.

By dividing the spectral admittance of the coated beam by the spectral admittance of the uncoated beam, the effectiveness of the layer can be determined. The effectivness is the ratio of the velocity of the coated beam over the velocity of the uncoated beam. The ratio of the admittances of the coated and uncoated beams yields the effectiveness since the measured velocities with and without the coating are corrected for differences in the force input.

To determine the wavenumber-frequency transmission loss, it was necessary to measure the spatial distribution of the forces on both sides of the layer. This was achieved using a thin array of force gauges, described in Chapter 4, on each side of the layer. The top array was directly below the shakers and the bottom array was "sandwiched" between the layer and the beam. For these measurements, the output from the central force gauge in the top array was used as the reference. By dividing the spatial transform of the normalized forces measured by the top array into the spatial transform of the normalized forces measured by the bottom array, the spectral transmission loss was determined.

Chapter 4

DESCRIPTION OF THE EXPERIMENTS

A description of the measurements, along with the transducers and instrumentation, are presented in this chapter.

4.1 Description of the shakers

In measuring both the admittance and the transmission loss, the beam was driven by an array of force drives (or shakers). These shakers were developed by Grosh [13]. A schematic of one of these units can be seen in Figure 4.1. The shakers, which have an overall length of approximately 6 cm and a diameter of 1.27 cm, consist of three sections; the drive, decoupler, and force gauge sections.

The drive section consists of two PZT-4 (Lead Zirconate Titonate) piezoceramic disks, three nickel electrodes, and a brass tail mass. The PZT-4 disks and the brass tail mass are 0.635 cm long. The PZT-4 disks are the active elements of the drive. By arranging the PZT-4 disks so that they are both polarized toward the center electrode, it was possible to connect them electrically in parallel. At low frequencies, both disks act together like a single disk of PZT-4 of twice the force output sensitivity. Shielding of the piezoceramic disks from electromagnetic interference (EMI) is provided by the negative or outer electrodes.

The decoupler section consists of an aluminum cylinder, 1.905 cm long and 1.27 cm in diameter. This section was found by Grosh to increase the low frequency

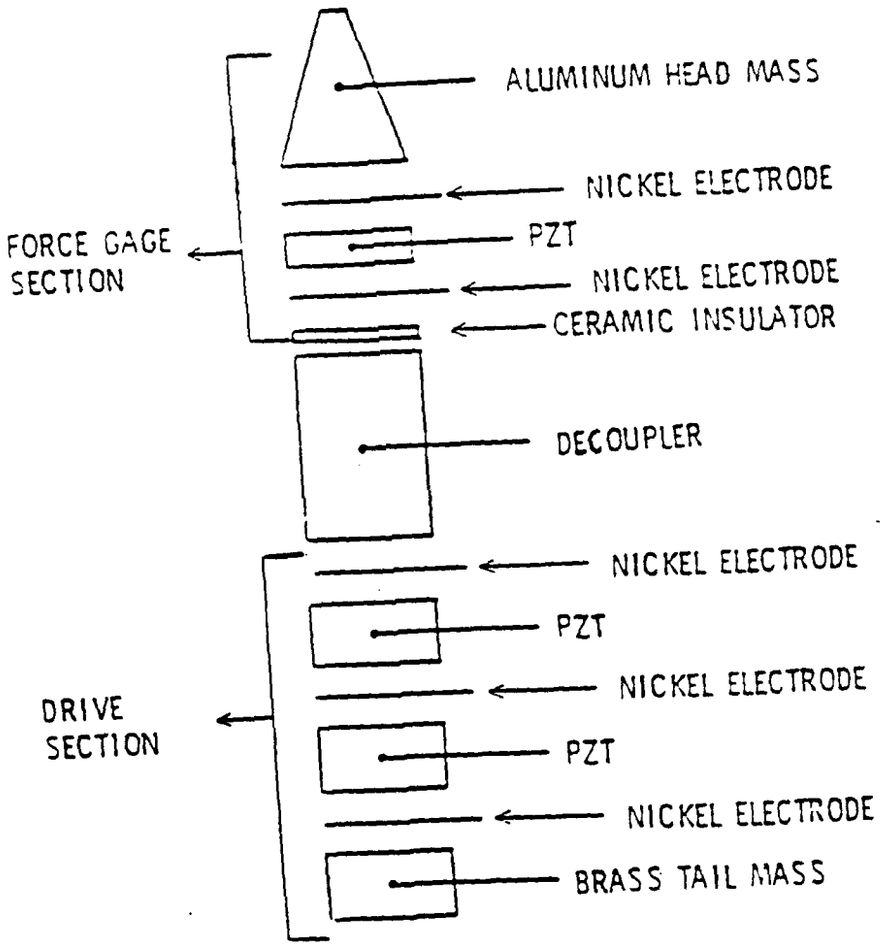

Figure 4.1: Single shaker/force gauge unit.

force output of the shaker [13]. The decoupler also reduces the effect of electronic cross talk between the drive and force gauge sections by increasing the distance between them. The decoupler is also grounded to provide EMI shielding for the force gauge section.

The force gauge section consists of an annular cylinder of PZT-4 (0.3175 cm long, 1.27 cm outer diameter, and 0.762 cm inner diameter), an aluminum head mass, an alsmaig ceramic insulator, and two nickel electrodes. The ceramic insulator insulates the positive electrode from the decoupler. Shielding for this section is provided by the negative electrode, the grounded head mass, and the grounded aluminum decoupler. The purpose of this section is to measure the force being transmitted from the drive section to the test structure. At the top or attachment point of the head mass, the cross section is narrowed to an area 0.3175 cm wide by 1.27 cm long to simulate a line force across the beam.

A detailed description of the development, construction, and the calibration of the shaker/force gauge combination is given by Grosh [13]. A listing of the force gauge sensitivities used in this thesis are given in Table 4.1.

4.2 Measurement of the admittance

4.2.1 Measurement instrumentation

A flow chart of the measurement system for admittance is shown in Figure 4.2. An IBM PC-AT controlled the experiment by operating an HP 4192A in the network analyzer mode through a General Purpose-Interface Bus (GP-IB). The network analyzer outputed a sinusoidal signal at a specified voltage level and

Table 4.1: Force gauge sensitivities.

Shaker number	Sensitivity (V/N)	Phase (deg.)
1	.94	179.
2	.88	179.
3	.95	180.
4	.88	180.
5	.93	180.
6	.92	181.
7	.99	181.
8	.94	181.
9	.98	181.
10	.98	181.
11	.97	180.
12	.97	181.
13	.97	181.
14	.97	180.
15	.99	180.
16	1.0	180.
17	.98	180.
18	1.0	180.
19	1.0	180.
20	.98	180.
21	.94	180.
22	.98	180.

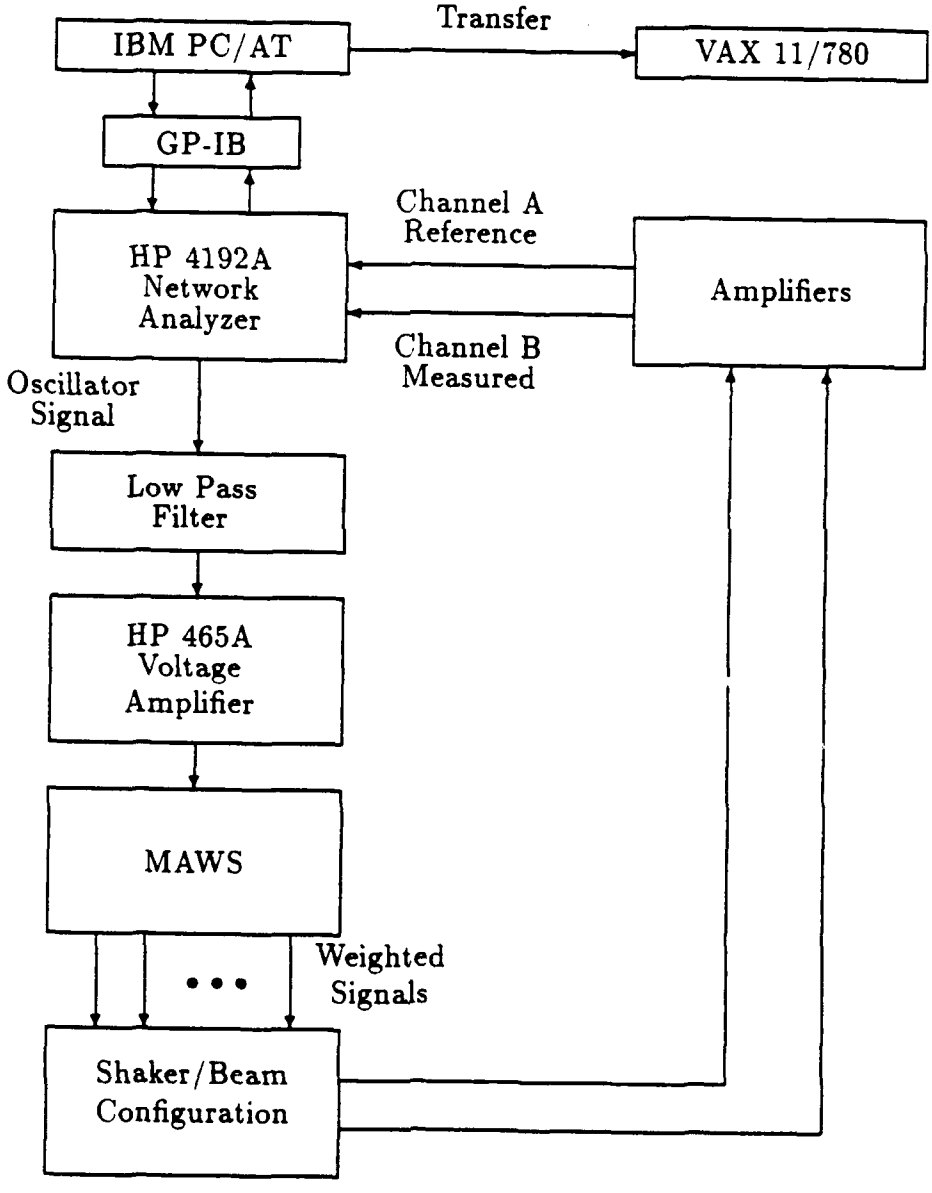

Figure 4.2: Flow chart of the measurement instrumentation.

frequency. This signal was sent through a low pass filter with the cut off frequency set to 13 kHz. The signal was filtered to reduce its harmonic content and to prevent the shakers from responding at their resonance frequency of approximately 30 kHz [13]. The filtered signal was then sent through an HP 465A voltage amplifier.

The filtered and amplified signal was input to the Multi-channel Amplitude Weighting System (MAWS). This system makes it possible to generate ten separate voltage signals of selectable amplitudes with zero or 180 degrees phase. Using the attenuator controls in the MAWS, it is possible to weight (or steer) an array of up to twenty shakers to a desired wavenumber using the technique described in Section 3.3.

Three beams were cut from the same stock and milled to identical dimensions of 37.8 cm long, 1.27 cm wide, and 1.92 cm thick. When running the experiment, the beam was supported on the ends by two open-cell foam wedges like those used in acoustical anechoic chambers. This support was found to closely simulate free-free boundary conditions at the ends of the beam [12].

When measuring the admittance of the bare beam, seventeen shakers were mounted directly onto the beam with a spacing of 2 cm between them. The bond was made with a cyanoacrylate adhesive (Eastman 910) after cleaning the beam and the attachment surface of the shaker with a three-part cleaning process[1]. The cleaning process involved soaking a cotton swab with toluene and scrubbing the surface until no residue was picked up by the swab. This was repeated with methanol alcohol and then acetone. Before bonding, a cyanoacrylate primer was applied to both surfaces

[1]Before cleaning, all metal surfaces were first scrubbed with a fiberglass brush to remove oxides.

to accelerate the bond and increase the bond strength.

When measuring the admittance of the coated beam, the elastomer layer was first bonded onto the beam. The natural rubber and neoprene layers were bonded with Devcon 5-minute epoxy after thoroughly cleaning both surfaces with the three part cleaning described above. For all of the bonds involving the 5-minute epoxy, the layers were clamped onto the beam using a jig and C-clamps to assure a strong, uniform bond. For the polyurethane layer, a jig was set up so that a layer of desired thickness could be poured directly onto the beam. The freshly poured layer was allowed to gel overnight before curing in an oven. Next, a 0.010 inch thick strip of steel was bonded to the layer with 5-minute epoxy. This was done to provide a good surface for shaker attachment. The strip also prevented localized deformation near the shaker attachment points.

The voltage outputs from the force gauges were connected to a channel selector. The selector was really just a switch that made it possible to select the output from a single force gauge and feed it into an amplifier. The force gauge of the center shaker was used as a reference so the signal from it was fed directly into channel A of the network analyzer. Depending upon which experiment was being conducted, the amplified signal from a force gauge or the amplified signal from the accelerometer was fed into channel B of the network analyzer.

The accelerometer was glued to a samarium-cobalt magnet so that it could be moved along the beam without the need to use glue for every measurement. In addition to the magnet, a small piece of steel, 0.1 cm thick, with the same dimensions as the shaker contact area (1.27 cm by 0.3175 cm) was glued onto the

bottom of the magnet to reduce the area in contact with the beam. When attached to the beam, a small amount of Kistler force gauge grease was used between the beam surface and the accelerometer assembly (used as a velocity probe) to enhance the response [13].

4.2.2 Procedure

The frequency range of all the measurements was 2–12 kHz where the shaker force gauge sensitivities were flat [13]. Also, the level of the forces generated by the shakers rolled off below 2 kHz so that the lower measurement frequency limit was 2 kHz. For each admittance measurement, two experiments were conducted. The first experiment involved measuring the ratios of the force gauge outputs to the output from the central force gauge output as described in Chapter 3. First, one of the end force gauge outputs was selected using the channel selector. A BASIC program in the IBM PC-AT was then used to instruct the network analyzer, via the GP-IB, to step through frequency and return the amplitude ratio and the phase difference between the force gauge outputs. This ratio was adjusted by the program for the difference in the force gauge sensitivities and any difference in the channel gains. This provided the normalized force at the selected position. Then, the frequency, normalized force, and phase were written to a file for each frequency step. The next force gauge output was selected and the experiment was repeated until all of the forces, excluding the center one, had been measured. It is important to keep the measurements in order for the purpose of spatial transform. From these measurements, the wavenumber-frequency spectra of the forcing function will be calculated.

The second experiment involved measuring the velocity at 37 locations along the beam (1 cm apart) with respect to the central force gauge output. These locations were marked on the beam by lines that were scribed onto the side of the beam. In a similar manner to the force measurements, the accelerometer was positioned on the beam and the computer ran a program that caused the network analyzer to step through the frequency and return the ratio between the voltage output of the accelerometer to the output from the central force gauge. The acceleration was converted into a velocity by dividing the measured ratio by the angular frequency ω and shifting the phase by 90 degrees. Using the sensitivities of the force gauge and the accelerometer, the ratio of their outputs was converted into the normalized velocity. The program then wrote the frequency, the normalized velocity, and the phase to a file for each frequency step. This was repeated until measurements of all 37 locations had been conducted.

4.2.3 Data reduction

Each experiment created two data files. One file contained the spatial distribution of the force over the frequency range while the other file contained the spatial distribution of velocity normalized with respect to the central force. These files were transferred to a VAX 11/780 mainframe computer for the data reduction.

Spatial Discrete Fourier Transforms (DFT's) were taken of the force and velocity files using a Fast Fourier Transform (FFT) technique [17]. The transforms were taken with 128 points and either a rectangular, a Hanning, or a Kaiser-Bessel window was applied to the data before the transform. These transforms produced the wavenumber-frequency spectra of the force and the velocity. It should be noted

that before the transform of the force file was taken, a simple program was run to insert a reference shaker (of unity value) in the middle of the file and zeroes were inserted between the force gauge values. These zeroes caused interpolation within the transform [17] so that the wavenumber-frequency spectrum of the force would have the same bin size as the velocity spectrum.

With the spectra of the force and velocity ready, the admittance of the beam was calculated by dividing the velocity spectrum by the force spectrum. In this division, the normalization factor provided by the central force is eliminated. The measured admittance is accurate only at the driven wavenumber; therefore, in order to measure the wavenumber dependence of the admittance, it is necessary to weight (or steer) the drive array to several wavenumbers and repeat the experiments.

4.3 Measurement of the transmission loss

In order to measure the transmission loss of compliant layers, it is necessary to determine the spatial force distributions on both sides of the layer. These distributions were measured by thin arrays of PVDF force gauges. A description of these arrays and how they were constructed is given in this section. Next, the experimental set up, procedure and the data acquisition are described.

4.3.1 Description of the PVDF arrays

A schematic of the array/layer arrangement can be seen in Figure 4.3. The arrays consisted of individual pieces of polyvinylidene fluoride (PVDF) piezoelectric film bonded between a 0.002 inch copper coated Kapton pc board and a 0.001 inch

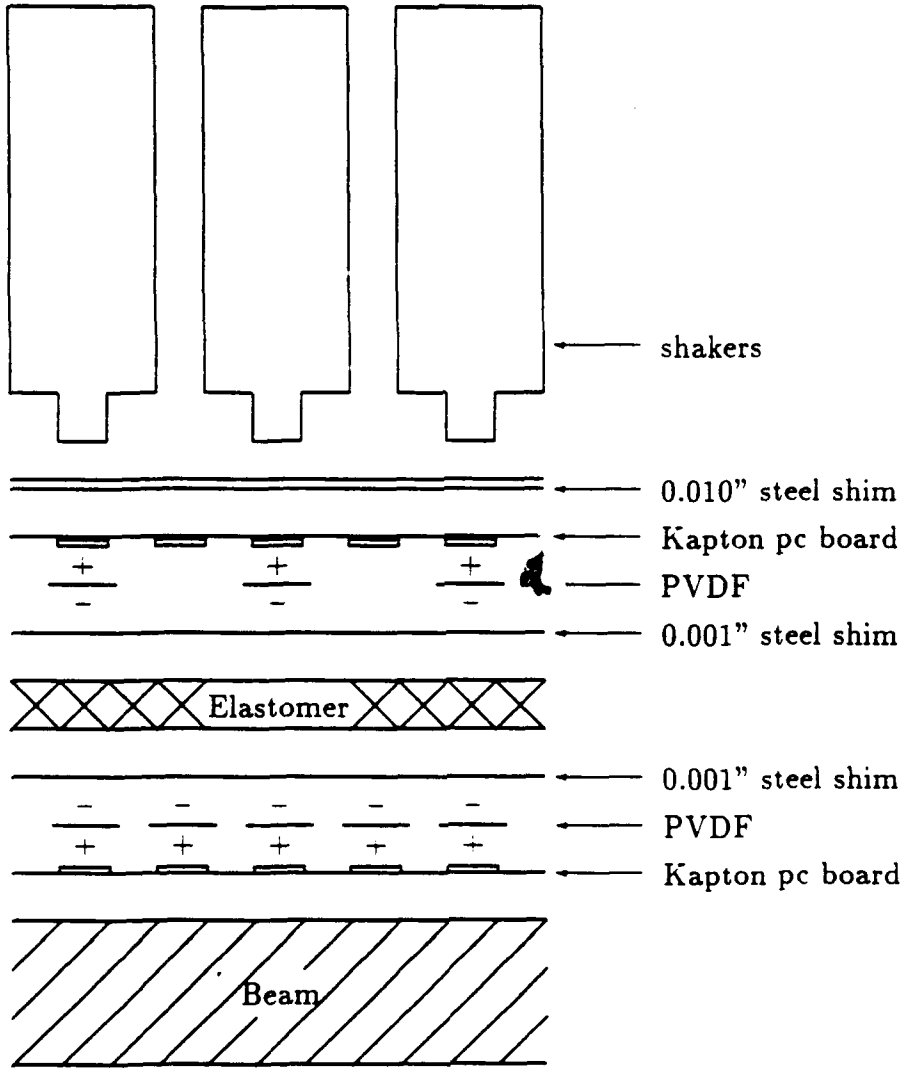

Figure 4.3: Schematic of the array/layer arrangement on the beam.

strip of stainless steel shim. The copper on the pc board and the steel shim acted as the positive and negative leads respectively by capacitive coupling through the bond layer and the piezoelectric film. It can be seen in the Figure 4.3 that EMI shielding was provided by grounded negative leads and either the beam or the 0.010 inch steel shim.

The pieces of PVDF were cut from strips of KYNAR piezo film that was purchased from the Penwalt Corporation in King of Prussia, Pennsylvania. A variety of PVDF materials of different thicknesses and different electrode coatings was available. The film that was used in this thesis was 52 μm thick and had nickel-aluminum electrode coatings. Before completion of the arrays, the PVDF pieces were cut into pieces 3/4 inch long and 7 mm wide. Great care was taken to keep track of the polarities of each of the pieces to insure that they would all be in phase when the array was finished. This was done by marking one electrode with a red felt tip pen.

To construct what became the positive leads of the arrays, a sheet of double sided, copper plated Kapton pc board (approximately 3 mills thick) was photographically etched. This etching left the Kapton with no copper on one side and 37 strips of copper 5 mm wide and 5 mm apart on the other side. The sheet of Kapton was then cut into strips 3/4 inch wide and approximately 44 cm long. This extra length was used to hold the strip down with tape during construction. A representation of a section of these strips is illustrated in Figure 4.4. The 0.001 inch steel strip was cut to dimensions identical to the those of the Kapton (44 cm x 3/4 inch).

Before construction, all of the surfaces were cleaned. The PVDF pieces

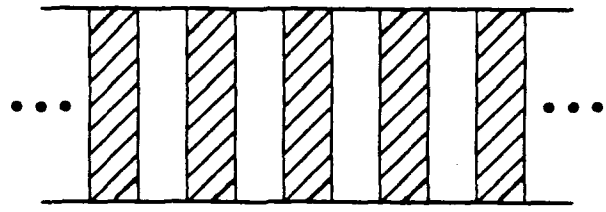

Figure 4.4: Kapton strip.

were cleaned with freon solvent and cotton swabs. Freon was used since most other solvents (namely toluene and acetone) can chemically attack the PVDF. Again, care was taken to keep track of the polarities by marking the electrodes of the PVDF with a felt tip pen. The Kapton and steel strips were cleaned using the same three part process described in Section 4.2.1, remembering to scrub the copper strips with a fiberglass brush beforehand to remove any oxide coating.

To prepare for the construction of the arrays, a thick plate (1/8 inch) of steel was covered with Teflon tape. Using a ruler, several pieces of PVDF were taped down with the desired spacing and with the positive electrodes facing upward. For the bottom array which had a total of 37 transducers, ten of the pieces, at a time, were taped down with a 1 cm spacing from center to center. For the top array which had 19 transducers, five pieces were taped down with a 2 cm spacing from center to center. Only five or ten pieces were installed at a time to insure good, uniform

bonds for each transducer.

Next, a thin layer of Devcon 5-minute epoxy was applied to the appropriate copper strips on the Kapton strip. A thin layer was achieved by first applying a small amount of epoxy and then wiping the area with a damp cotton swab. The epoxy was applied to an area of 1.27 cm by 0.7 cm on each copper strip so that the remaining 0.635 cm by 0.7 cm area of copper could be used as the positive lead for each transducer in the array. The Kapton strip was then placed onto the PVDF pieces so that only the epoxied areas of the Kapton strip came in contact with the PVDF, leaving 1.27 cm of each copper strip in contact with 1.27 cm of PVDF. The Kapton strip was then held in place with tape at the ends. Next, the Kapton and PVDF pieces were clamped with C-clamps between a beam that was coated with Teflon tape and the plate of steel that was also coated with Teflon tape. It was important to make sure that the clamps were not screwed too tight or the PVDF strips might have been damaged or displaced. Each bond was allowed to set for at least half an hour before the clamps were removed.

When all of the PVDF pieces were bonded onto the Kapton strip, their surfaces were once again cleaned with freon solvent. Next the Kapton was trimmed down to a length of 38 cm. The strip was then taped down with the PVDF facing upward. The tape covered the exposed parts of the copper strips. Next, a thin layer of 5-minute epoxy was applied to the steel strip and it was taped down so that it covered only the PVDF pieces. The array was then clamped as before. When the bond was set, one of the excess ends of the steel strip was removed, leaving the other end to act as the negative lead for the whole array. Finally, the excess PVDF

and steel was carefully removed using a pair of scissors. This technique produced arrays of 19 or 37 force gauge transducers with similar sensitivities and phases.

The bottom array (with 37 transducers) was then mounted onto the beam with 5-minute epoxy. Next, the elastomer layer was mounted on top of the array. Then the top array (19 transducers) was mounted and then the 0.010 inch steel shim was mounted on top of the array to prevent localized deformation around the shaker attachments and to protect the PVDF array on top of the layer. The polyurethane layer had to be molded separately (instead of poured in place as before) since the oven cure temperature that was required would have destroyed the PVDF arrays.

4.3.2 Experimental set up

The same system that was used to drive the beam in the admittance experiments was used to drive the beam for the transmission loss. Namely, the same combination of the personal computer, network analyzer, and MAWS was used to drive the array of shakers mounted onto the beam.

A new method of supporting the beam was used, however. This was required to keep the foam from interfering with the operation of the PVDF arrays. Notches were cut into the exposed parts of the arrays between the first and second transducers from each end and rubber bands (three to an end) were used to support the beam. The rubber bands were supported by metal rods held by buret clamps on chemical laboratory stands. This new arrangement also made it possible to increase the aperture of the force array by adding one more shaker at each end, increasing the number of shakers from seventeen to nineteen in all.

It is very important at this point to describe how the signals were obtained

from the PVDF transducers. As mentioned before, the 0.001 inch steel snim was used for the negative lead. The 0.010 inch steel strip and the beam were electrically grounded to provide electrical shielding for the arrays. The positive signal from the copper lead of each transducer was picked up by a miniature electrical spring hook probe. A small microphone amplifier was glued onto the back of the hook. The signal from the hook was soldered to the amplifier input, the output of the amplifier was soldered to the positive lead of a coaxial cable, and the ground of the amplifier was soldered to the ground lead of the cable. The microphone amplifier was then potted with 5-minute epoxy. The entire hook was then carefully wrapped with aluminum foil that was grounded to provide the necessary electrical shielding for the amplifier. A Micro-tech cable end was attached at the other end of the coaxial cable. When in use, the end of the cable was connected to a box with two channels that provided the necessary voltage (9 volts) and a bias resistor (6.81 ohms) for each channel. Between the positive posts of the inputs and outputs of the box, there were capacitors (1 μFarad each) to prevent a large DC current from entering any of the instrumentation that was used in the system.

Using the hook as a probe combined with an amplifier, it was possible to get a strong, clean signal from each of the transducers in the arrays. The small amplifier was necessary because the PVDF impedance was high and attaching a cable directly to the transducer would have attenuated the signal. Two of these probes were constructed and the gains of each probe was measured so that the data could be adjusted accordingly.

4.3.3 Procedure and data reduction

The procedure and data reduction of this experiment were fairly straightforward. One of the probes was clipped onto the center PVDF force gauge of the top array, the output of which was inputted to channel A of the network analyzer as the reference. The other probe was used to measure the response of each PVDF force gauge relative to the reference force gauge over the frequency range of 2–12 kHz. A computer program was used to step the frequency, adjust for the gains, and write the ratios of the output signals to a file. Only voltage ratios were needed in the calculations since the sensitivity of the force gauges were similar.

For each experiment, this process created two files (one for the top array and one for the bottom array). These files were transferred to the VAX for reduction. Fourier transforms were taken of each of these files. As in the data reduction for the admittance experiments, the file for the top array had the center transducer response (unity) inserted and zeroes were added so that the transform would have the same bin size as the transform of the bottom array. These transforms represented the wavenumber-frequency spectra of the force distributions on each side of the layer. The transmission loss was then calculated by taking the spectrum of the bottom array and dividing it by the spectrum of the top array. Data are reported only at the wavenumbers which were being driven. Again, to determine the wavenumber dependence, it is necessary to repeat the experiment for other wavenumbers.

Chapter 5

EXPERIMENTAL RESULTS

This chapter presents the results that were obtained from the experiments described in Chapter 4. A large number of experiments were conducted (a total of 24) and several comparisons were made. The experimental test matrix is given in Table A.1 of Appendix A.

The analysis and interpretation of measurements conducted on different materials and drive wavenumbers are presented. Using PVDF force gauge arrays, the transmission losses are measured at different wavenumbers for two different materials.

5.1 Results from the bare beam

5.1.1 Experimental verification

It was necessary to verify the set up by repeating an identical experiment performed by Grosh [13] and comparing the results. The seventeen shakers were steered to a wavenumber of approximately $\pi/4$ cm^{-1}. This corresponded to experiment #8 of Grosh's thesis. The force spectrum obtained in this mesurement is shown in Figures 5.1 and 5.2. The features of the force spectrum are similar to those reported by Grosh [13]. These features include the forced wavenumber ridge, the grating lobe ridge, and the free bending wavenumber ridge. The forced

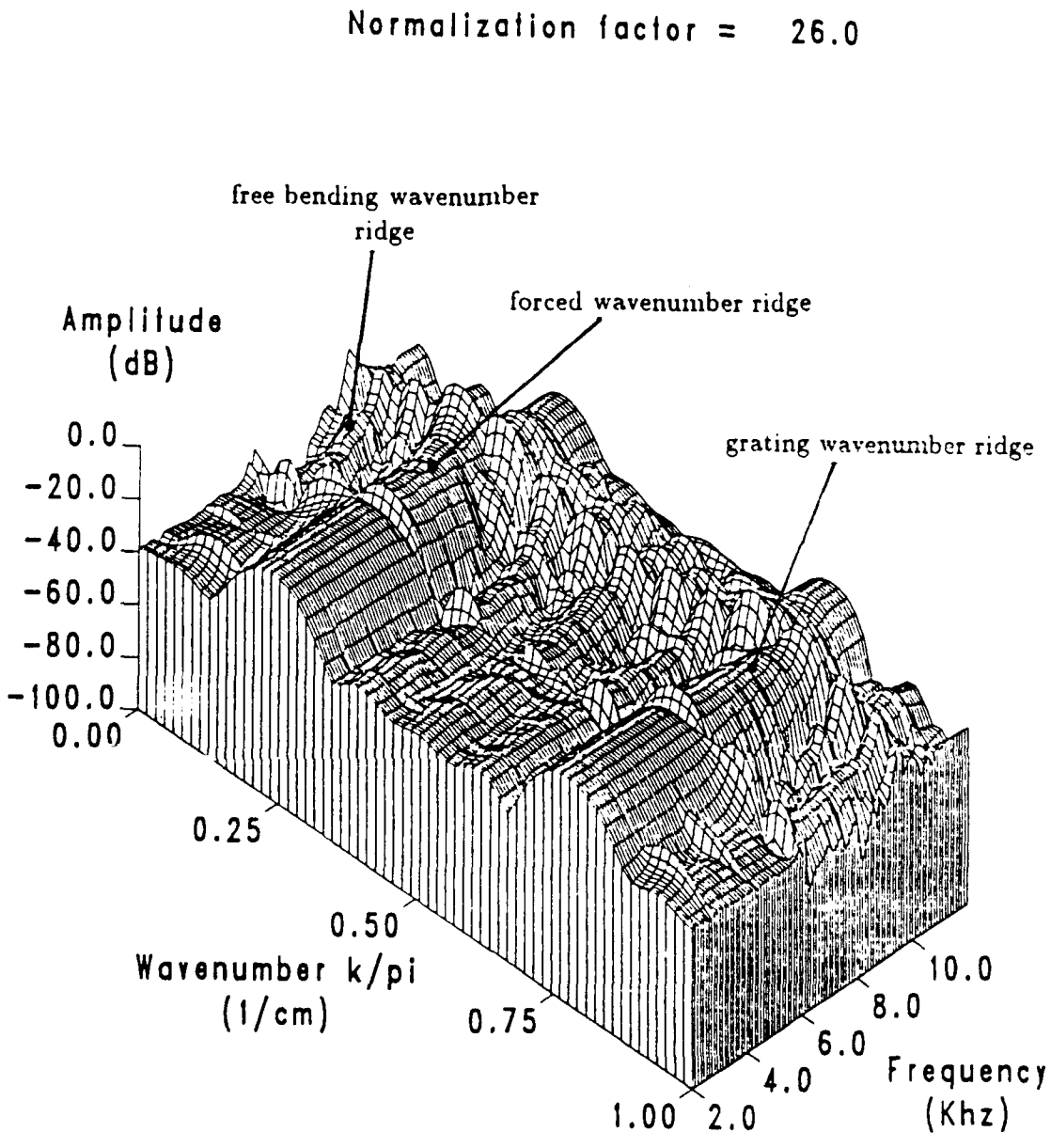

Figure 5.1: Surface plot of the force spectrum for $k_d = \pi/4$ cm^{-1}.

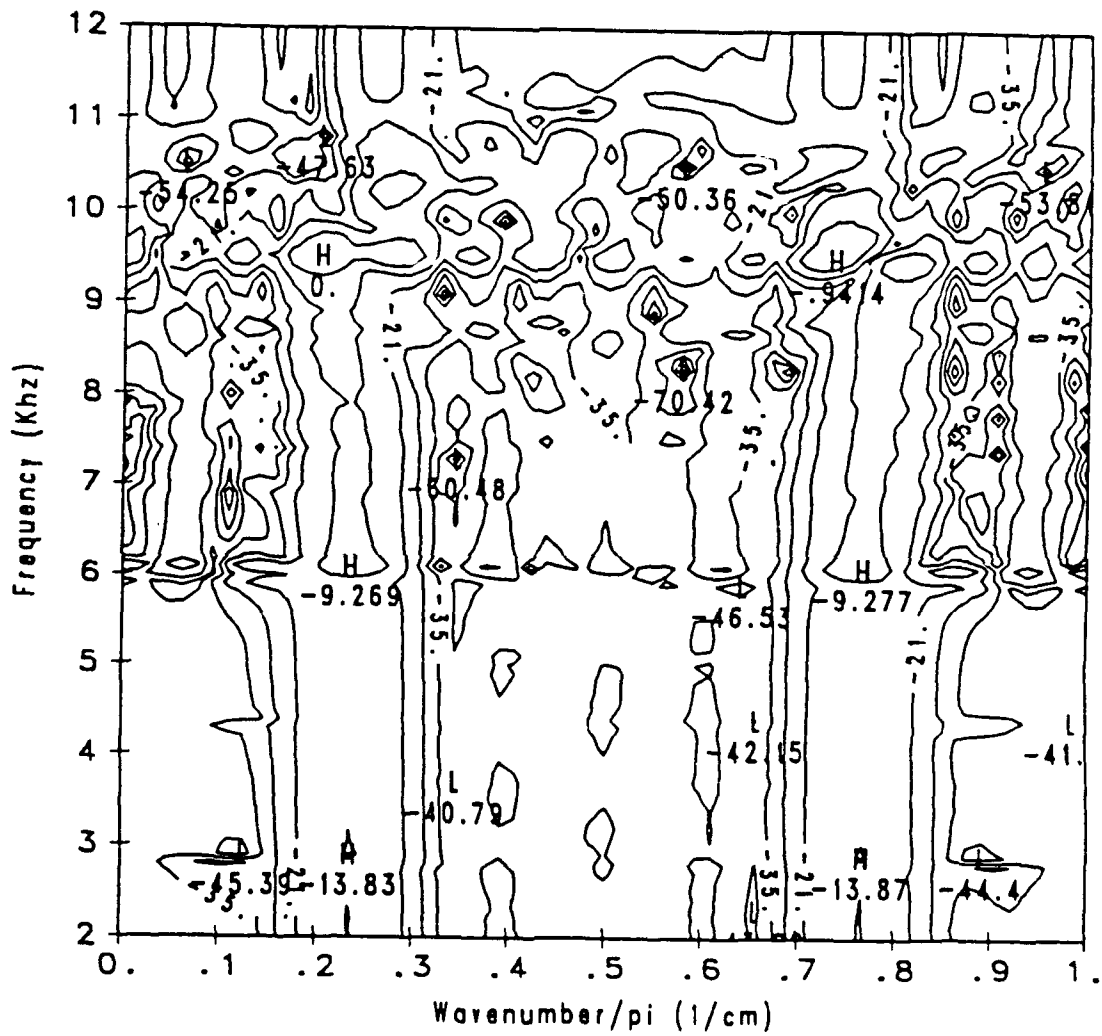

Figure 5.2: Contour plot of the force spectrum for $k_d = \pi/4$ cm^{-1}.

wavenumber ridge exists at the wavenumber to which the shaker array has been weighted. The grating lobe exists at $k_x = \pm(2\pi/\Delta x - k_d)$ as predicted in Chapter 3. As can be seen by these figures, the force spectrum closely resembles the spectrum of the applied shaker voltages shown in Chapter 3 except at high frequencies where the close proximity of the free bending wavenumber ridge causes the forced ridge to shift in wavenumber [13]. Figure 5.3 compares the values of force obtained by the new experiment with those values obtained by Grosh [13] over frequency at the driven wavenumber, $\pi/4$ cm^{-1}. The values of both curves are similar.

The measured velocity spectrum at the same drive wavenumber of $\pi/4$ cm^{-1} is shown in Figures 5.4 and 5.5. Again, the characteristics seen in this spectrum closely match those observed by Grosh [13]. The response of the beam to the driven wavenumber is apparent as is the free bending wavenumber ridge of the beam. The response of the beam at the grating lobe wavenumber can not be seen because of the low admittance of the beam at the grating lobe wavenumber. A comparison of the velocity values obtained by this thesis and those obtained by Grosh [13] at the driven wavenumber $\pi/4$ cm^{-1} is given in Figure 5.6. Again, the curves are similar.

5.1.2 Improvement of the velocity measurement

One of the problems encountered by Grosh [13] was the poor signal to noise ratio experienced at higher wavenumbers. An example of this problem can be seen in Figures 5.7 and 5.8 which show the velocity spectrum with the drive wavenumber equal to $\pi/2$ cm^{-1}. These plots were produced from data measured by Grosh. As can be seen, the response of the beam at the drive wavenumber ($\pi/2$ cm^{-1}) can barely be resolved from the surrounding "noise." Also, there exists a large response

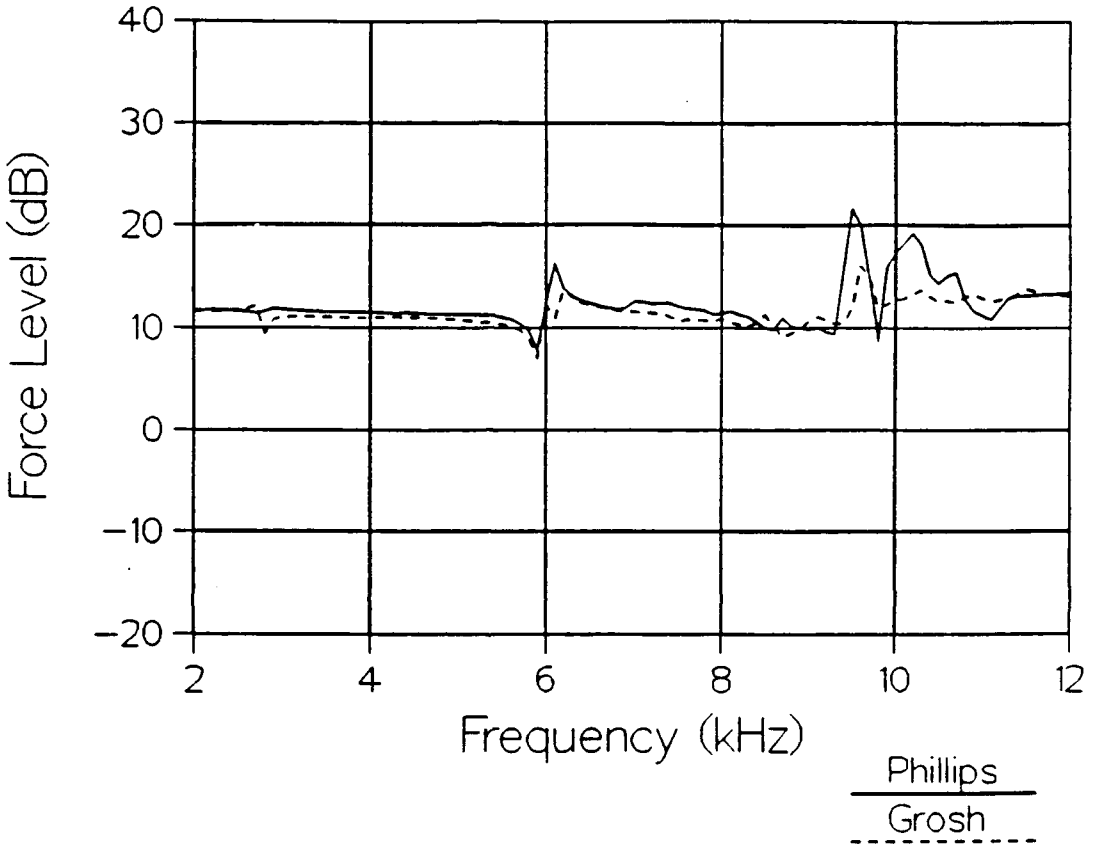

Figure 5.3: Comparison of force obtained by this thesis and Grosh [13] at $k_d = \pi/4$ cm^{-1}.

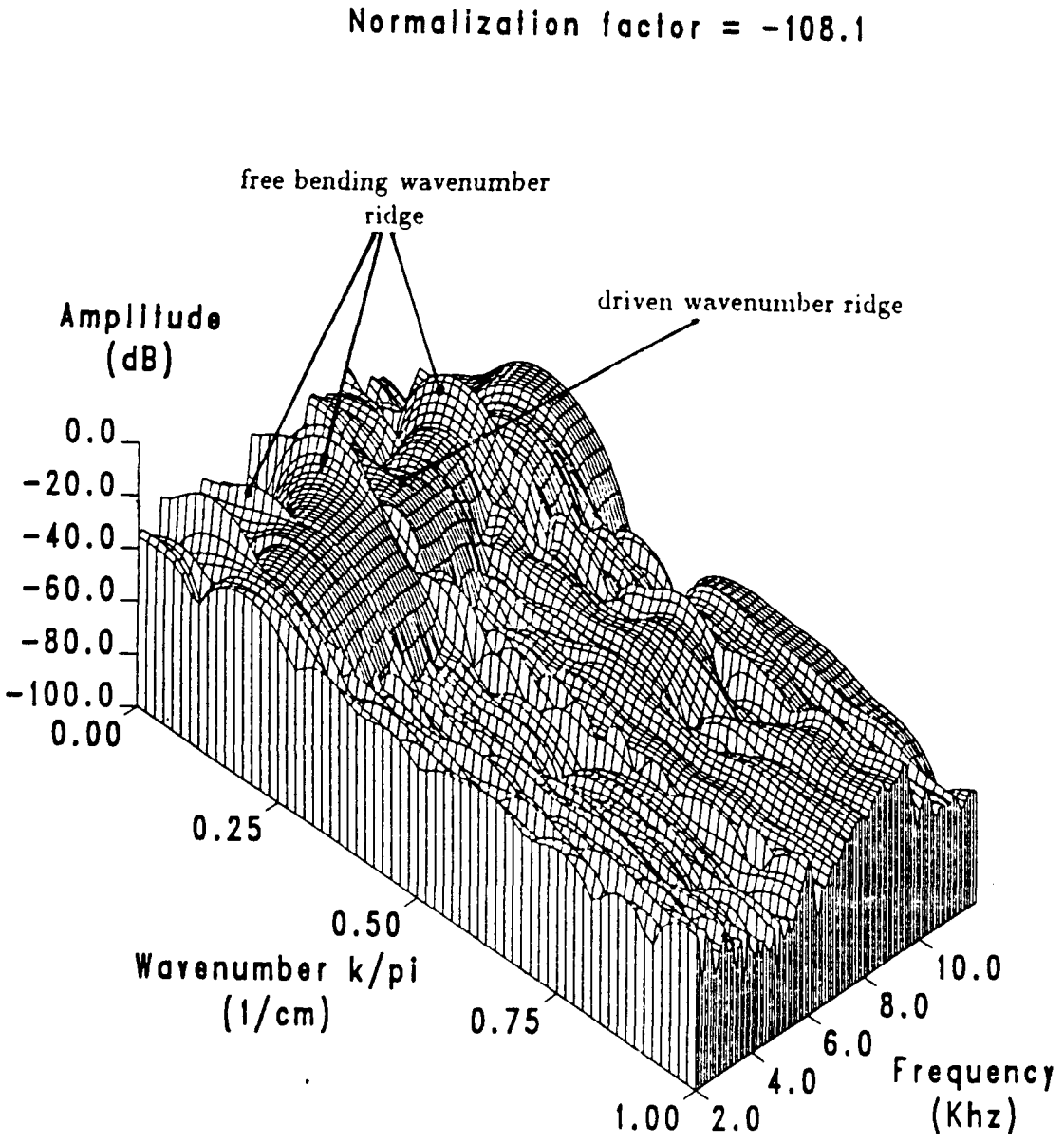

Figure 5.4: Surface plot of the velocity spectrum for $k_d = \pi/4$ cm^{-1}.

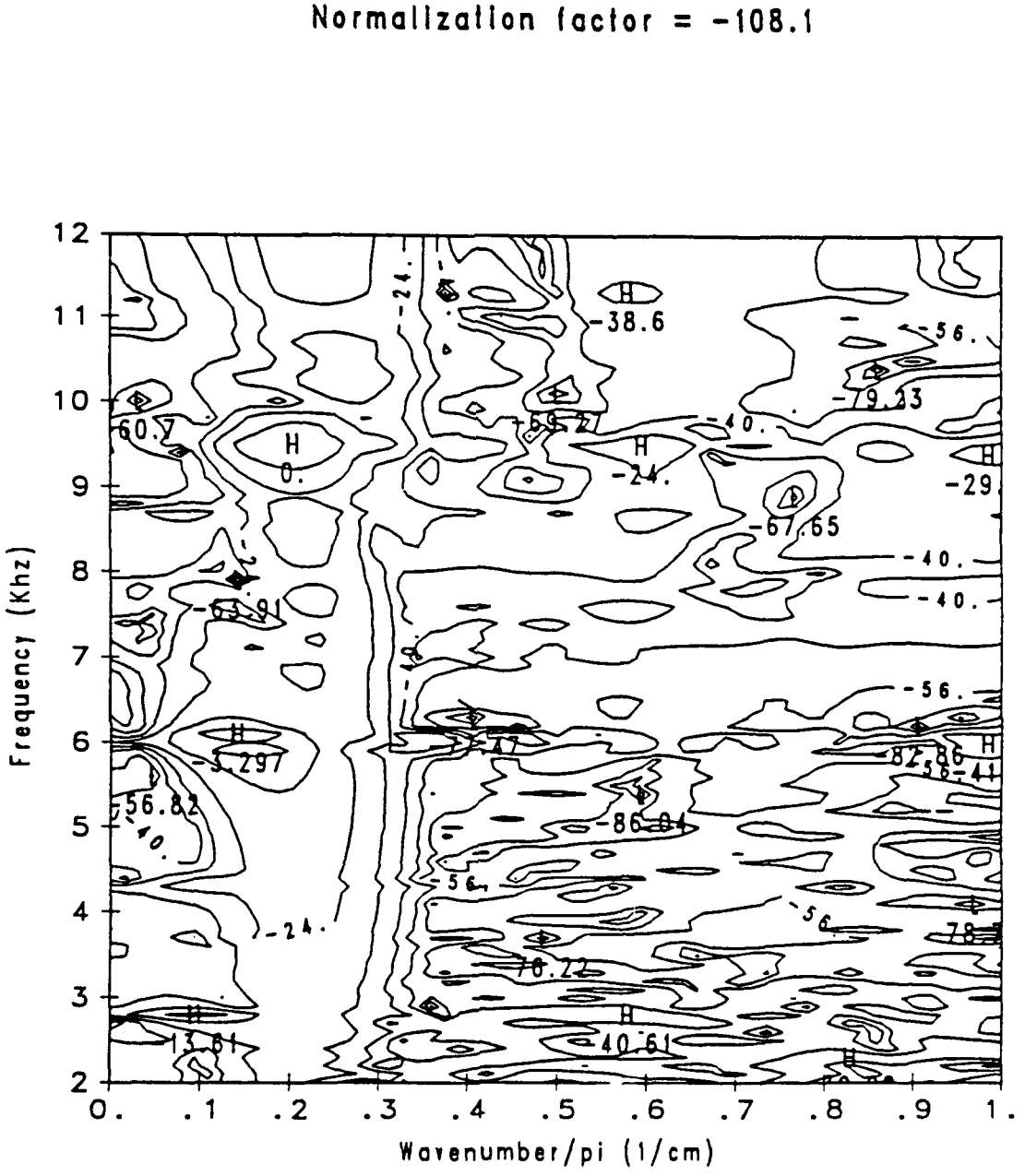

Figure 5.5: Contour plot of the velocity spectrum for $k_d = \pi/4$ cm^{-1}.

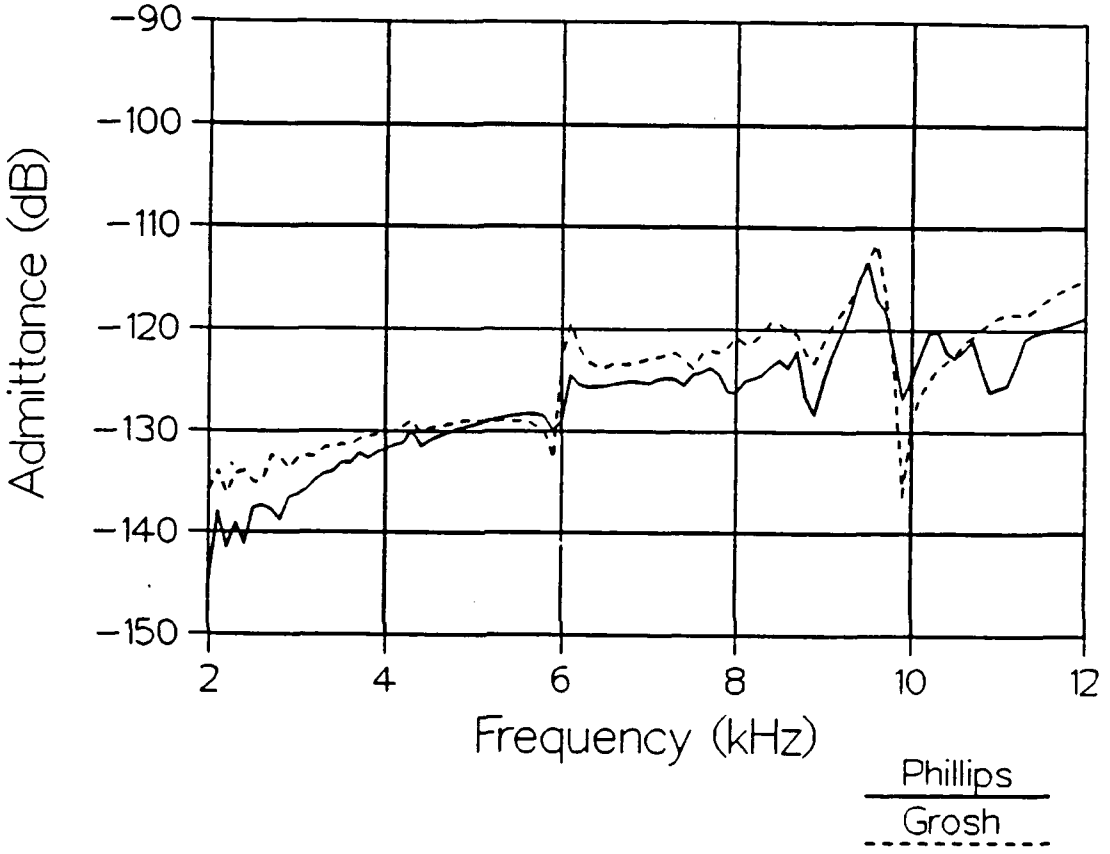

Figure 5.6: Comparison of velocity obtained by this thesis and Grosh [13] at $k_d = \pi/4$ cm^{-1}.

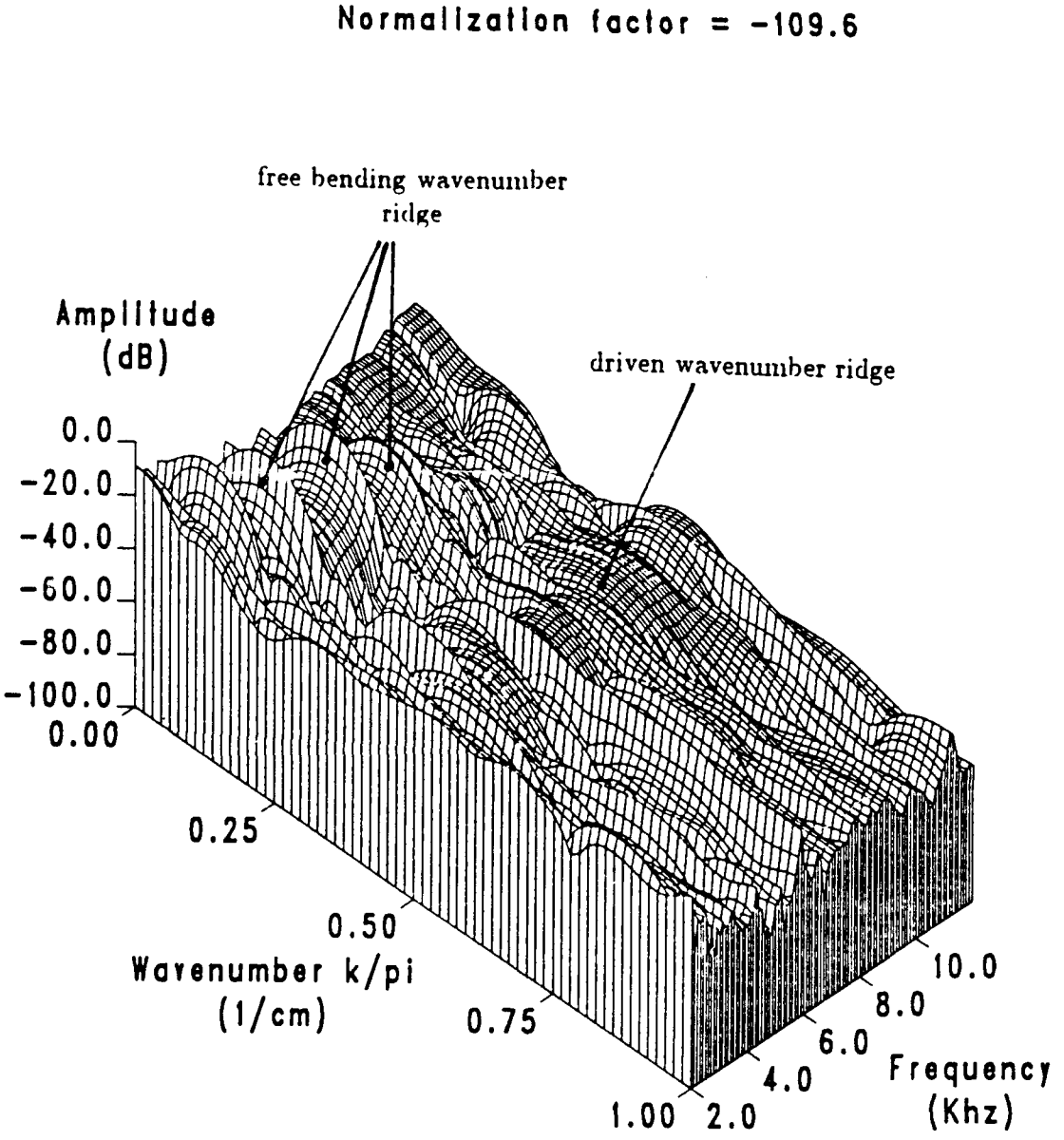

Figure 5.7: Surface plot of the velocity spectrum for $k_d = \pi/2$ cm^{-1} measured by Grosh [13].

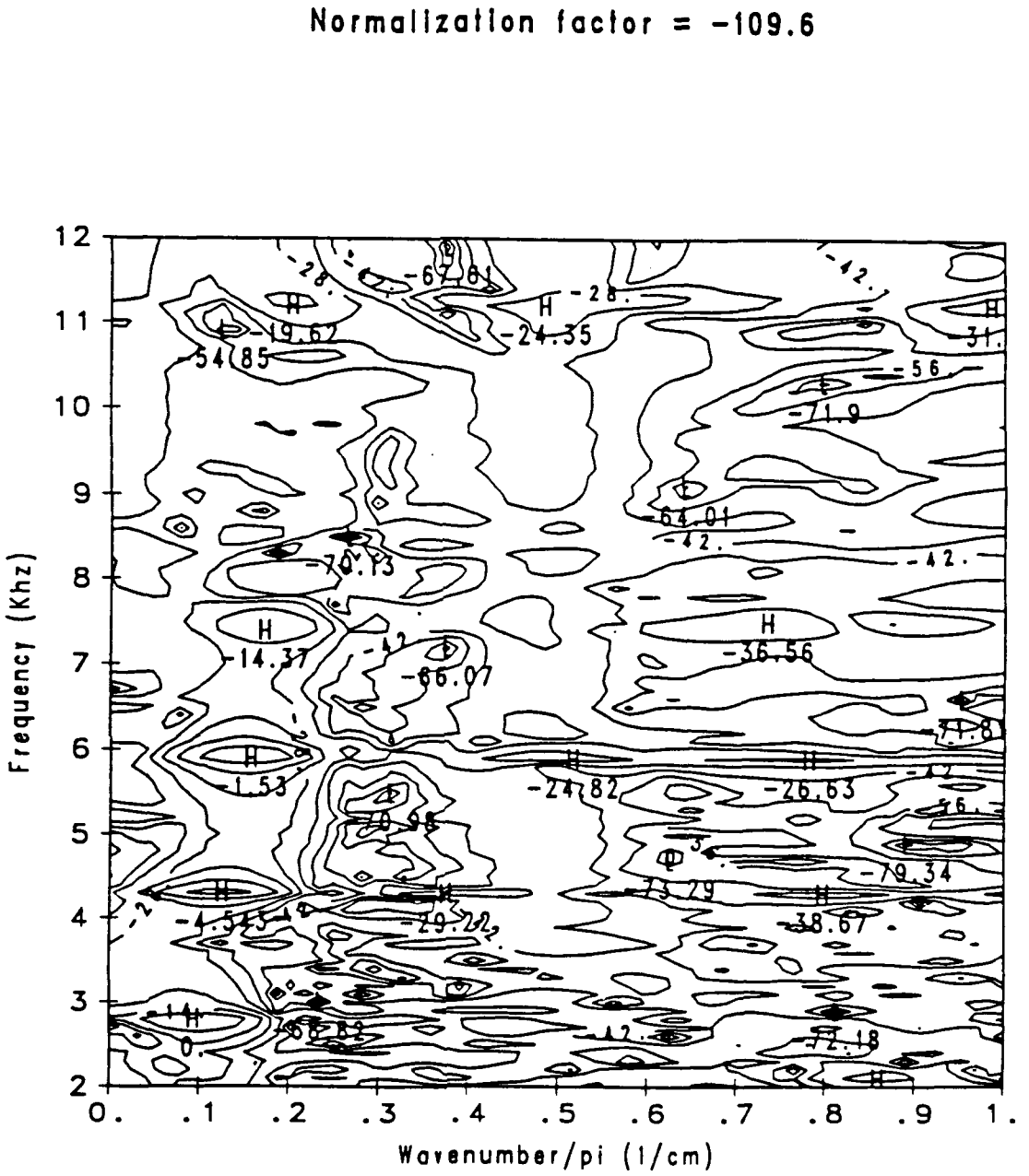

Figure 5.8: Contour plot of the velocity spectrum for $k_d = \pi/2$ cm^{-1} measured by Grosh [13].

at the free bending wavenumber ridge with peaks along this ridge which correspond to resonances of the beam.

The reason for the poor response at the driven wavenumber is the combination of the low admittance of the beam and the attenuation of the signal caused by the size of the accelerometer which is comparable to the measurment wavelengths. Whereas nothing can be done to increase the admittance of the beam, the attenuation of the signal due to the spatial averaging of the sensor can be reduced. The accelerometer used earlier was mounted onto a samarium-cobalt magnet which had a diameter of 1 cm. At a wavenumber of $\pi/2$ cm^{-1}, the wavelengths on the beam are 4 cm. Therefore, the magnet was too large (1/4 the measurement wavelength) to accurately measure the response. The measured response was improved by mounting a piece of steel (1.27 cm x 0.3175 cm x 1/32 in) onto the bottom of the magnet, giving the accelerometer the same contact area as the shakers. The improvement in the resolution of the driven wavenumber ridge at $\pi/2$ cm^{-1} can be seen by comparing the velocity response measured by the new probe shown in Figures 5.9 and 5.10 with the velocity response meausured by the old probe shown in Figures 5.7 and 5.8.

5.1.3 Additional measurements on the bare beam.

At a certain frequency, the response of the beam is high at free bending wavenumbers. Earlier work proved that it was possible to force the beam to respond at wavenumbers other than free bending wavenumbers. However, previous drive wavenumbers had wavelengths that fit onto the beam in half wavelength multiples [13]. When measuring the wavenumber dependence of the transfer admittance, it

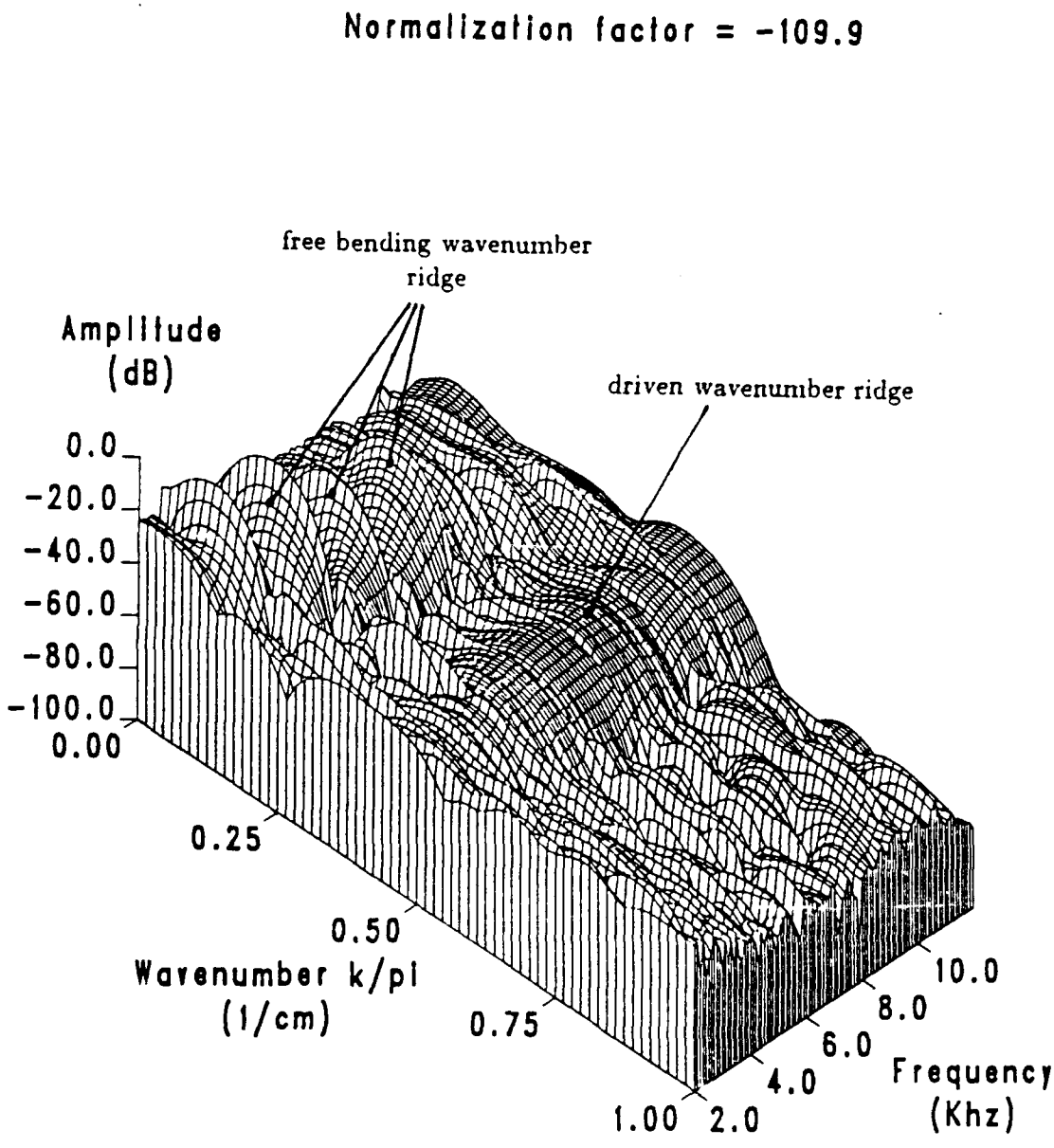

Figure 5.9: Surface plot of the velocity spectrum for $k_d = \pi/2$ cm^{-1} measured with the improved velocity probe.

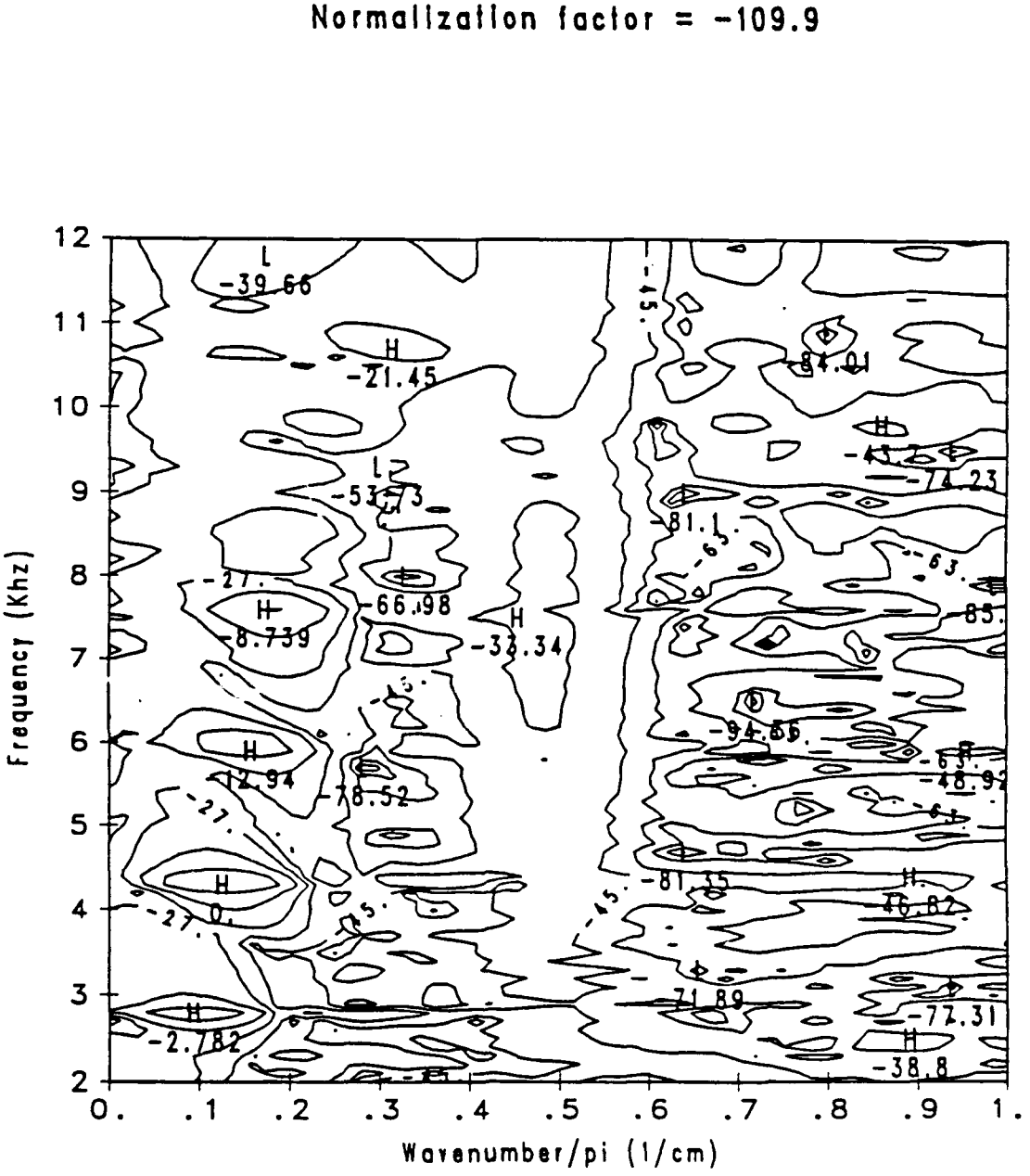

Figure 5.10: Contour plot of the velocity spectrum for $k_d = \pi/2$ cm^{-1} measured with the improved velocity probe.

became apparent that wavenumbers whose wavelengths did not fit so "nicely" onto the beam should be measured.

Force and velocity measurements were made on the bare beam driven at a wavenumber of 0.28π cm^{-1}. This corresponded to approximately 7.14 wavelengths on the beam. The force and velocity spectra of this experiment can be seen in Figures 5.11–5.14. It can be seen from the strong response in both spectra at the driven wavenumber that the system worked well when the length of the beam was not a half multiple of the driven wavelength.

5.2 Results from the coated beam

This section presents the results from the force and velocity measurements conducted on the coated beams. Several materials, all of which had the same thickness, 0.635 cm, were tested at several drive wavenumbers.

The first test involved a layer of natural rubber with a hardness of 65 durometer, referred to as "Natural Rubber I" to distinguish it from an other natural rubber used later. The drive wavenumber for this experiment was $\pi/4$ cm^{-1}. The wavenumber-frequency force spectrum is shown in Figures 5.15 and 5.16. The force spectrum for the coated beam is much smoother than the spectra for the bare beam, especially at the high frequencies. This can be attributed to the decoupling of the shakers from each other due to the elastomer and to the feedback from the beam response with the coating. Also, with the coating, the drive impedance is lowered so that the shakers appear more as force sources where the forces are less affected by the impedance of the driven structure. It can also be seen in Figures

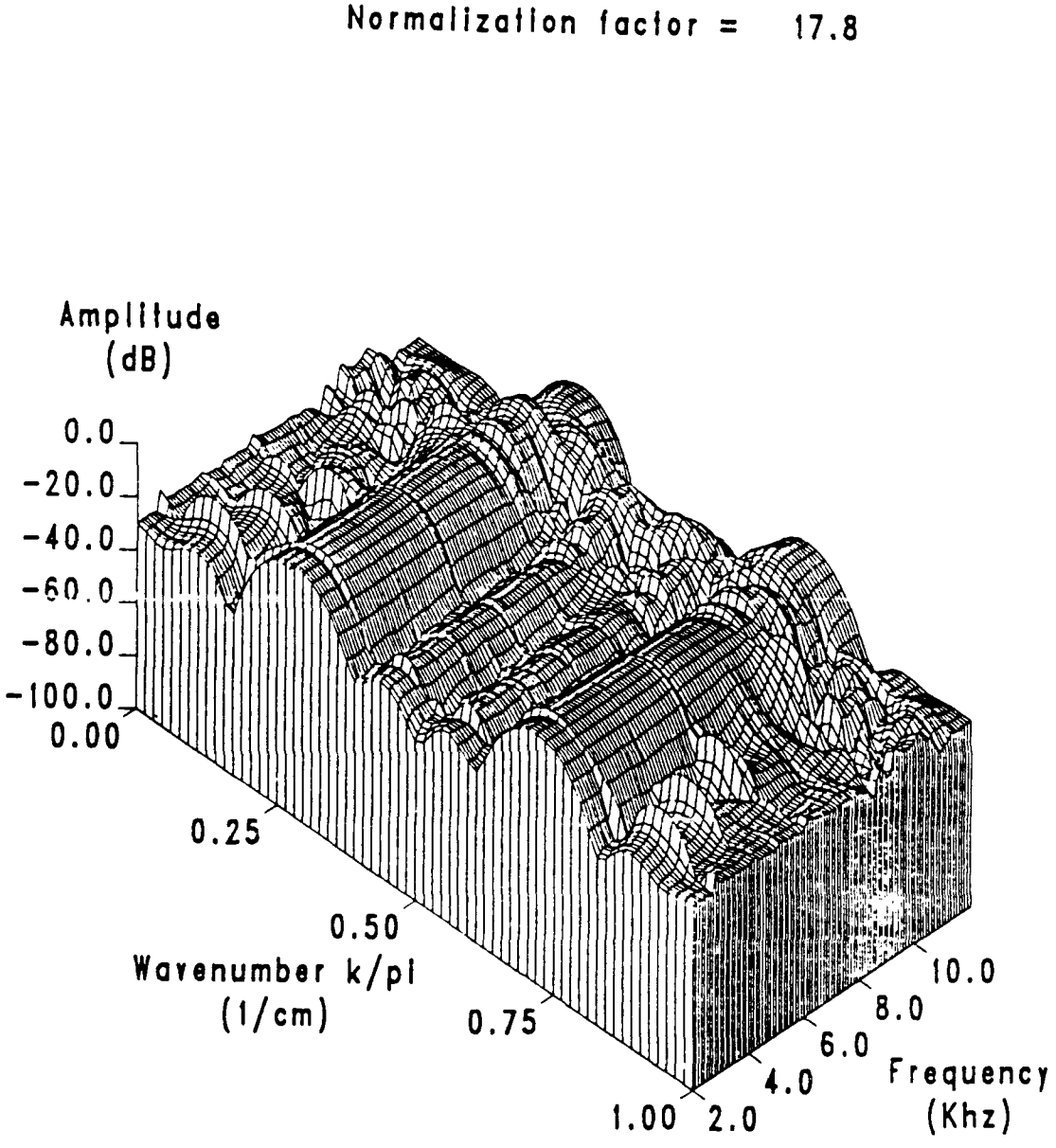

Figure 5.11: Surface plot of the force spectrum for $k_d = 0.28\pi$ cm^{-1}.

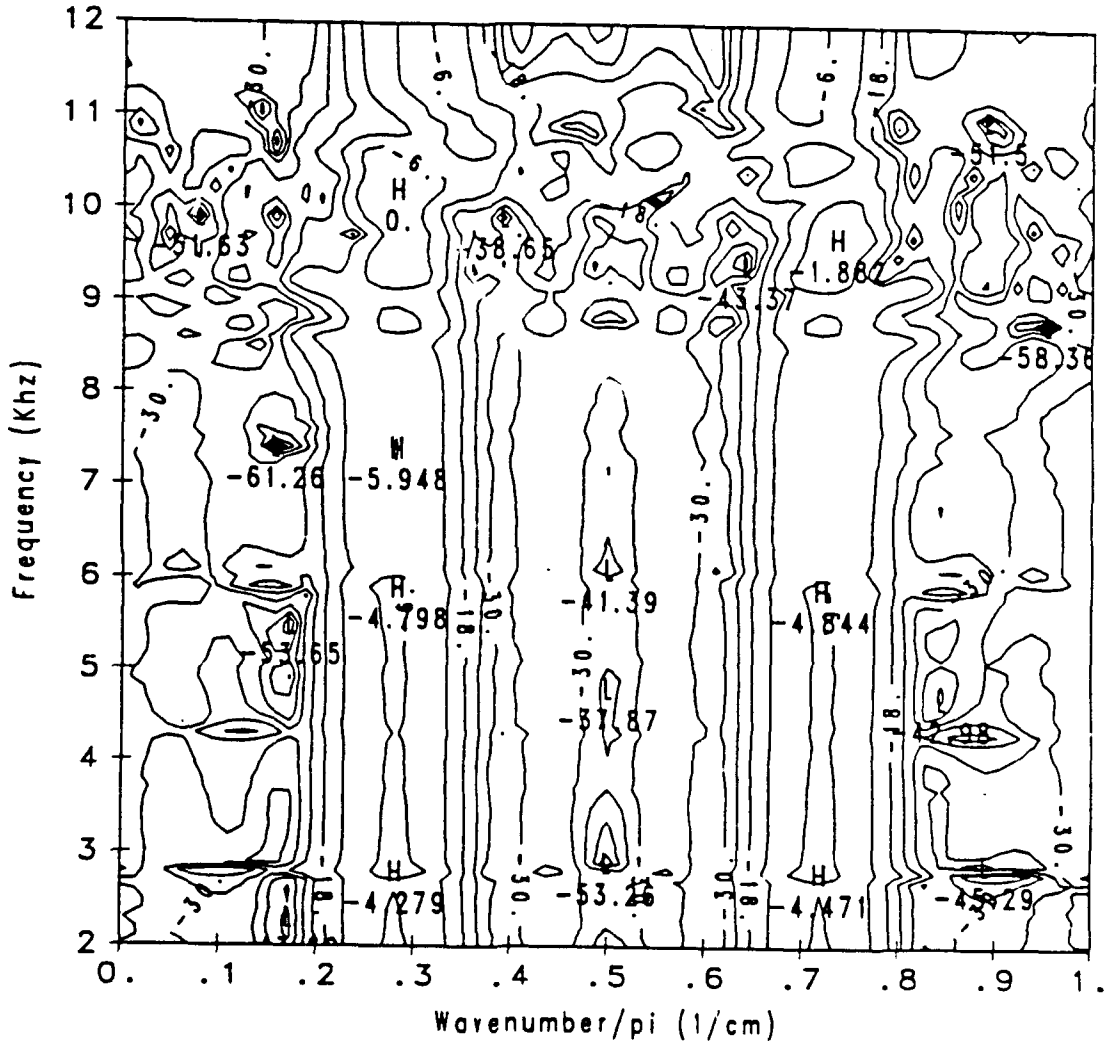

Figure 5.12: Contour plot of the force spectrum for $k_d = 0.28\pi$ cm^{-1}.

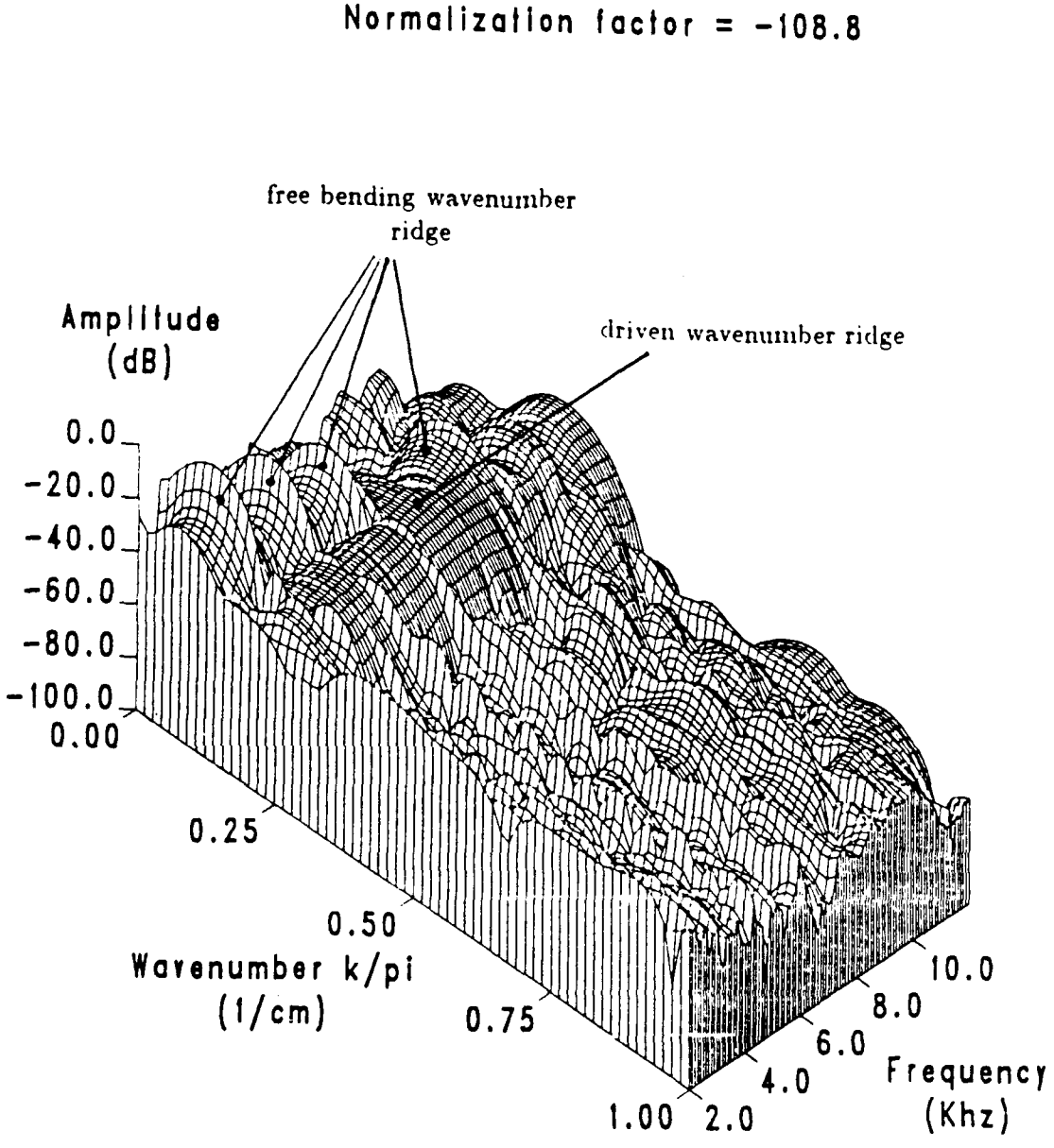

Figure 5.13: Surface plot of the velocity spectrum for $k_d = 0.28\pi$ cm^{-1}.

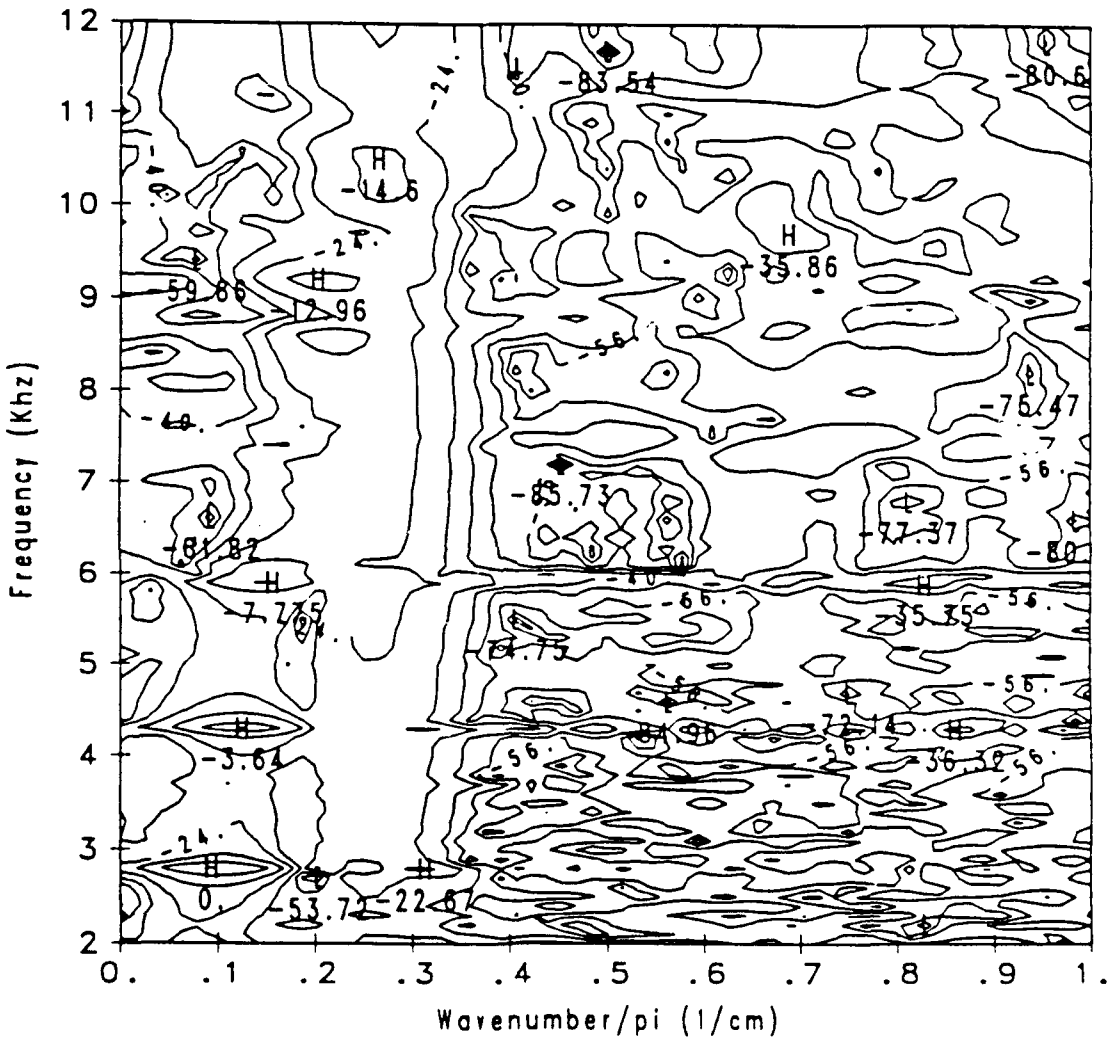

Figure 5.14: Contour plot of the velocity spectrum for $k_d = 0.28\pi$ cm^{-1}.

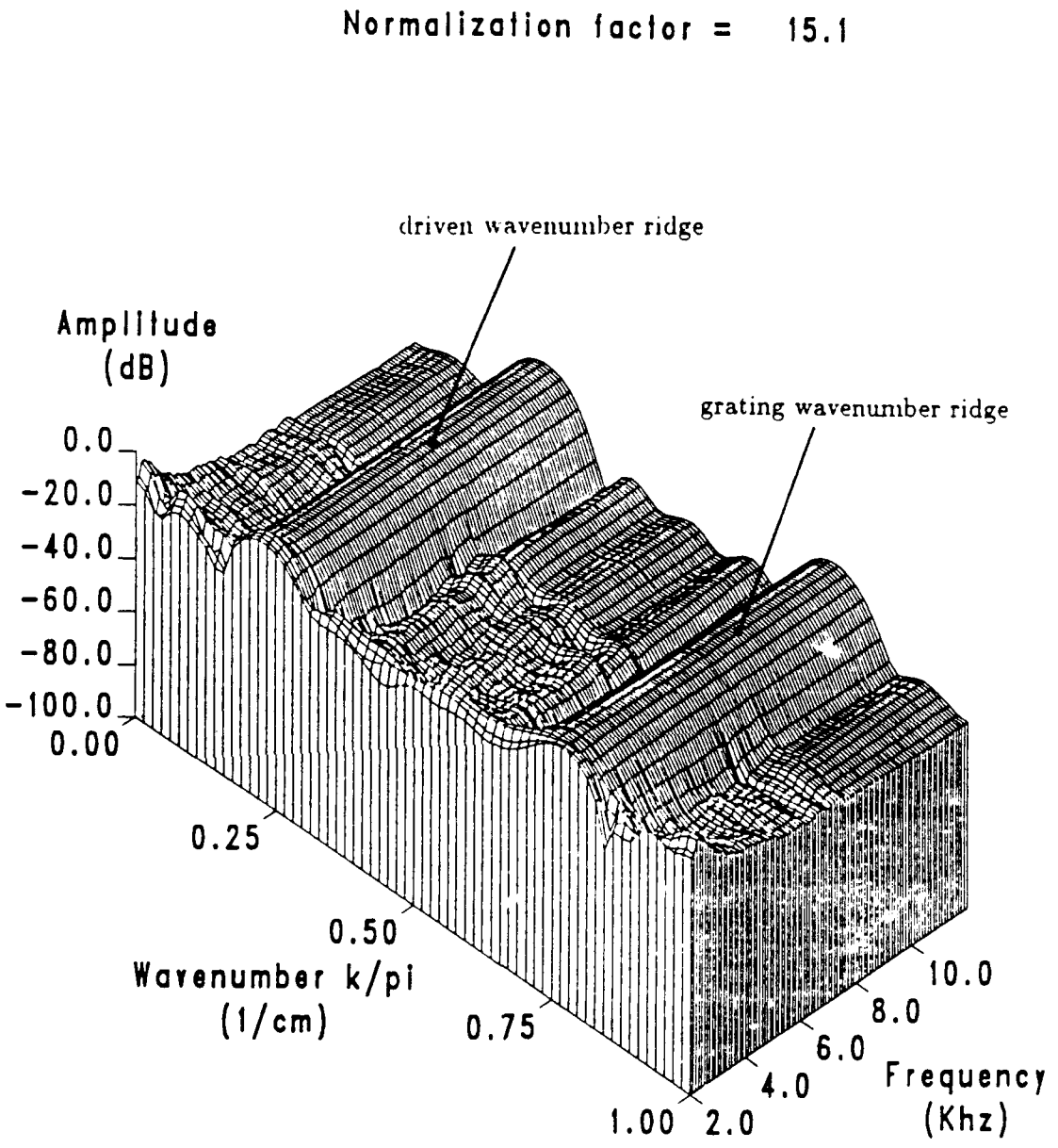

Figure 5.15: Surface plot of the force spectrum for Natural Rubber I with $k_d = \pi/4$ cm^{-1}.

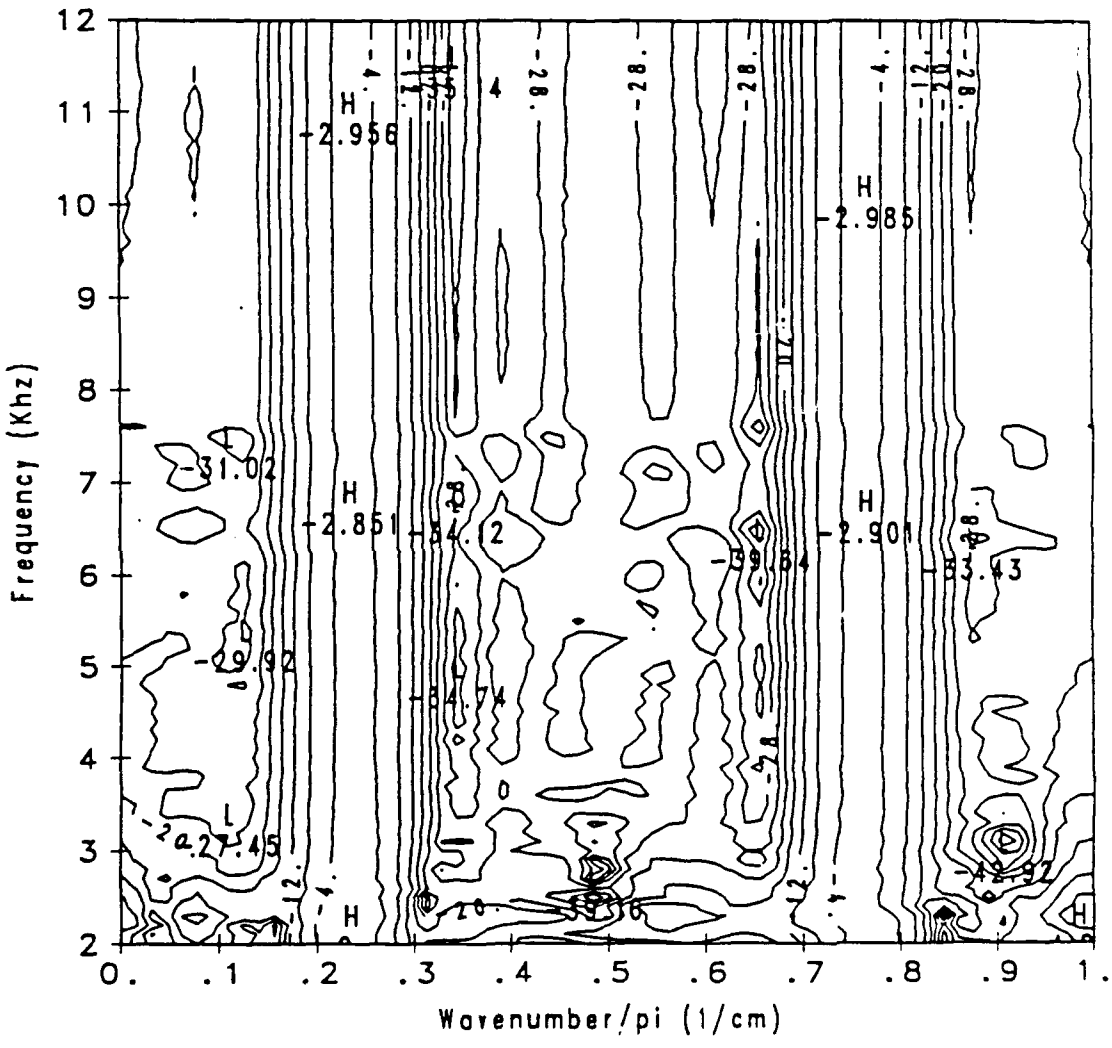

Figure 5.16: Contour plot of the force spectrum for Natural Rubber I with $k_d = \pi/4$ cm^{-1}.

5.15 and 5.16 that the free bending wavenumber ridge of the coated beam had no influence on the input force spectrum.

The wavenumber-frequency spectrum of the velocity response of the beam coated with Natural Rubber I is given in Figures 5.17 and 5.18. Generally, the beam did respond to the driven wavenumber except at the lower frequencies where the driven wavenumber ridge is partially masked by the increased response due to resonance introduced by the insertion of the layer.

The next experiment involved a neoprene layer with a hardness of 60 durometer, referred to as "Neoprene I" to distinguish it from a second neoprene sample. The drive wavenumber was $\pi/4$ cm^{-1} as before. The wavenumber-frequency force spectrum of this experiment can be seen in Figure 5.19. As was the case with Natural Rubber I, this spectrum is smooth and the free bending wavenumber ridge had little or no effect on this measurement. The velocity spectrum of this experiment is shown in Figure 5.20. Here, the same characteristics of the velocity spectrum for Natural Rubber I are evident. The driven wavenumber ridge is partially masked by low frequency resonances.

In the next experiment, the admittance of the beam coated with a layer of polyurethane with a hardness of 90 durometer was measured at a drive wavenumber of $\pi/4$ cm^{-1}. The force spectrum obtained on this layer is shown in Figures 5.21 and 5.22. The force spectrum contains a "new" feature which is a ridge at approximately 3.8 kHz for all wavenumbers. This ridge is a system resonance of the shaker/layer/beam combination similar to the mass-spring resonance observed for the sample section in Figure 2.2. This resonance occurred for the other experiments

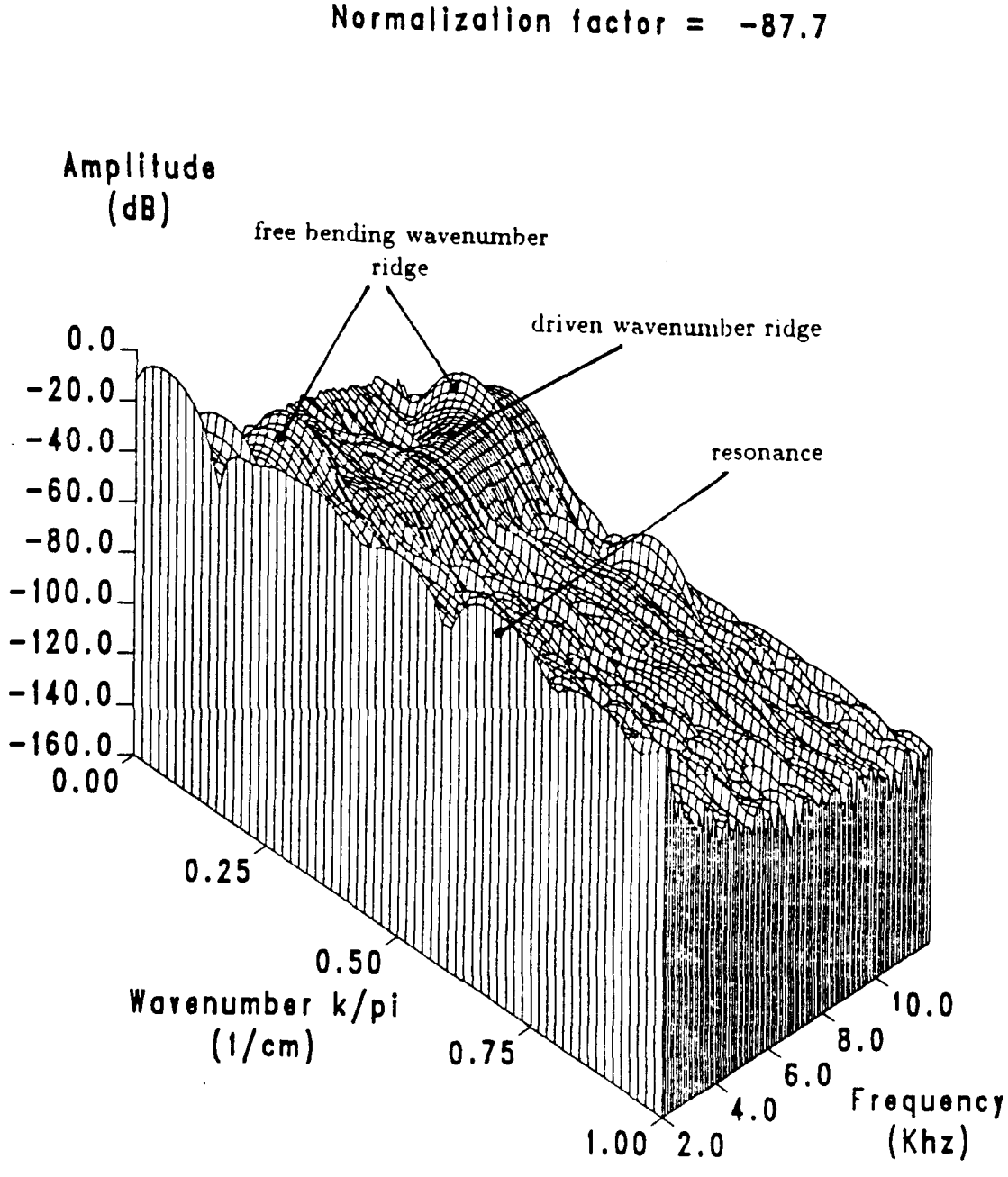

Figure 5.17: Surface plot of the velocity spectrum for Natural Rubber I with $k_d = \pi/4$ cm^{-1}.

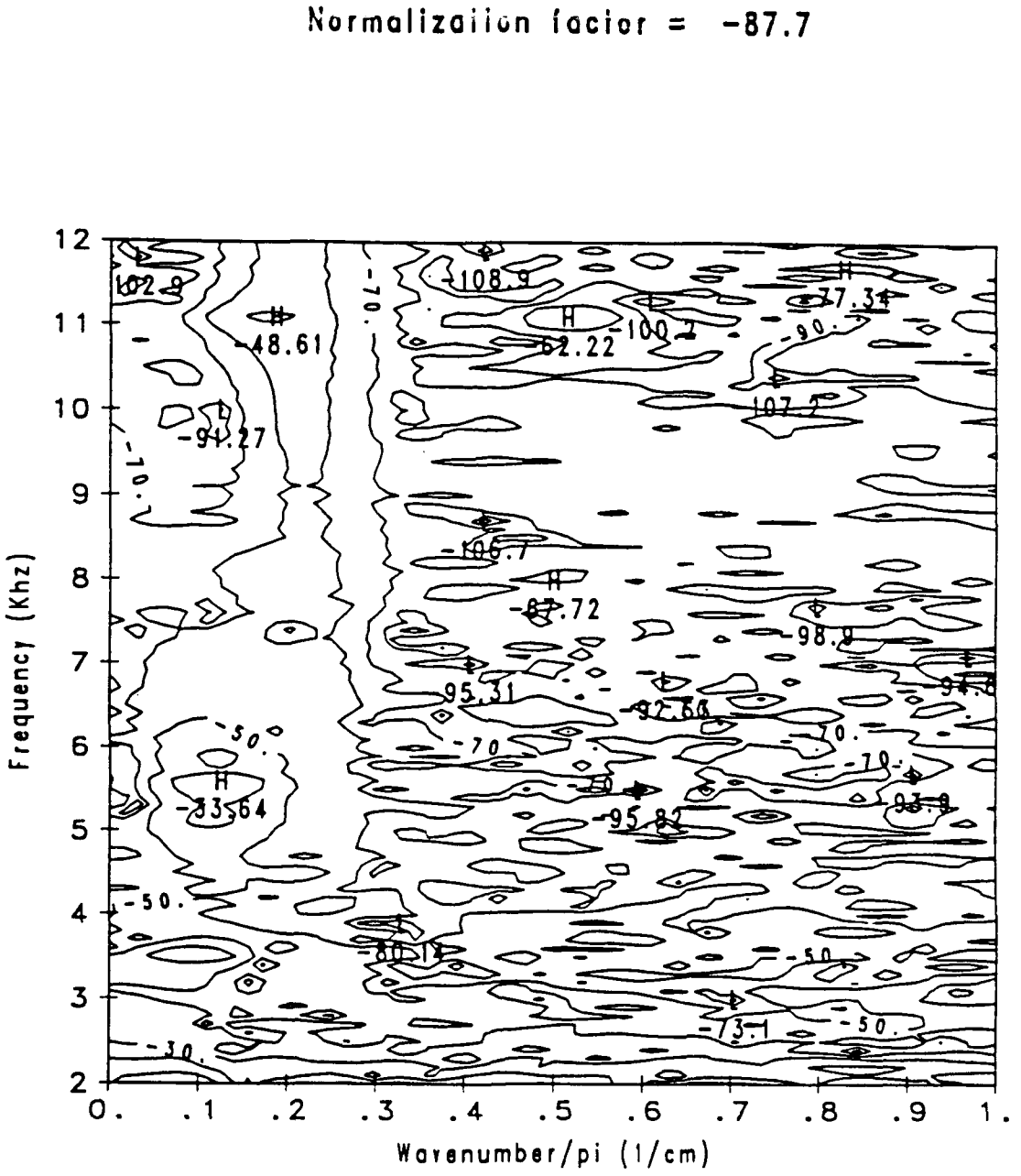

Figure 5.18: Contour plot of the velocity spectrum for Natural Rubber I with $k_d = \pi/4$ cm^{-1}.

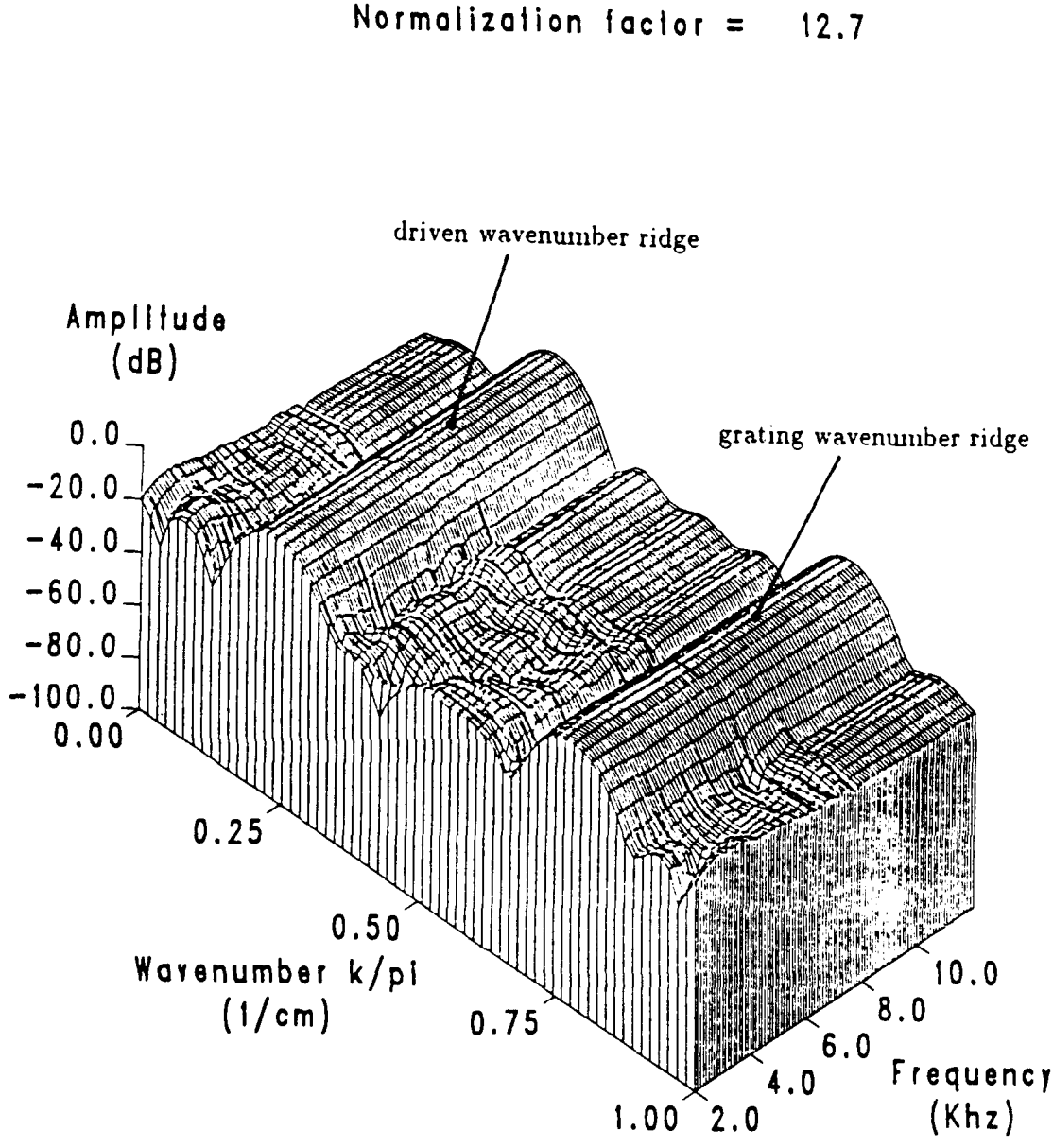

Figure 5.19: Surface plot of force spectrum for Neoprene I with $k_d = \pi/4$ cm^{-1}.

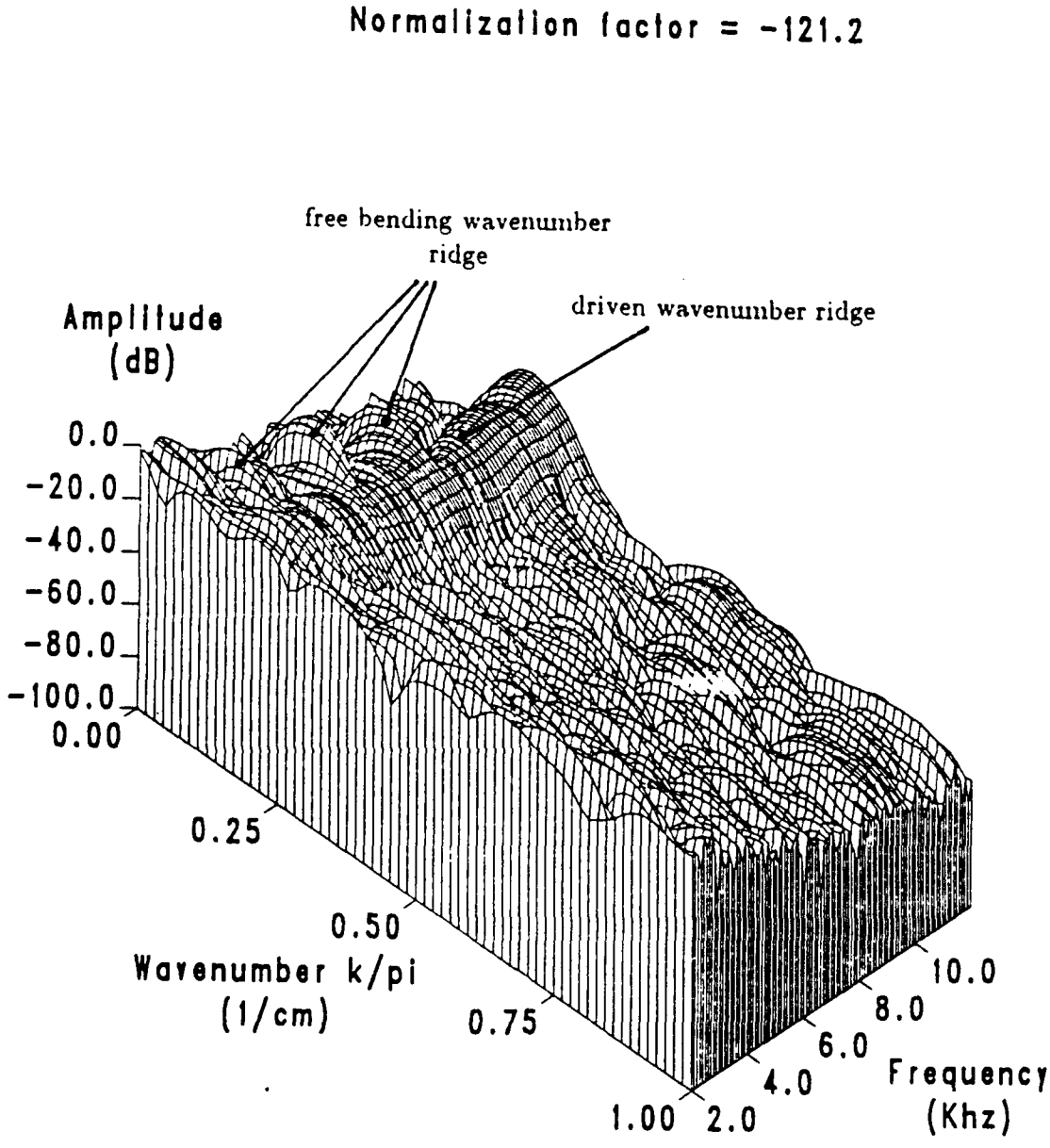

Figure 5.20: Surface plot of the velocity spectrum for Neoprene I with $k_d = \pi/4$ cm^{-1}.

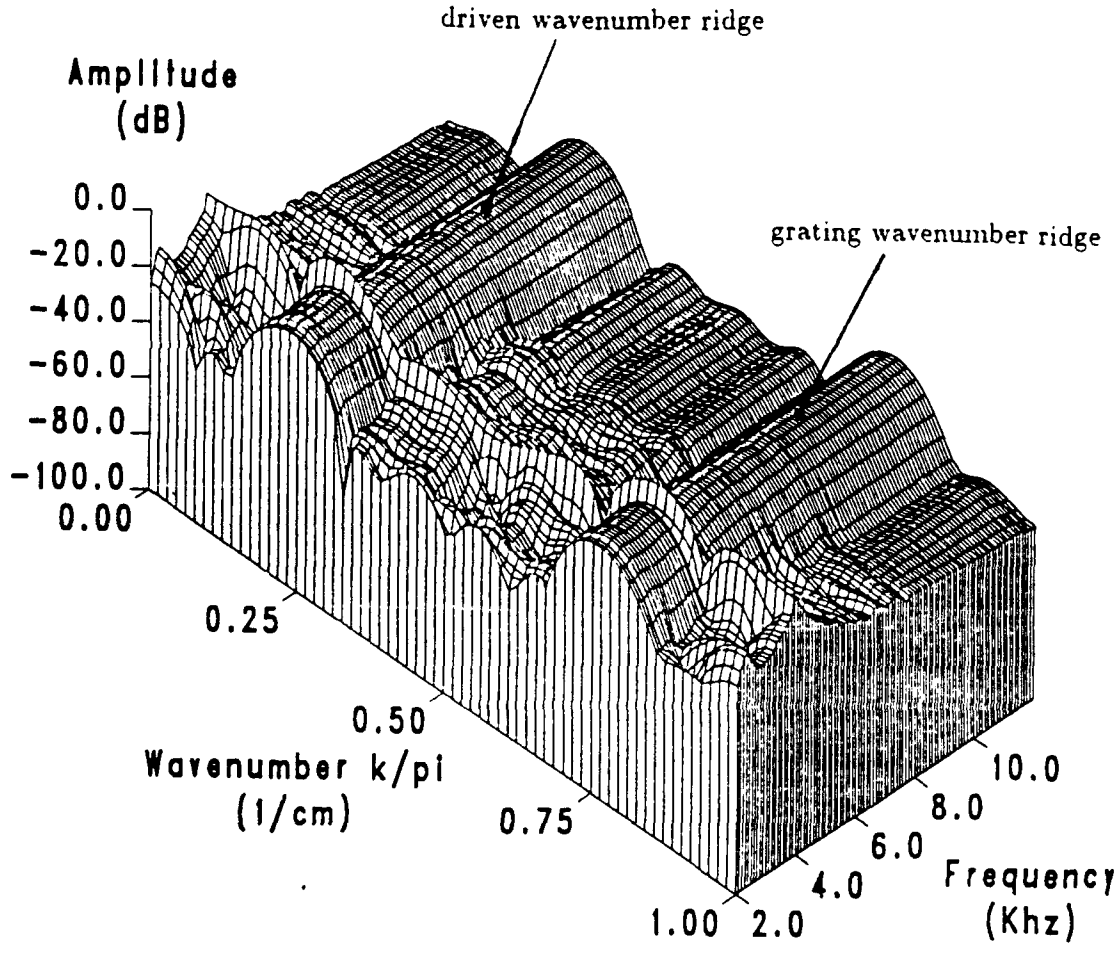

Figure 5.21: Surface plot of force spectrum for polyurethane with $k_d = \pi/4$ cm^{-1}.

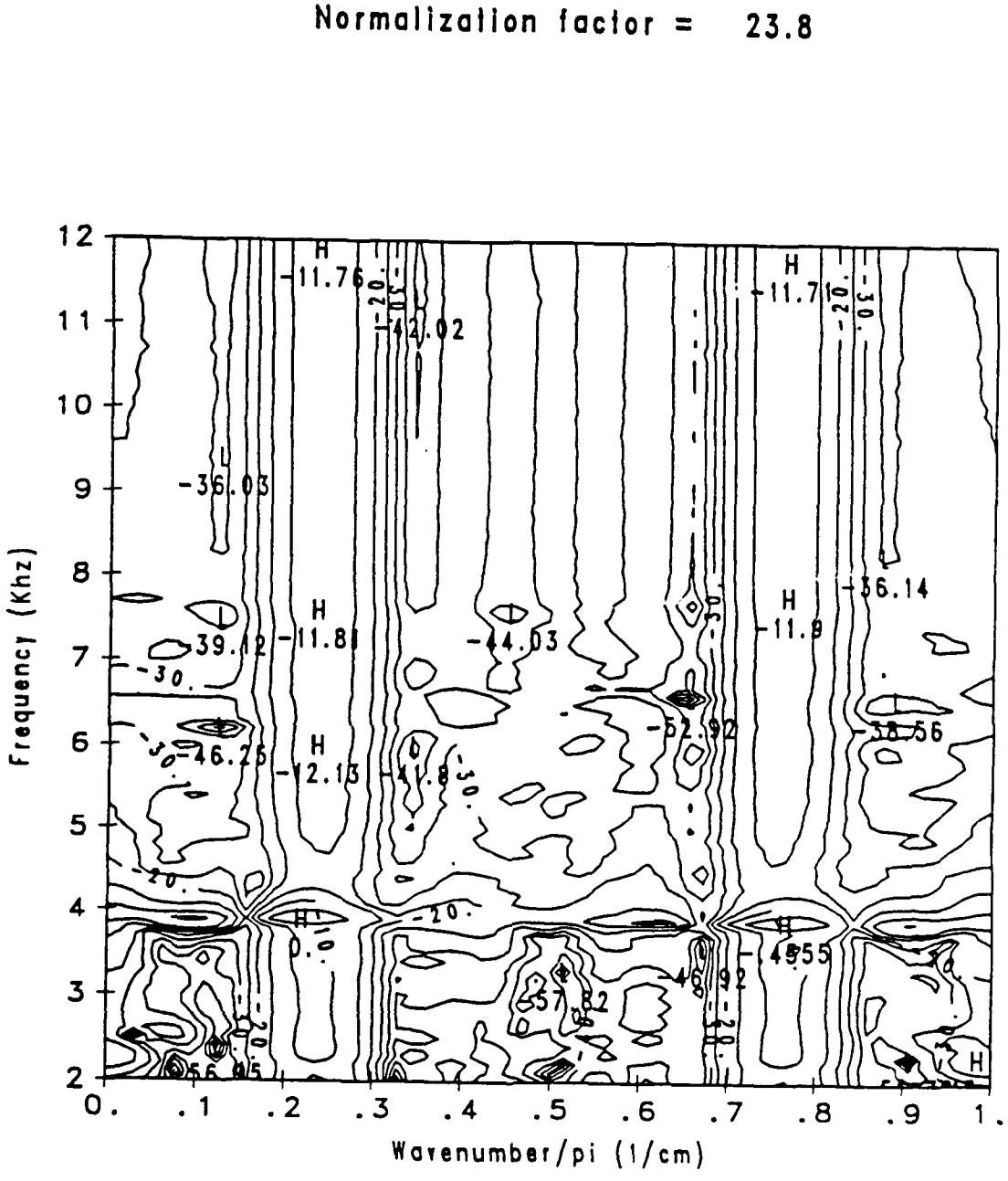

Figure 5.22: Contour plot of force spectrum for polyurethane with $k_d = \pi/4$ cm^{-1}.

as well, yet at lower frequencies, near the lower frequency limit of the measurement range. The resonance frequency of the polyurethane is at a higher frequency than that of either natural rubber or neoprene because polyurethane is stiffer than the other materials.

The velocity spectrum of the polyurethane layer driven at $\pi/4$ cm^{-1} can be seen in Figures 5.23 and 5.24. These figures show a better response at the driven wavenumber than with the neoprene due to the stiffer nature of the polyurethane. The free bending wavenumber ridge and the resonance at 3.8 kHz can be seen in Figures 5.23 and 5.24. An additional resonance can be seen at approximately 8.2 kHz which is probably dependent upon the lower resonance.

The next experiment was conducted using a natural rubber layer with a hardness of 37 durometer referred to as "Natural Rubber II." Again, the drive wavenumber was $\pi/4$ cm^{-1}. The force and velocity spectra can be seen in Figures 5.25–5.27. The force spectrum has a smooth surface with little or no influence from the free bending wavenumber similar to the surfaces for the force spectra of Natural Rubber I and Neoprene I. The velocity spectrum shows little response at the drive wavenumber until high frequencies. Again, this is partially due to masking of the response by resonances. The free bending wavenumber ridge is very dominant in this measurement.

Next, a layer of neoprene with a hardness of 55 durometer, referred to as "Neoprene II," was examined at the drive wavenumber of $\pi/4$ cm^{-1}. The plots of the force and velocity spectra can be seen in Figures 5.28 and 5.29. The features of these plots resemble those of Neoprene I.

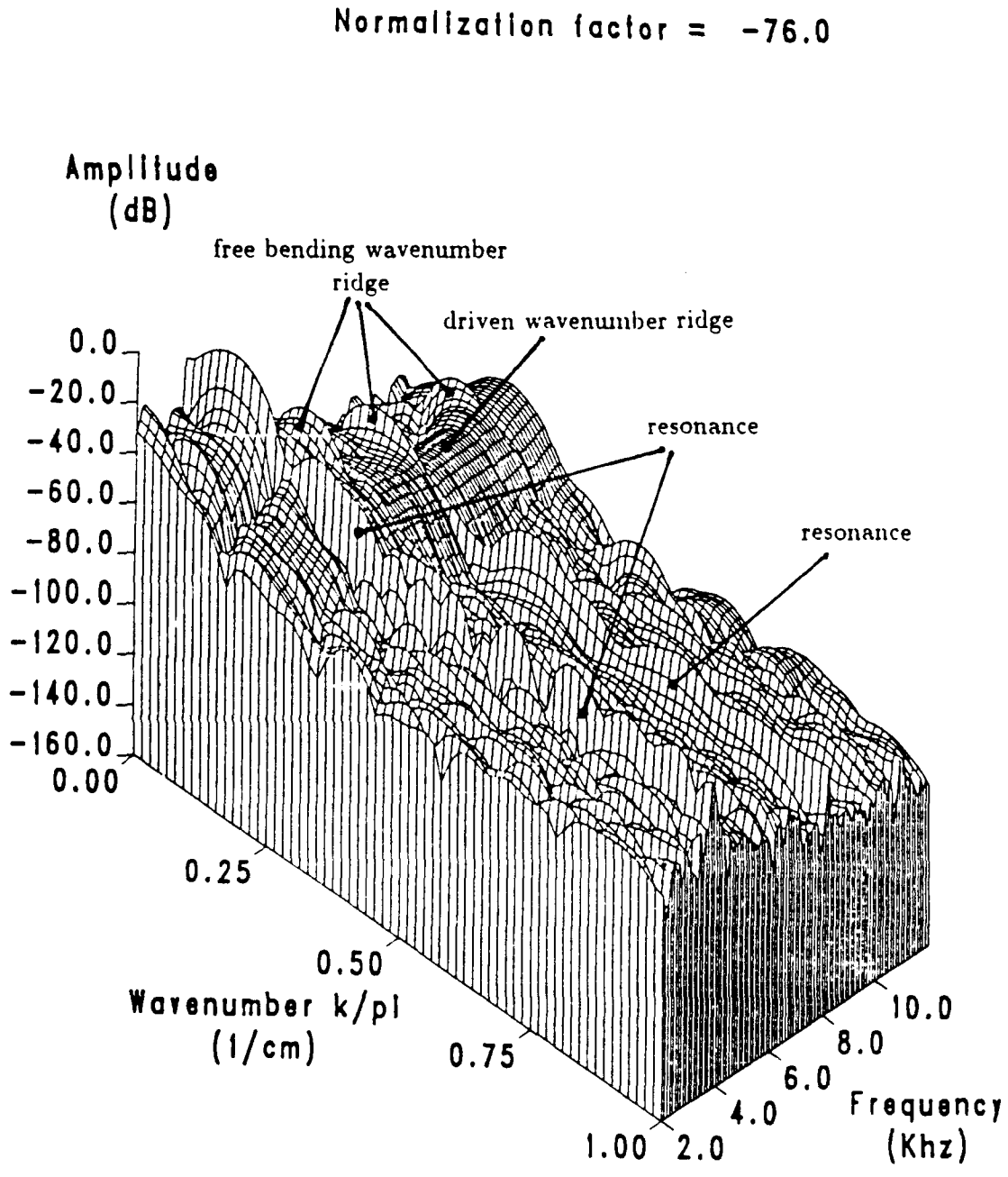

Figure 5.23: Surface plot of the velocity spectrum for polyurethane with $k_d = \pi/4$ cm^{-1}.

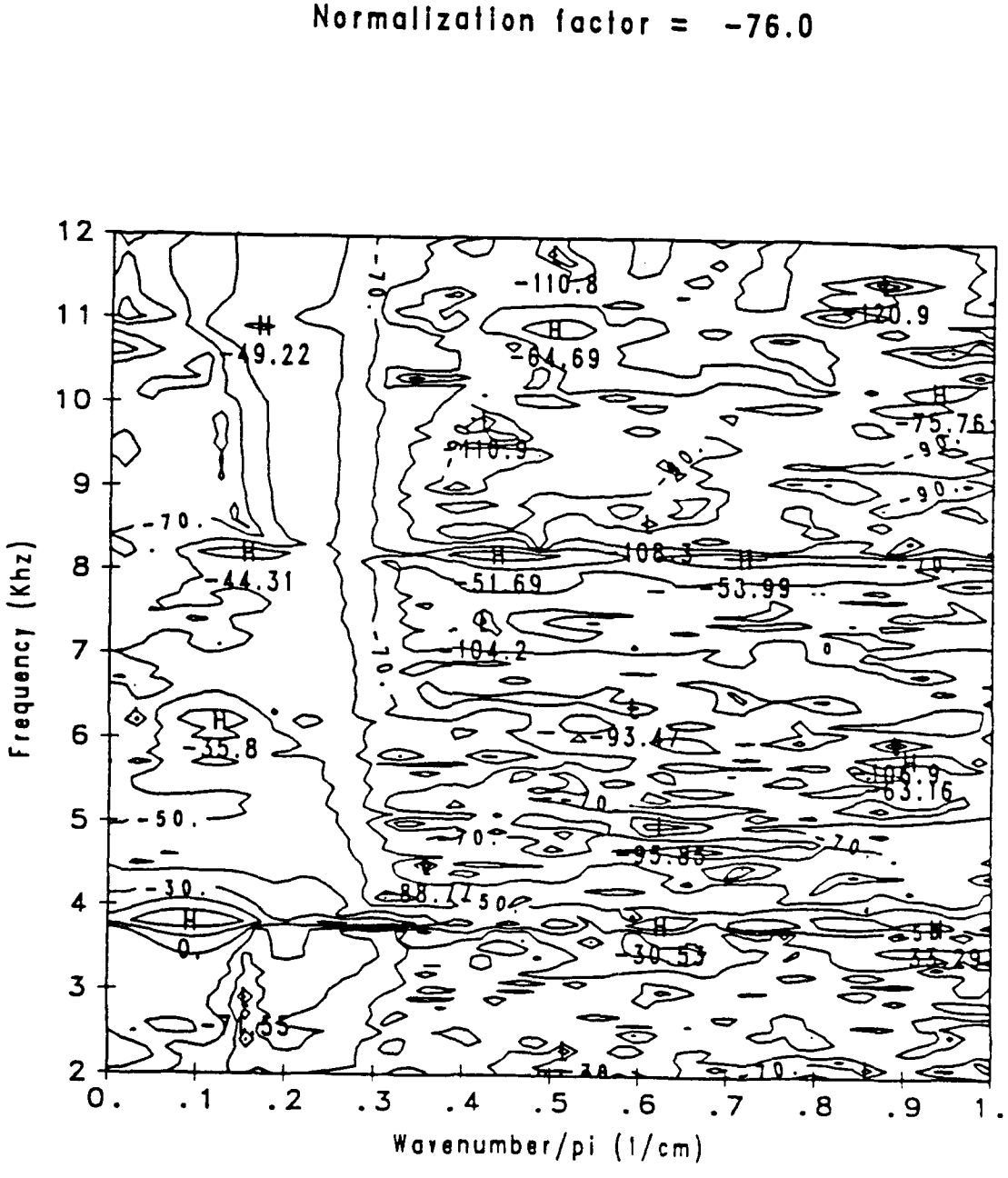

Figure 5.24: Contour plot of the velocity spectrum for polyurethane with $k_d = \pi/4$ cm^{-1}.

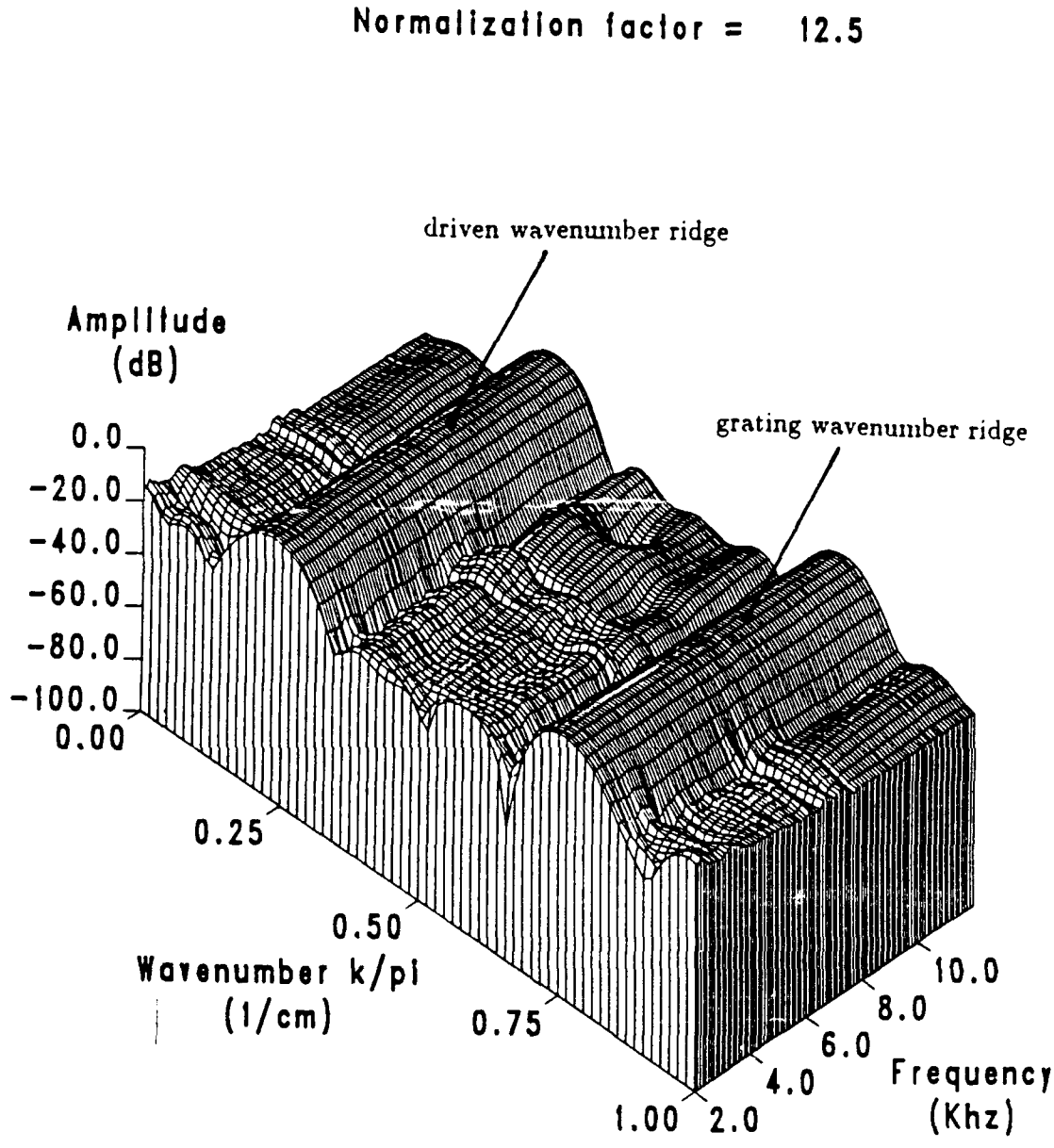

Figure 5.25: Surface plot of the force spectrum for Natural Rubber II with $k_d = \pi/4$ cm^{-1}.

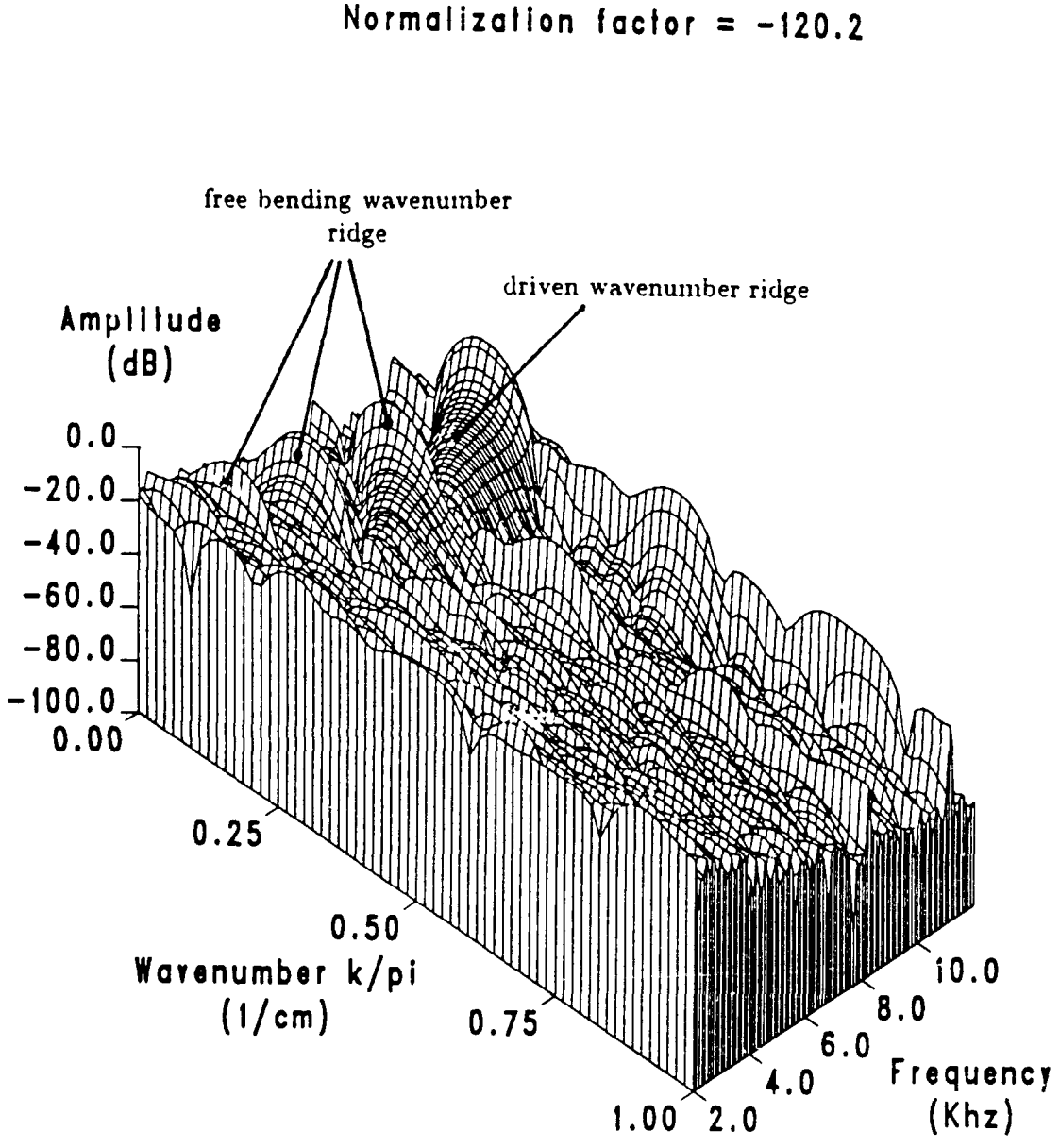

Figure 5.26: Surface plot of the velocity spectrum for Natural Rubber II with $k_d = \pi/4$ cm^{-1}.

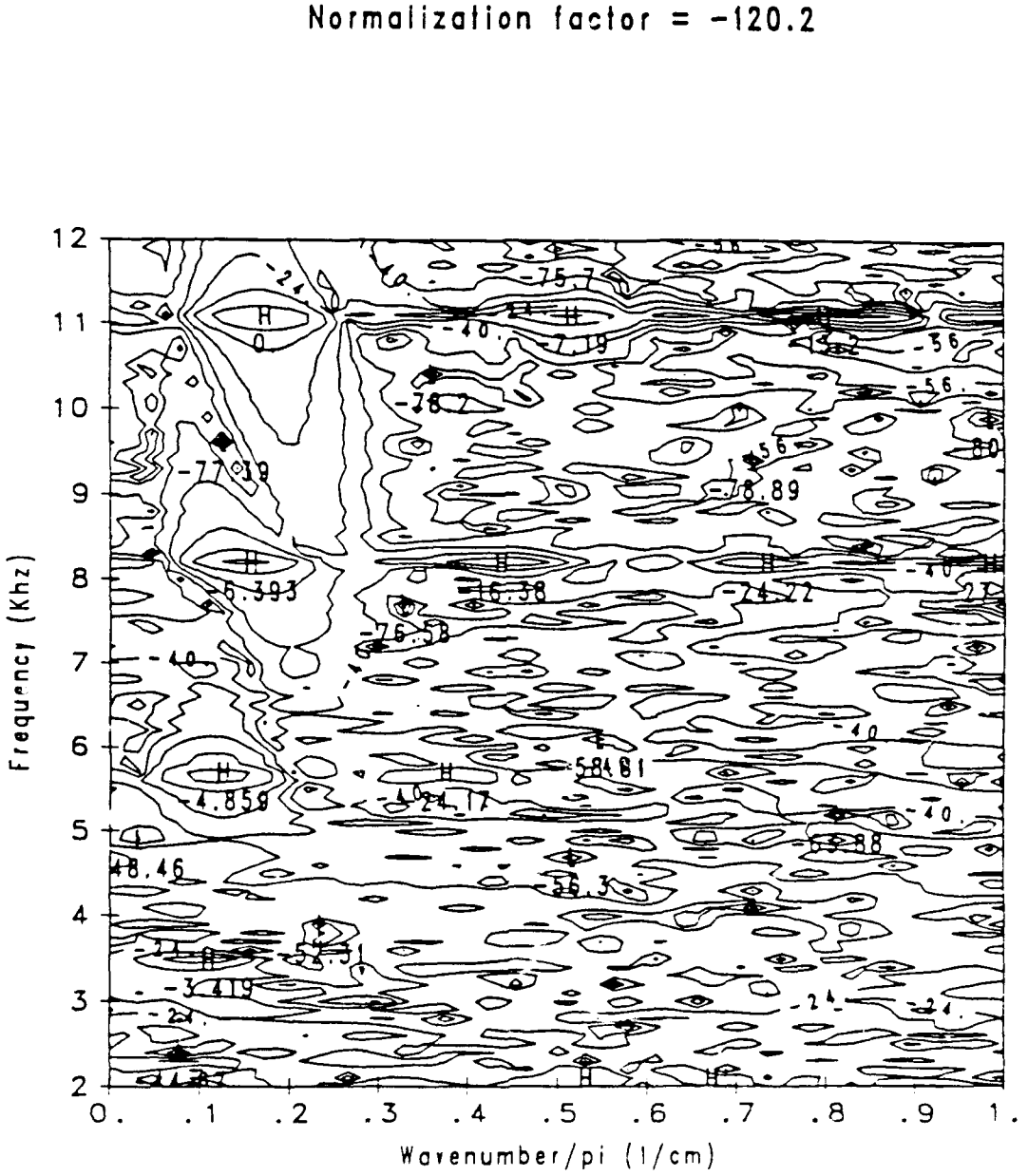

Figure 5.27: Contour plot of the velocity spectrum for Natural Rubber II with $k_d = \pi/4$ cm^{-1}.

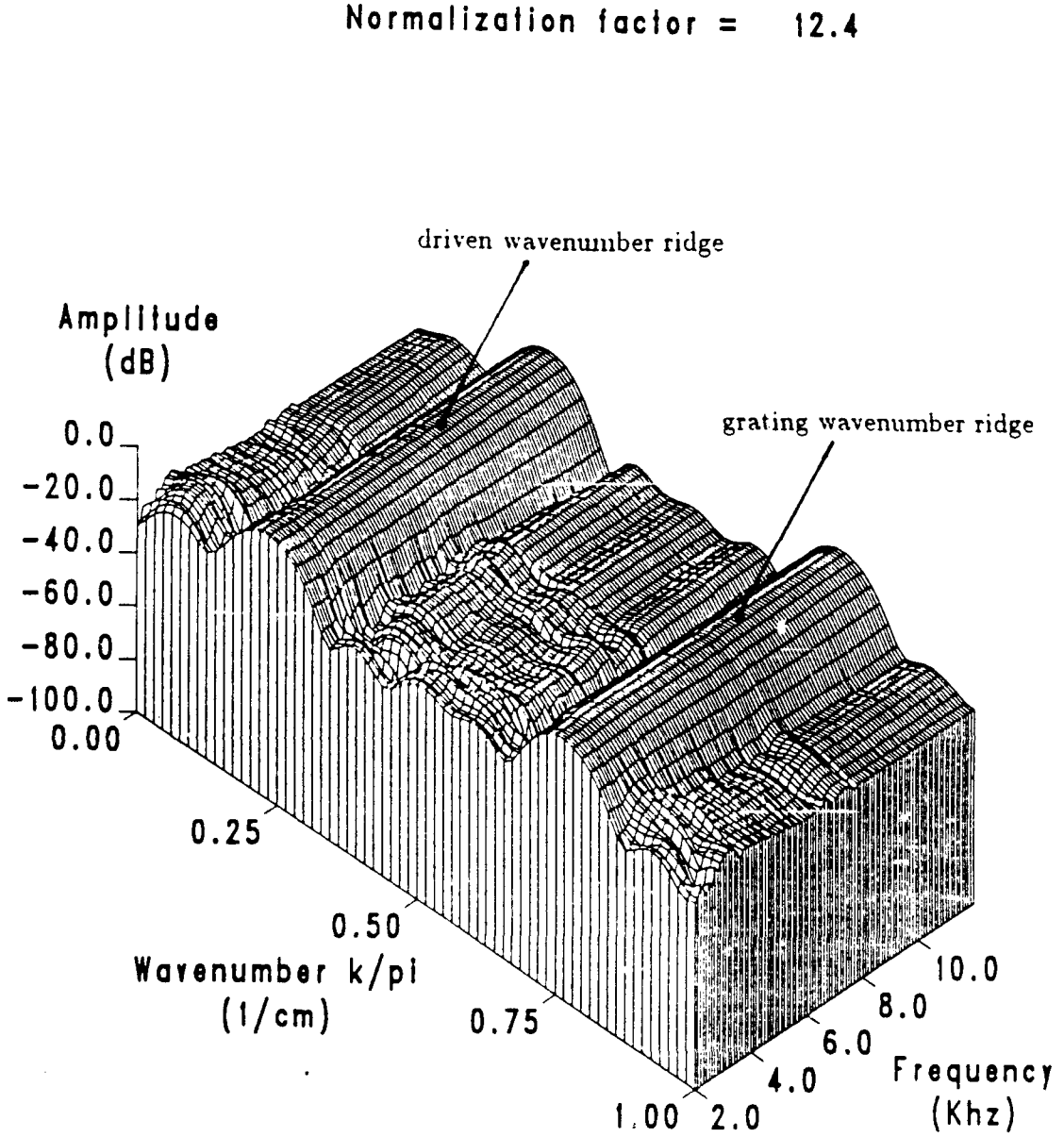

Figure 5.28: Surface plot of force spectrum for Neoprene II with $k_d = \pi/4$ cm^{-1}.

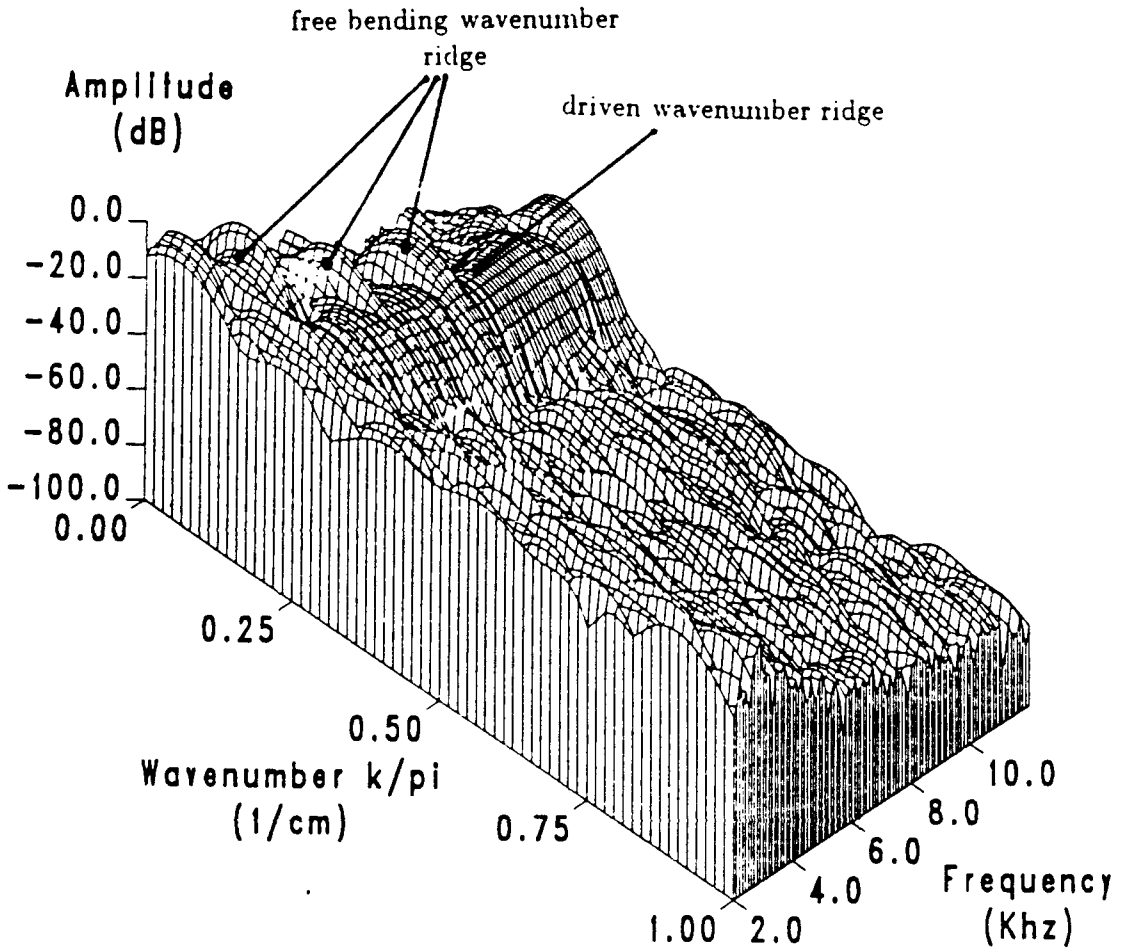

Figure 5.29: Surface plot of the velocity spectrum for Neoprene II with $k_d = \pi/4$ cm^{-1}.

Finally, the polyurethane layer was driven and measured at the wavenumbers 0, 0.28π, $\pi/3$, and $\pi/2$ cm^{-1}. The force and velocity spectra of these measurements can be seen in Figures 5.30–5.40. These spectra commonly exhibit characteristics found in the spectra of the same layer driven at $\pi/4$ cm^{-1}, particularly the system resonance at 3.8 kHz. Looking at the contour plots of the velocity spectra at $k_d = 0.28\pi$ cm^{-1} and $k_d = \pi/3$ cm^{-1} shown in Figures 5.34 and 5.37, the response of the beam at the driven wavenumber can be seen. Looking at the contour plot of the velocity spectrum at $k_d = \pi/2$ cm^{-1} in Figure 5.40, the velocity response at the driven wavenumber is very low and is partially masked by resonances of the coated beam.

5.3 Measured transfer admittances

The effectiveness of a layer in reducing the velocity response of the beam can be determined by comparing the transfer admittance of the coated beam to the transfer admittance of the bare beam. Taking the ratio of the coated beam transfer admittance to the bare beam transfer admittance will provide the ratio of the velocity of the coated beam to the velocity of the bare beam for the same input force spectrum. Figure 5.41 compares the forces on the polyurethane coated beam and the bare beam over frequency at the driven wavenumber $\pi/4$ cm^{-1}. It can be seen from the figure that the forces on both beams were at the same level.

Figure 5.42 compares the velocities of the polyurethane coated and uncoated beam. The resonance that masked the driven wavenumber ridge at lower frequencies for the coated beam can be seen in this figure. The large peak at ap-

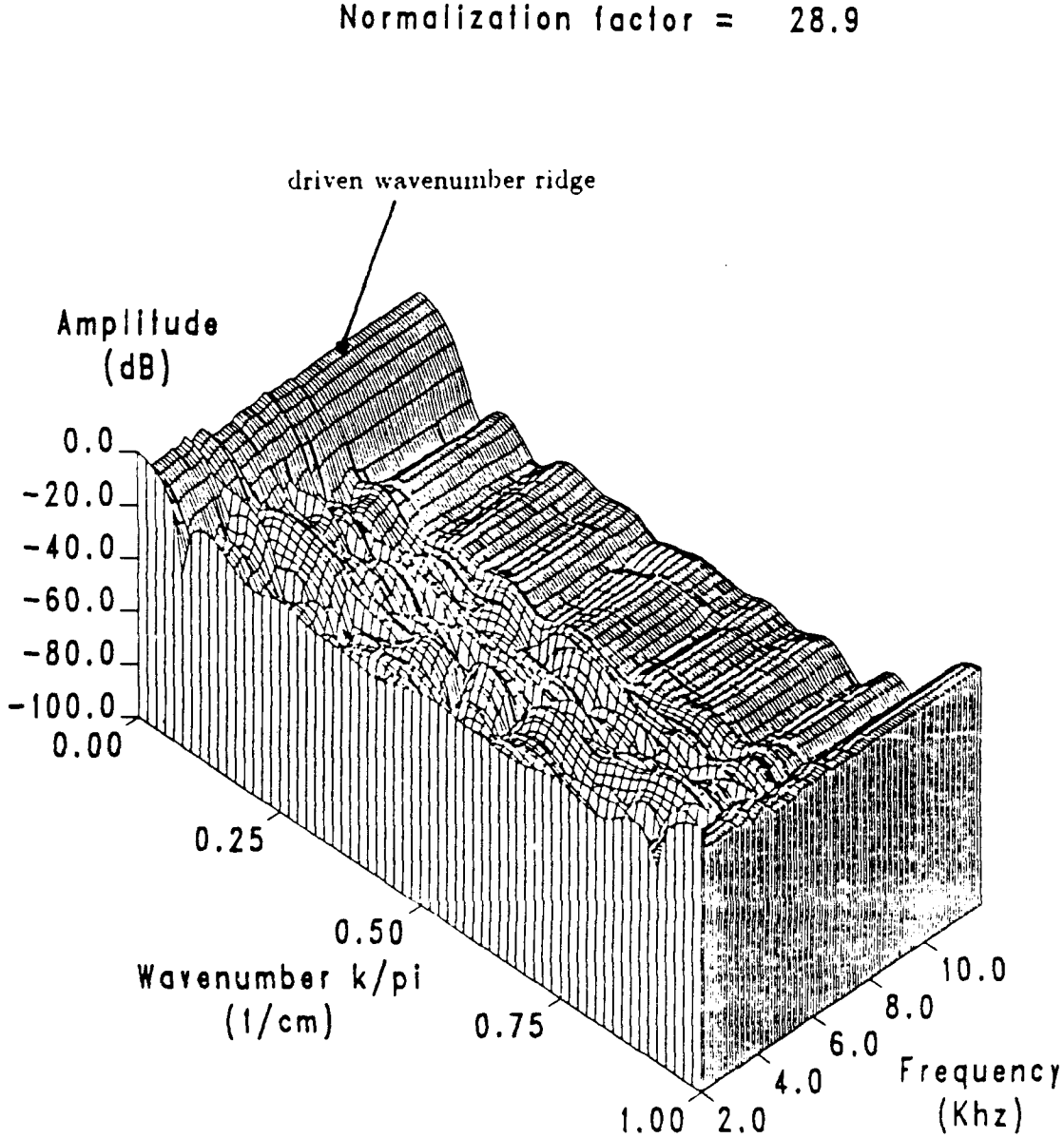

Figure 5.30: Surface plot of the force spectrum for polyurethane with $k_d = 0$.

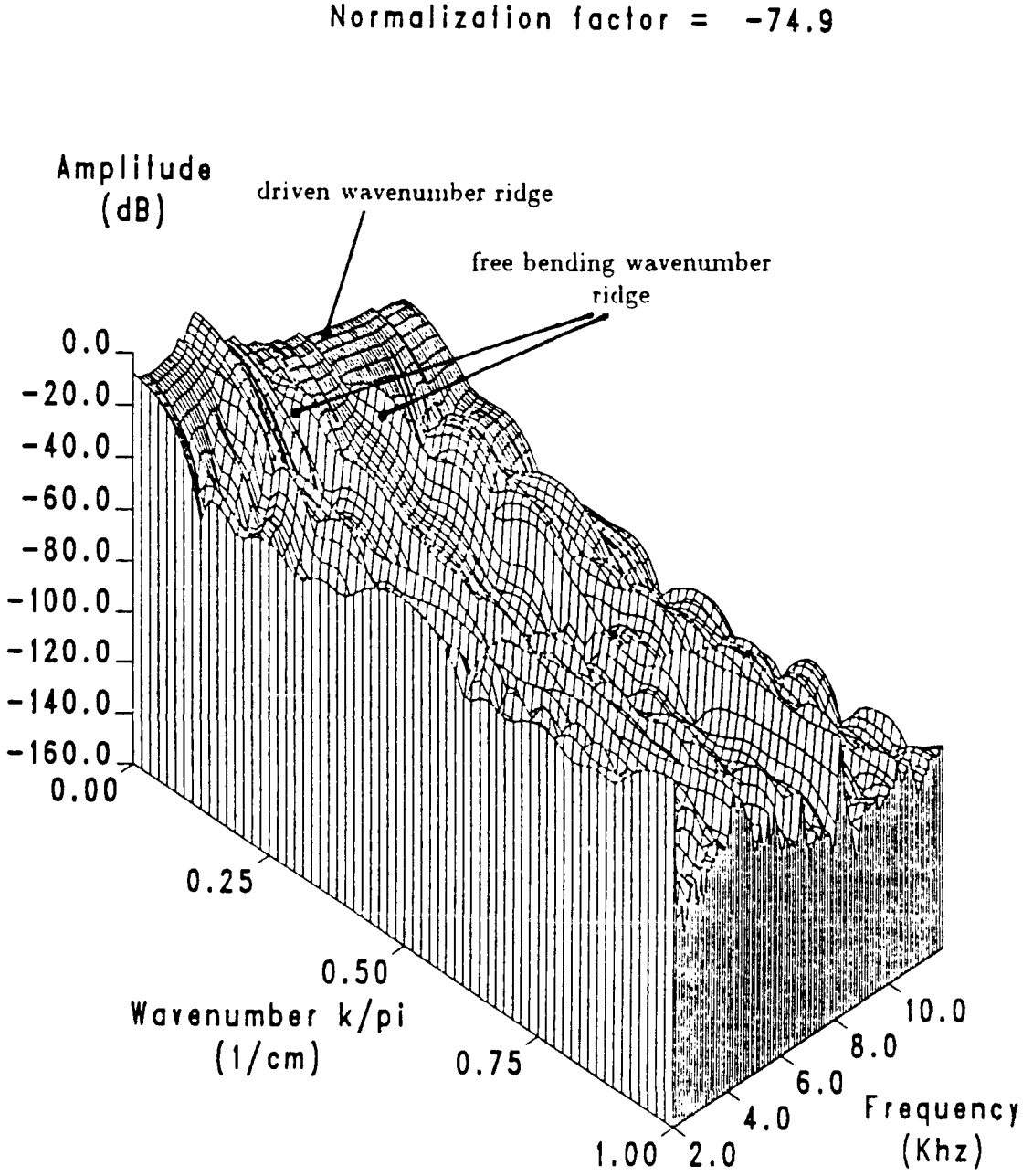

Figure 5.31: Surface plot of the velocity spectrum for polyurethane with $k_d = 0$.

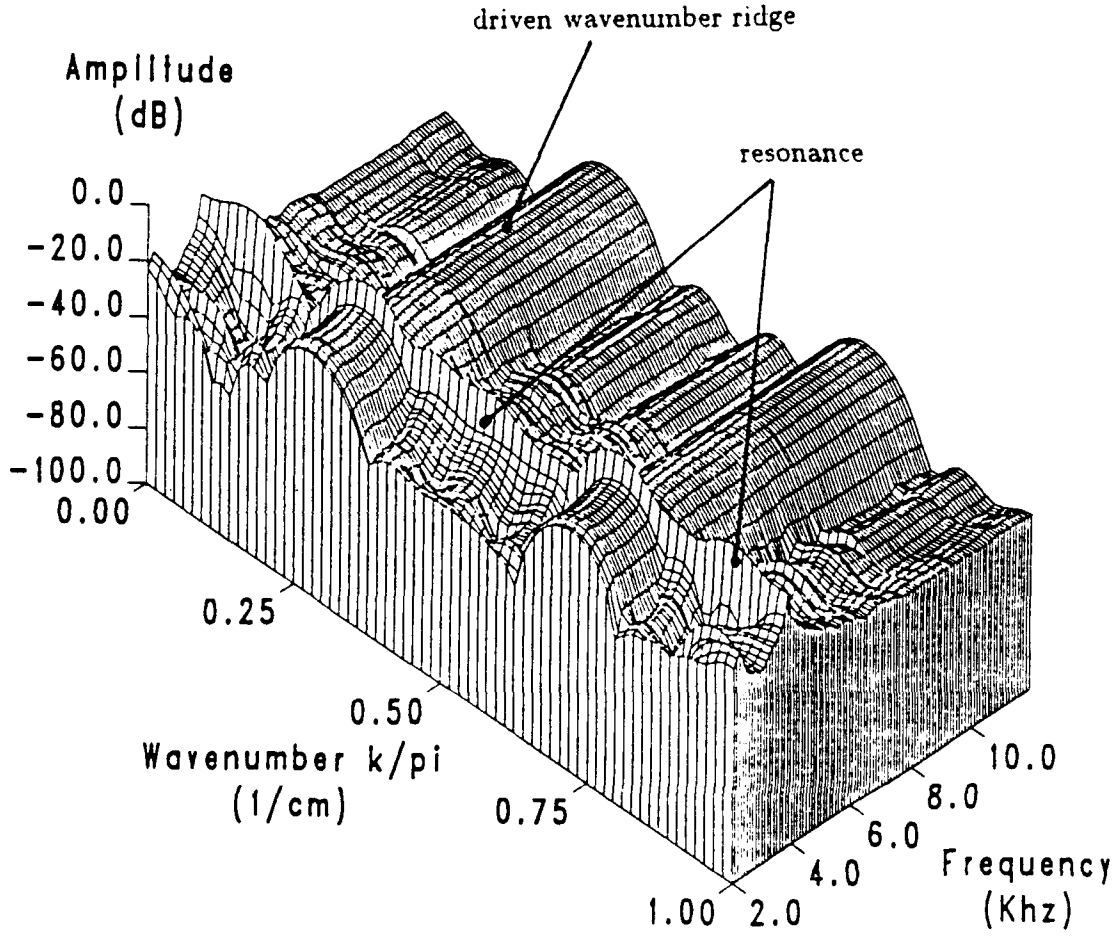

Figure 5.32: Surface plot of force spectrum for polyurethane with $k_d = 0.28\pi$ cm^{-1}.

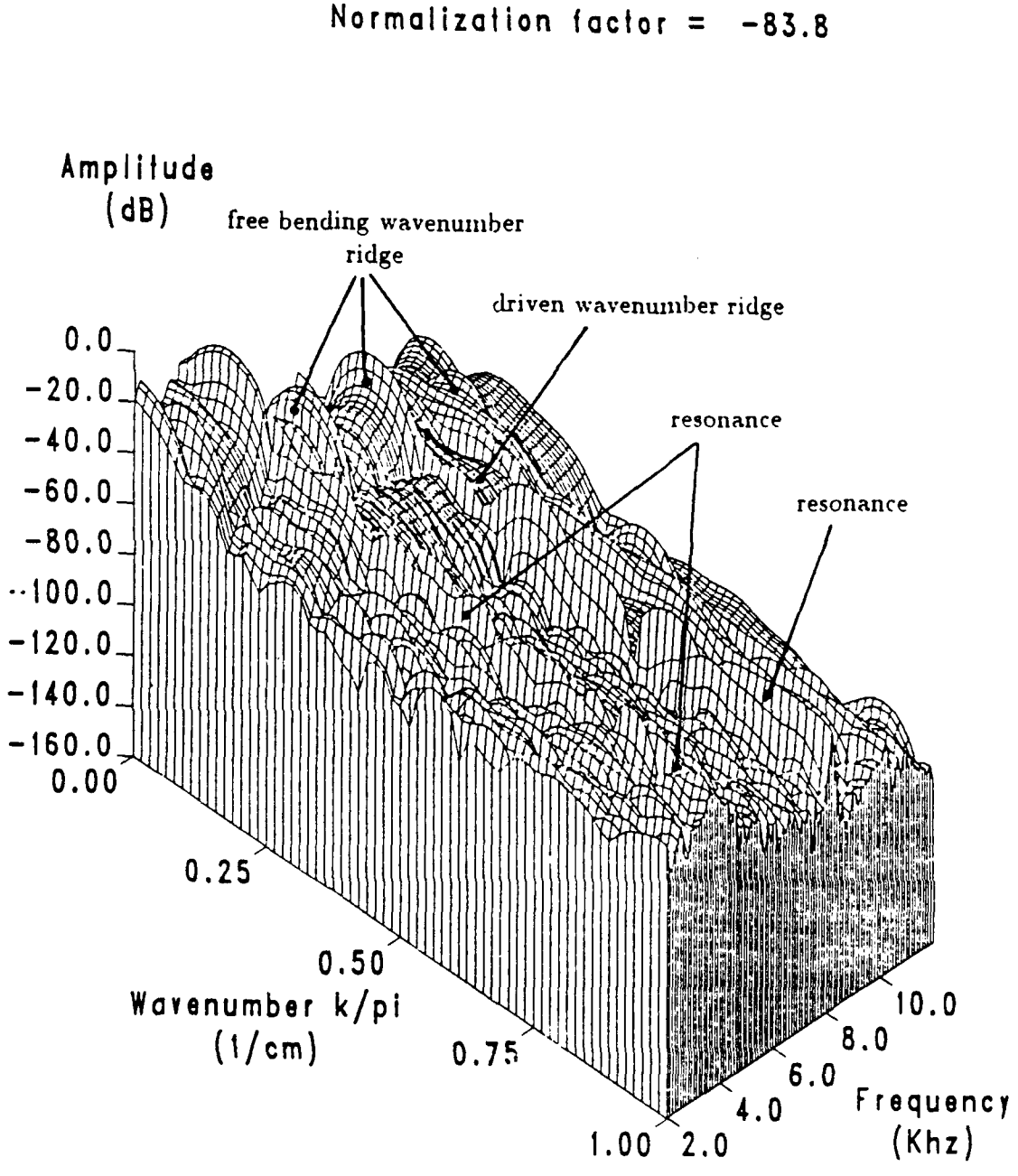

Figure 5.33: Surface plot of the velocity spectrum for polyurethane with $k_d = 0.28\pi$ cm^{-1}.

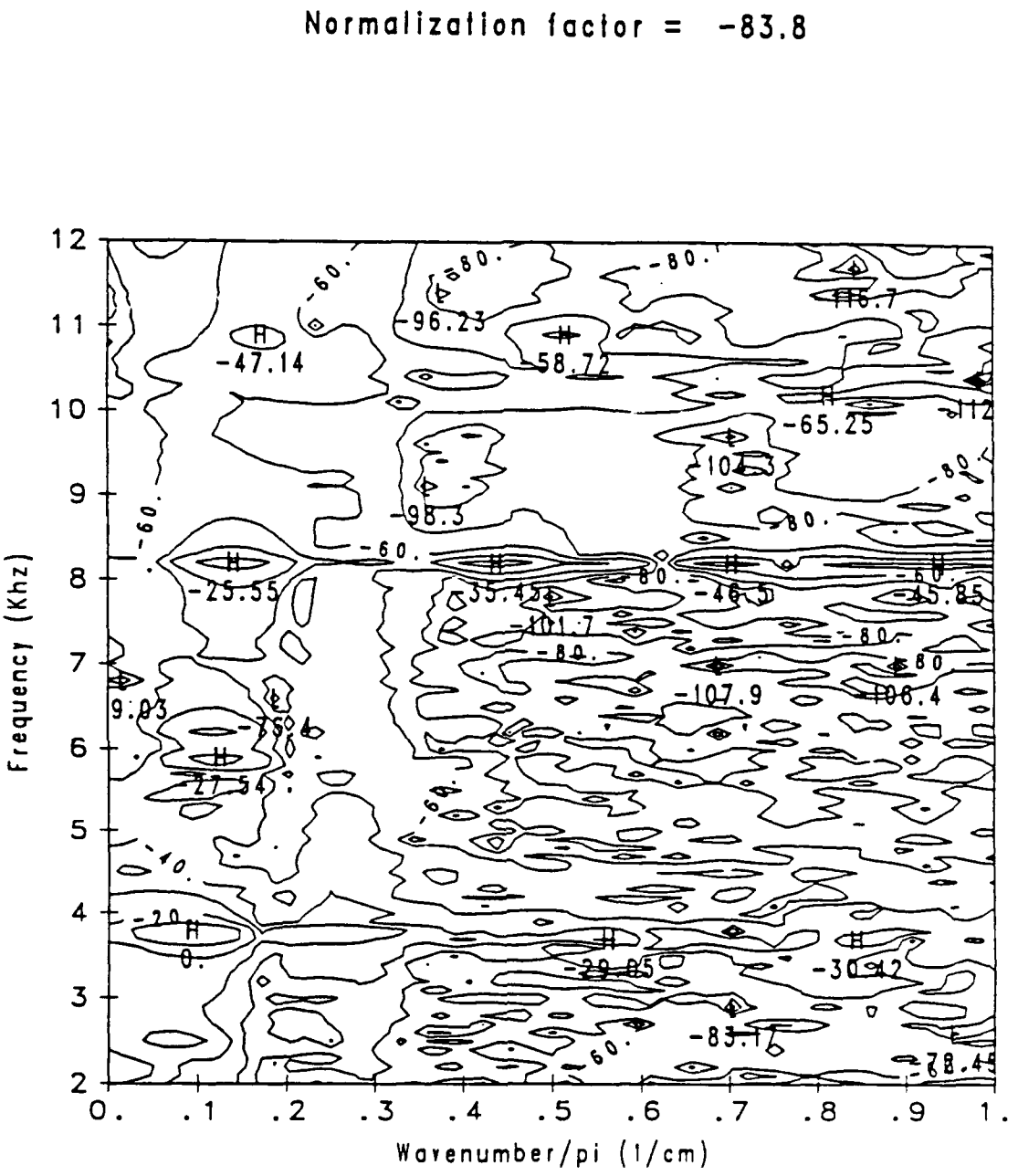

Figure 5.34: Contour plot of the velocity spectrum for polyurethane with $k_d = 0.28\pi$ cm^{-1}.

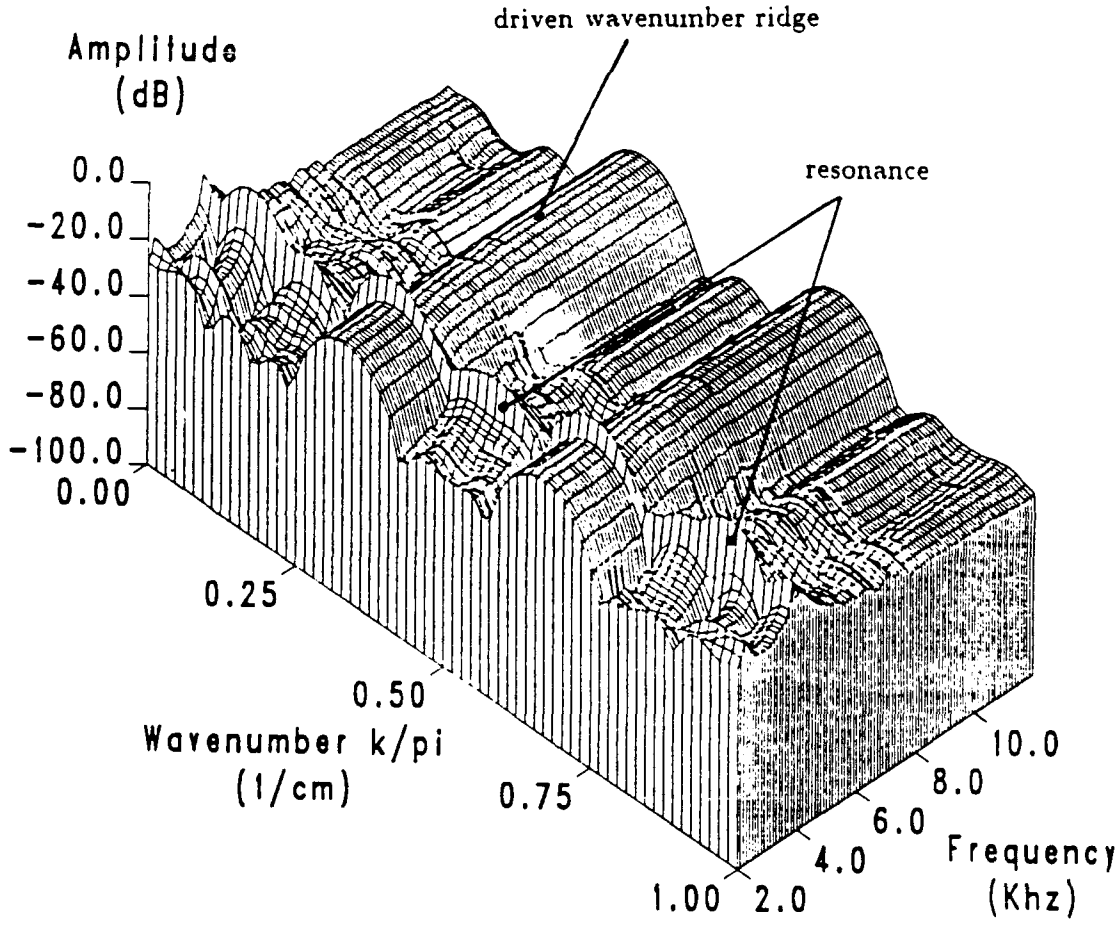

Figure 5.35: Surface plot of force spectrum for polyurethane with $k_d = \pi/3$ cm^{-1}.

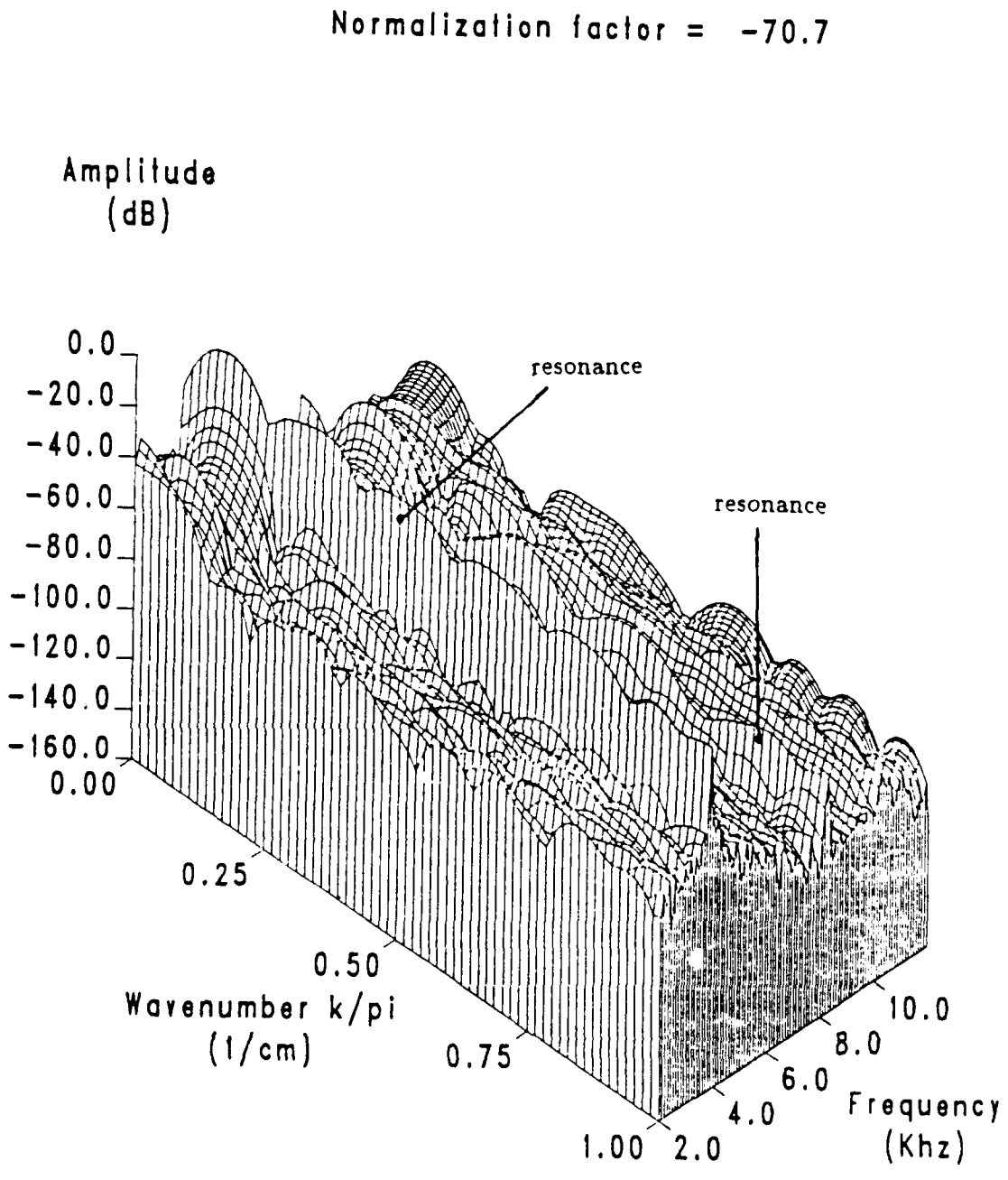

Figure 5.36: Surface plot of the velocity spectrum for polyurethane with $k_d = \pi/3$ cm^{-1}.

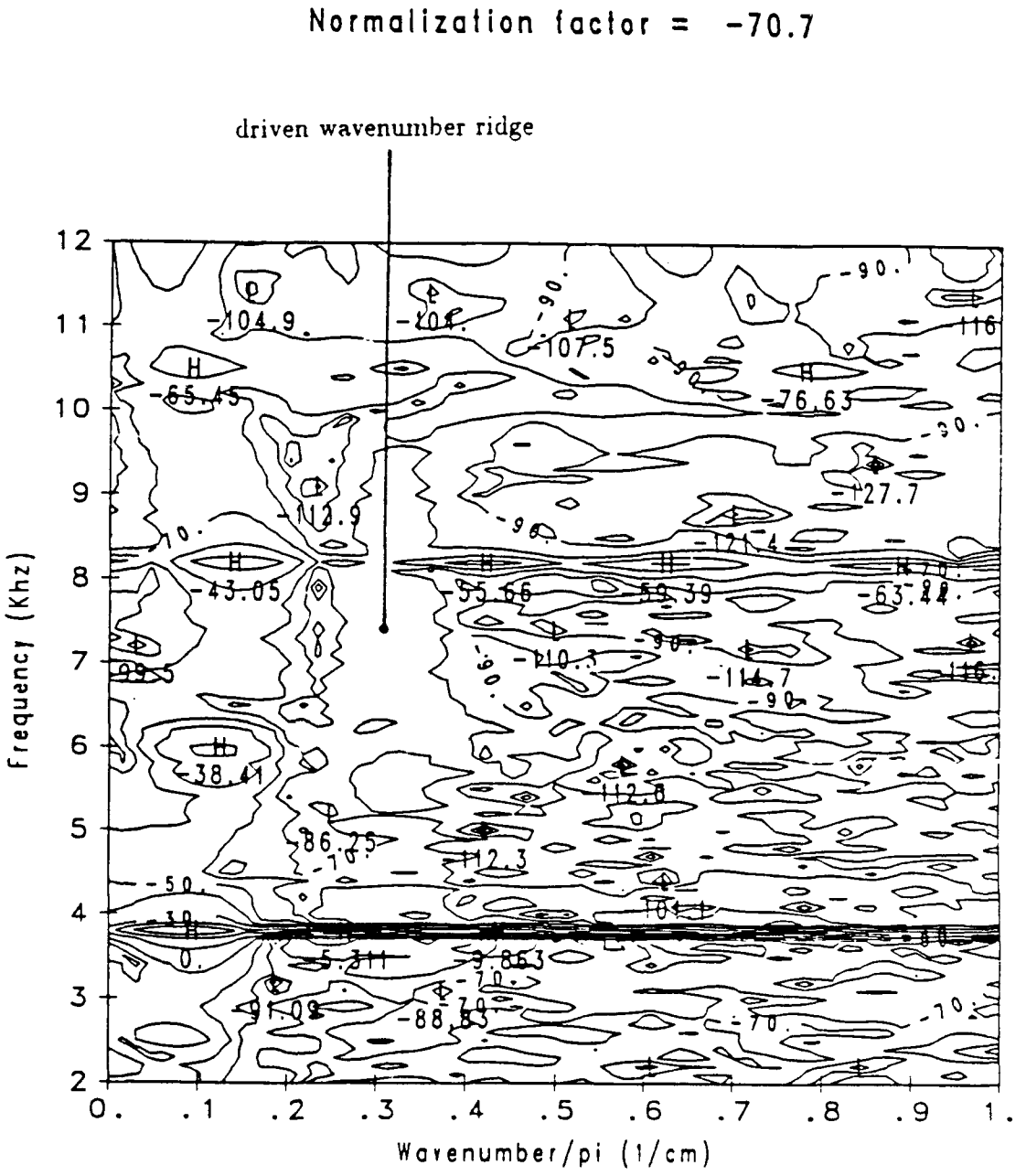

Figure 5.37: Contour plot of the velocity spectrum for polyurethane with $k_d = \pi/3$ cm^{-1}.

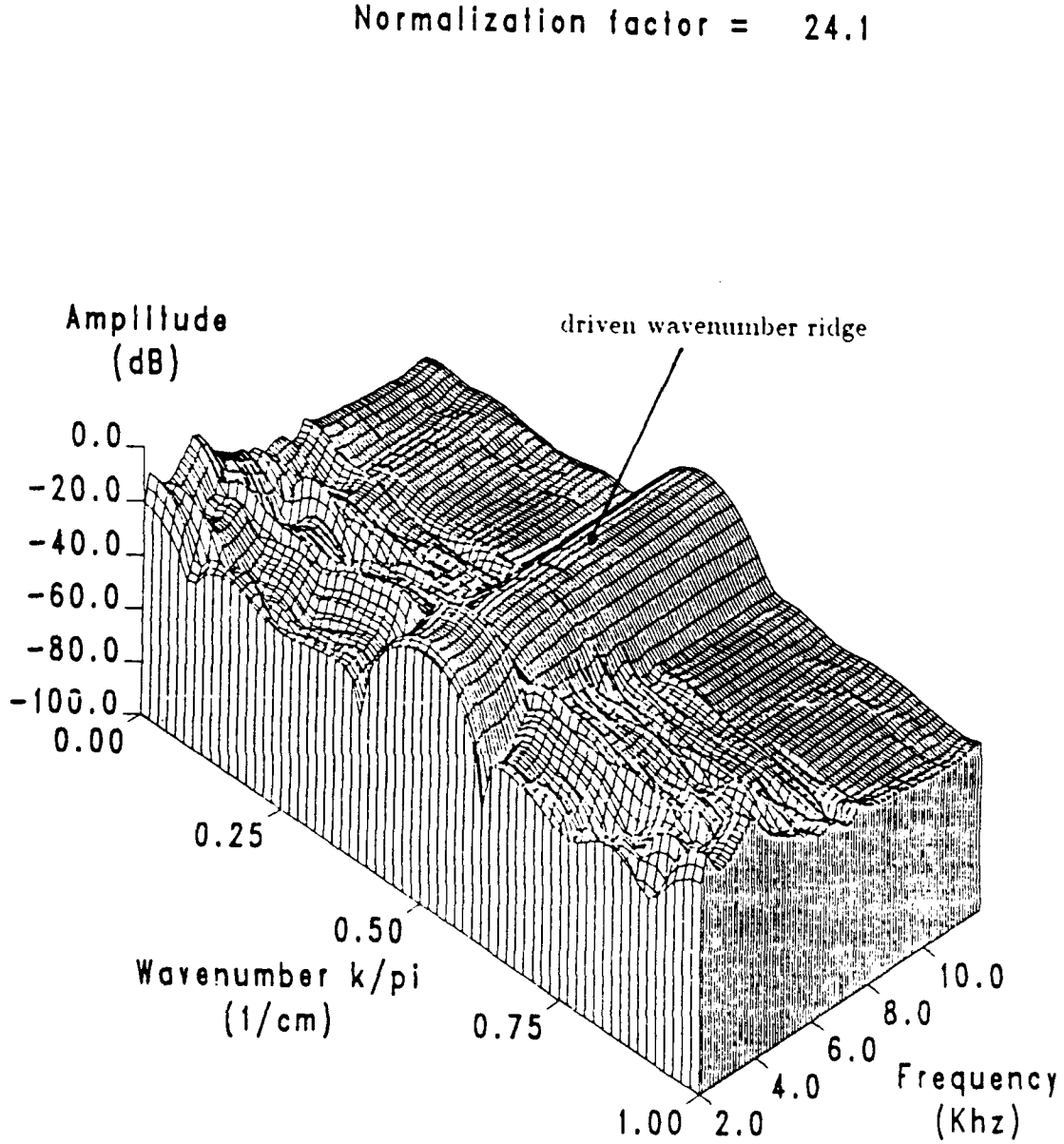

Figure 5.38: Surface plot of force spectrum for polyurethane with $k_d = \pi/2$ cm^{-1}.

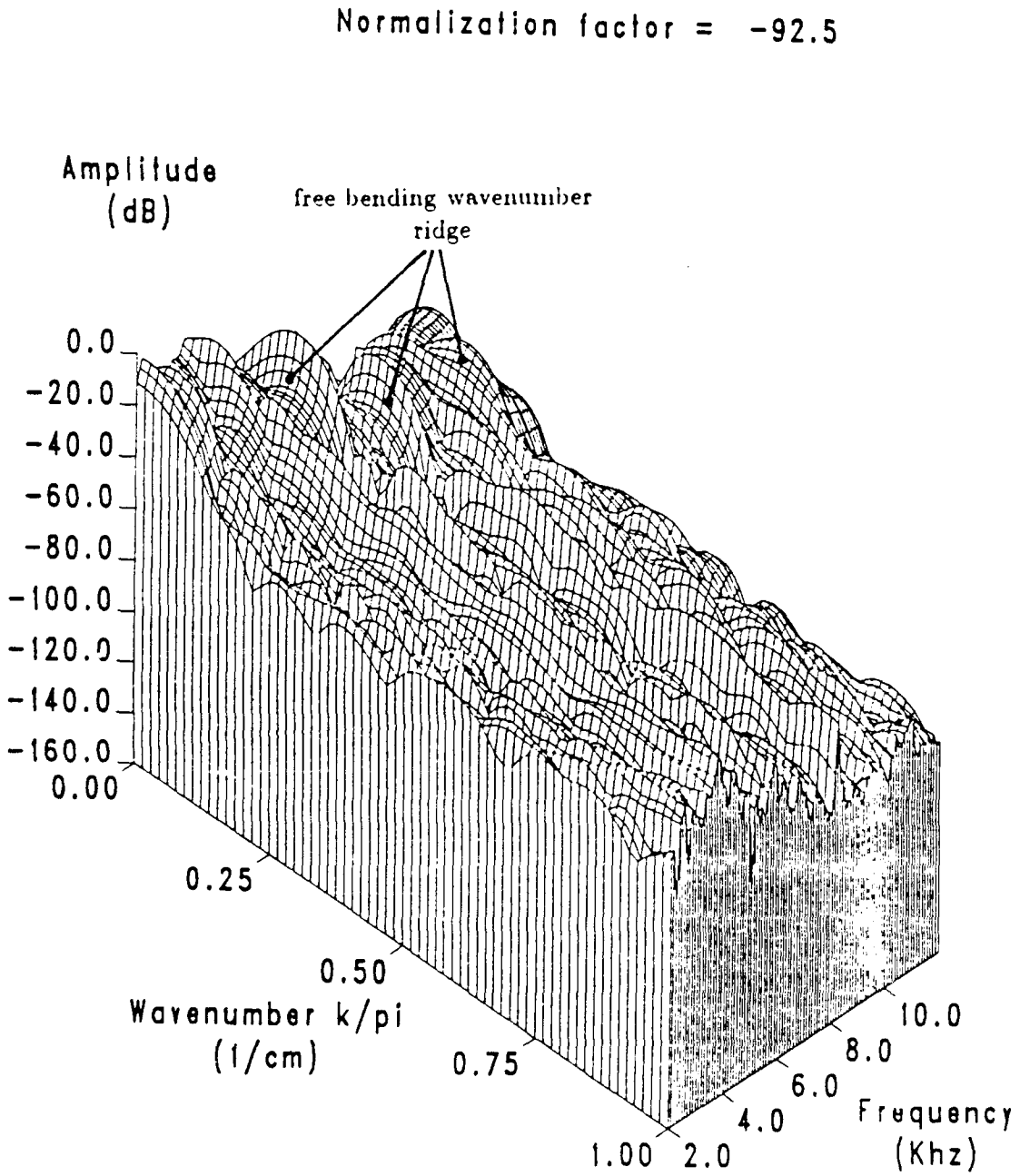

Figure 5.39: Surface plot of the velocity spectrum for polyurethane with $k_d = \pi/2$ cm^{-1}.

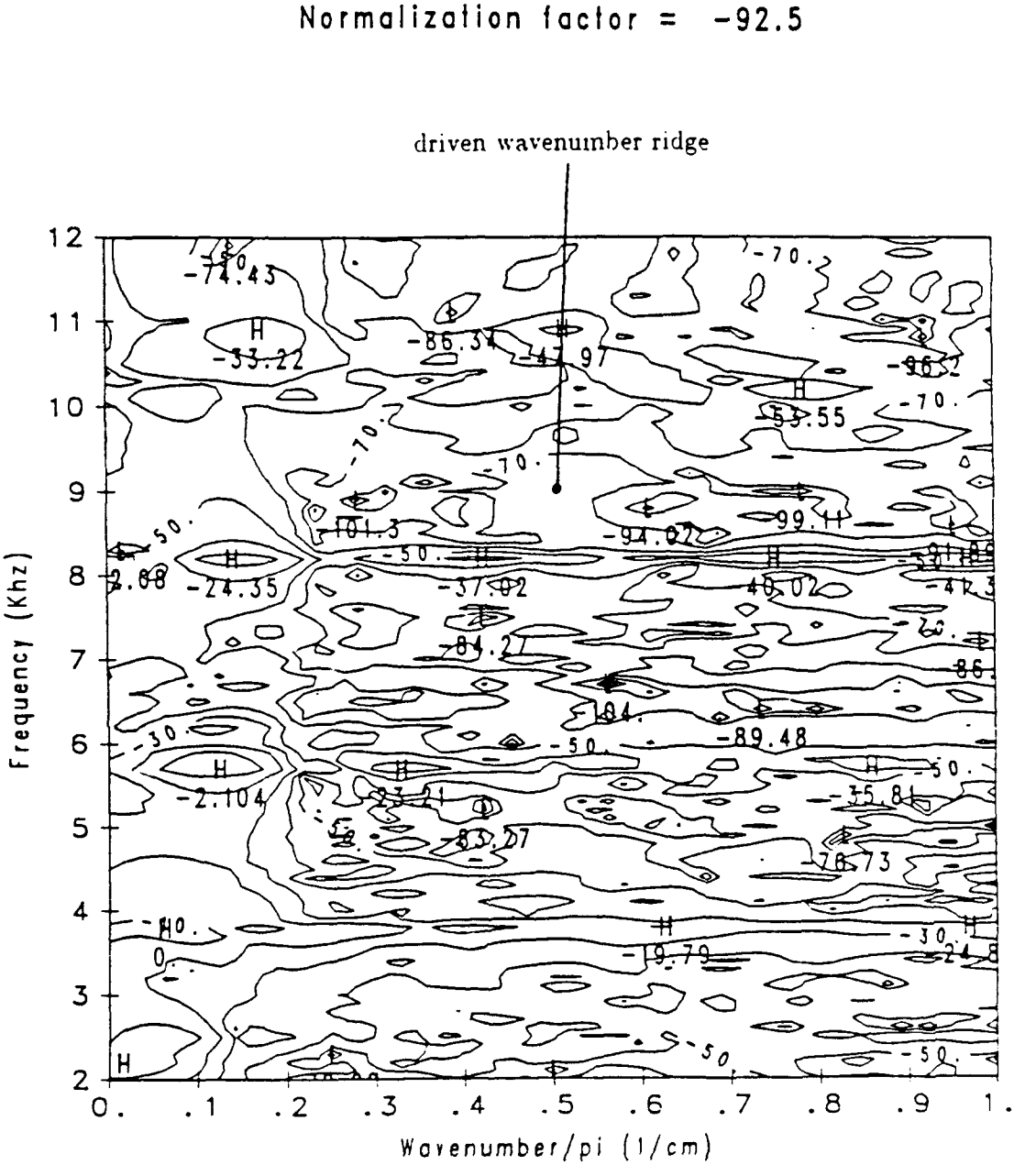

Figure 5.40: Contour plot of the velocity spectrum for polyurethane with $k_d = \pi/2$ cm^{-1}.

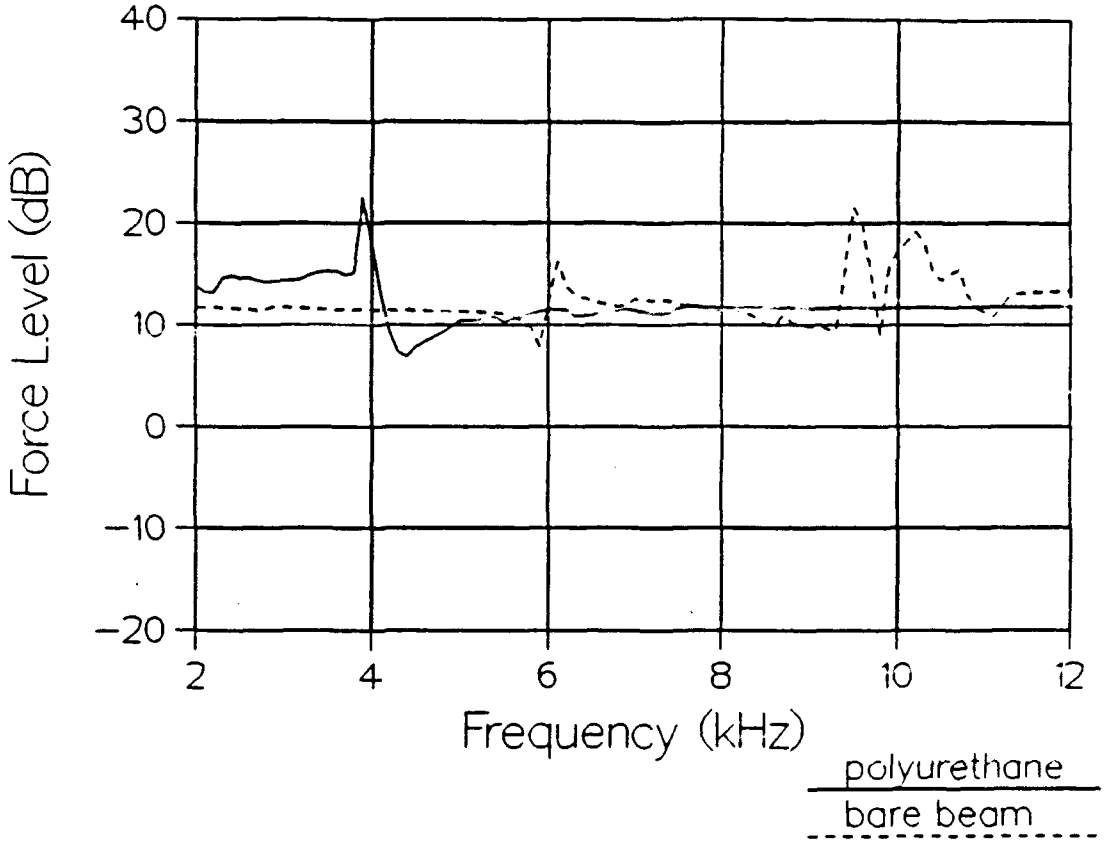

Figure 5.41: Comparison of the force on the polyurethane coated beam and the force on the bare beam driven at $k_d = \pi/4$ cm^{-1}.

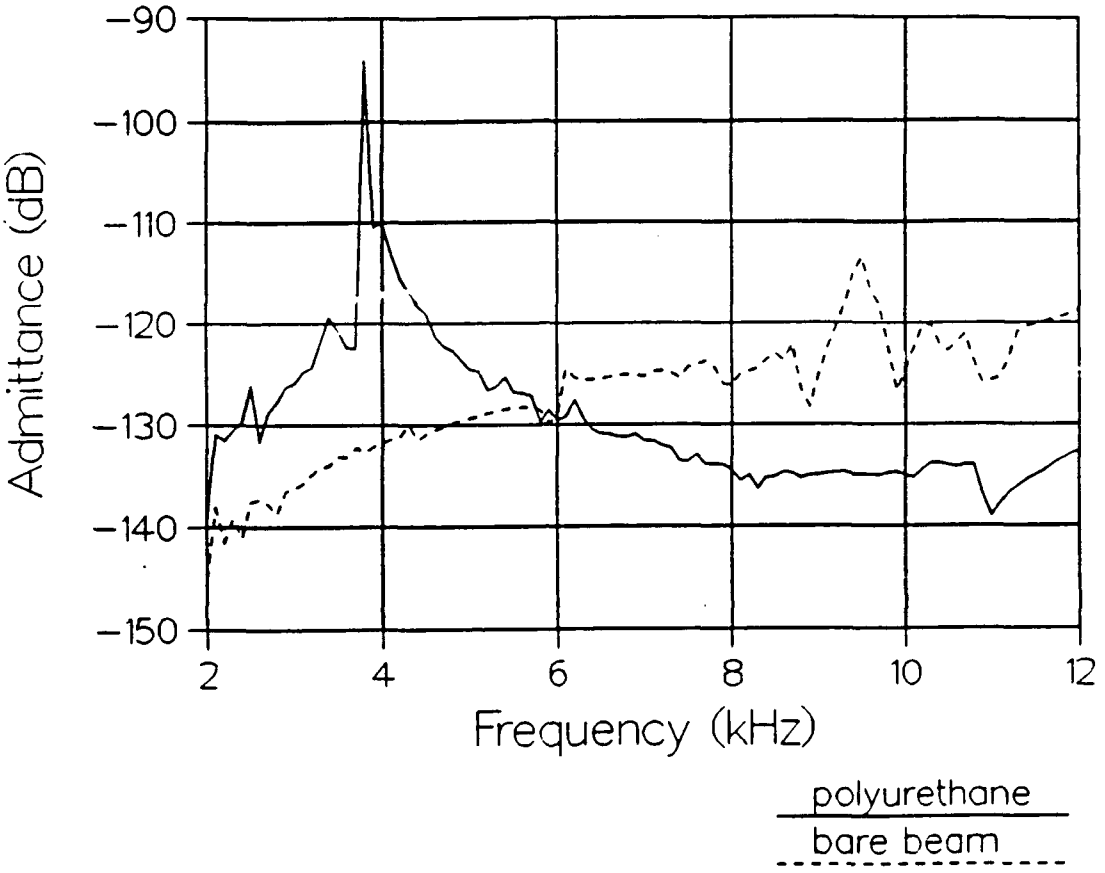

Figure 5.42: Comparison of the velocities of the polyurethane coated beam and the bare beam driven at $k_d = \pi/4$ cm^{-1}.

proximately 3.8 kHz appears to be erroneous, since no other peaks appear as sharp (see Figure 2.2). At a wavenumber of $\pi/4$ cm^{-1}, the transfer admittance of the bare beam and the transfer admittances of the beam coated with polyurethane, Natural Rubber I, and Neoprene I were calculated by taking the ratios of the corresponding force and velocity spectra. The effectiveness of each layer at the wavenumber $\pi/4$ cm^{-1} was calculated by dividing the transfer admittance of the bare beam into the transfer admittances of each coated beam. These admittances are compared in Figure 5.43. The peak of 3.8 kHz for the polyurethane has been removed. Because the polyurethane has the greatest stiffness, the highest resonance frequency occurs with the polyurethane. Also, the peak for the polyurethane layer occurs at a higher frequency (4.3 kHz) than the peak in the admittance of the single sample of polyurethane (3.8 kHz, see Figure 2.2). This indicates that the layer is stiffer than the single sample possibly because of Poisson's effect and the high bulk modulus of polyurethane. The curve for polyurethane is the highest curve on the plot indicating that the effectiveness is lowest. Yet, the amount of effectiveness does not seem to depend strictly upon stiffness. The Natural Rubber I appears to have a resonance at approximately 2 kHz whereas the Neoprene I appears to have a resonance at an even lower frequency, implying that the Neoprene I has a lower stiffness. However, in the plot comparing the effectiveness of each layer, the curve for Neoprene I is higher than the curve for Natural Rubber I. This implies that the effectiveness of the Neoprene I is less than the effectiveness of the Natural Rubber I, contrary to a linear relation between effectiveness and the apparent stiffness of the layer. There were some reservations about the validity of the Neoprene I (see Appendix B) which is

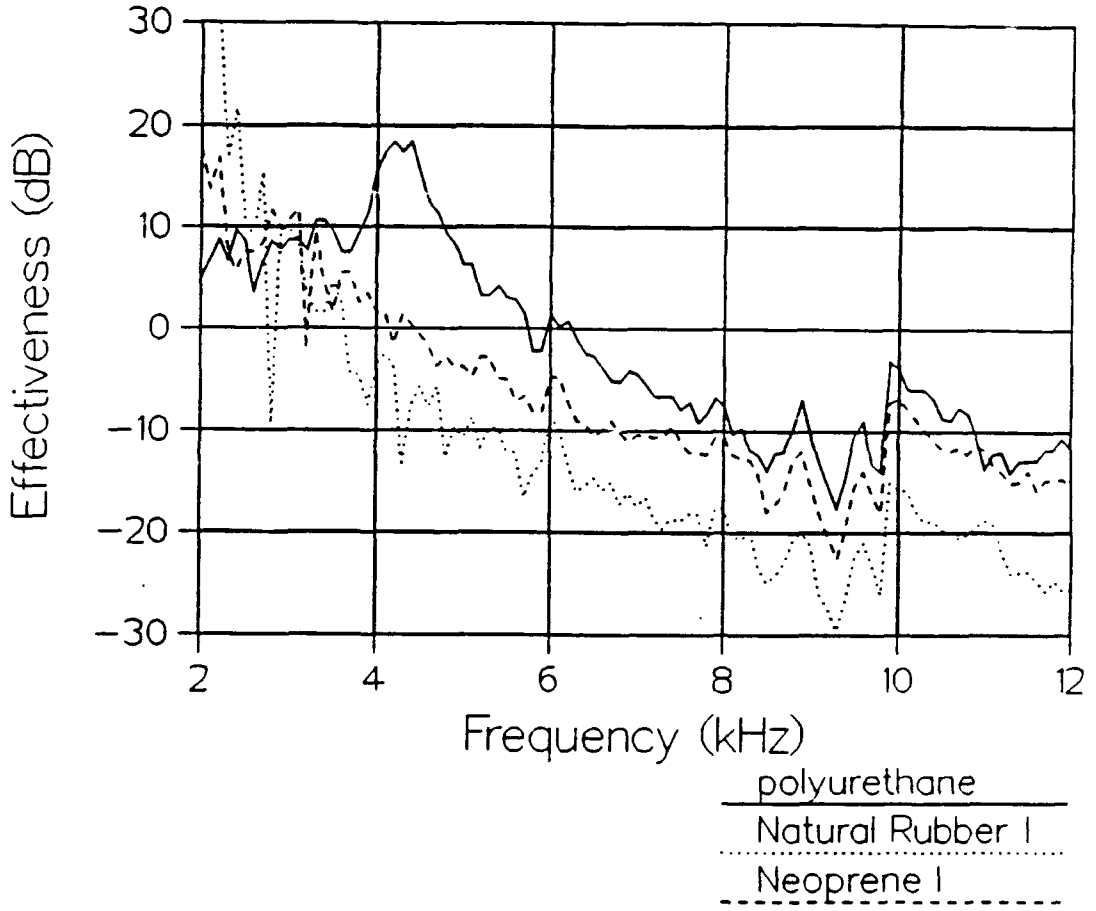

Figure 5.43: Comparison of the effectiveness of polyurethane, Natural Rubber I, and Neoprene I at $k_d = \pi/4$ cm^{-1}.

why the Neoprene II was measured. The plot of the effectiveness of the Neoprene II at a driven wavenumber of $\pi/4$ cm^{-1} is is compared to the effectiveness of Neoprene I in Figure 5.44. Agreement between the two measurements is good, indicating that the results for the Neoprene I are valid.

Measurements were conducted on the Natural Rubber II because the hardness of this material was much lower than any of the other materials considered here. The effectiveness of Natural Rubber II at the driven wavenumber of $\pi/4$ cm^{-1} is compared to the effectiveness of Natural Rubber I in Figure 5.45. It can be seen in Figure 5.45 that the softer material was much more effective at reducing the velocity of the beam.

A comparison of the effectiveness of the polyurethane layer at two different driven wavenumbers (0 and $\pi/3$ cm^{-1}) are shown in Figure 5.46. A slight increase in the effectiveness with increasing driven wavenumber can be seen between these two curves.

5.4 Results from the PVDF arrays

Because the polyurethane layer was molded in place for the transfer admittance experiments, a new layer had to be fabricated. Therefore, before the transfer loss results are shown, the results from the transfer admittance measurement (taken on the beam with the PVDF arrays) are presented so that the results can be compared to the previous transfer admittance experiments.

For these experiments, a 0.635 cm layer of polyurethane with a hardness of 90 durometer was mounted between the PVDF arrays as described in Chapter 4.

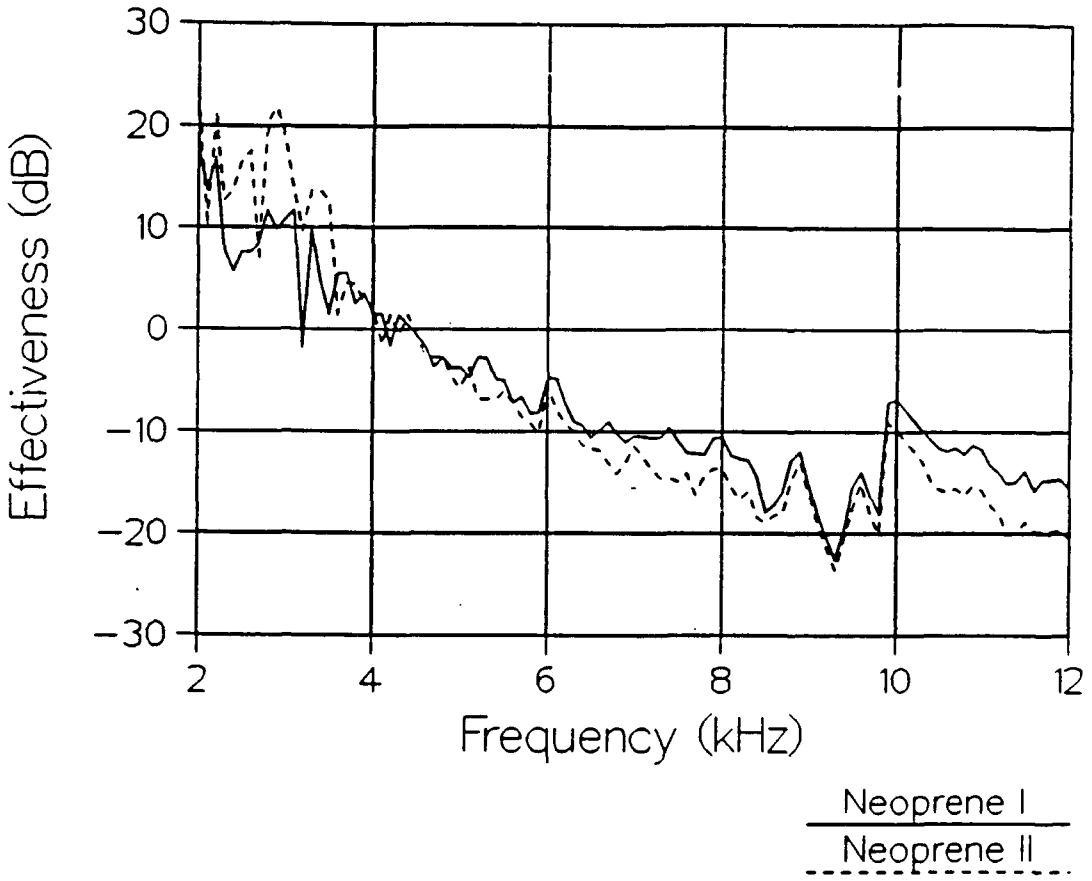

Figure 5.44: Effectiveness of Neoprene I and II at $k_d = \pi/4$ cm^{-1}.

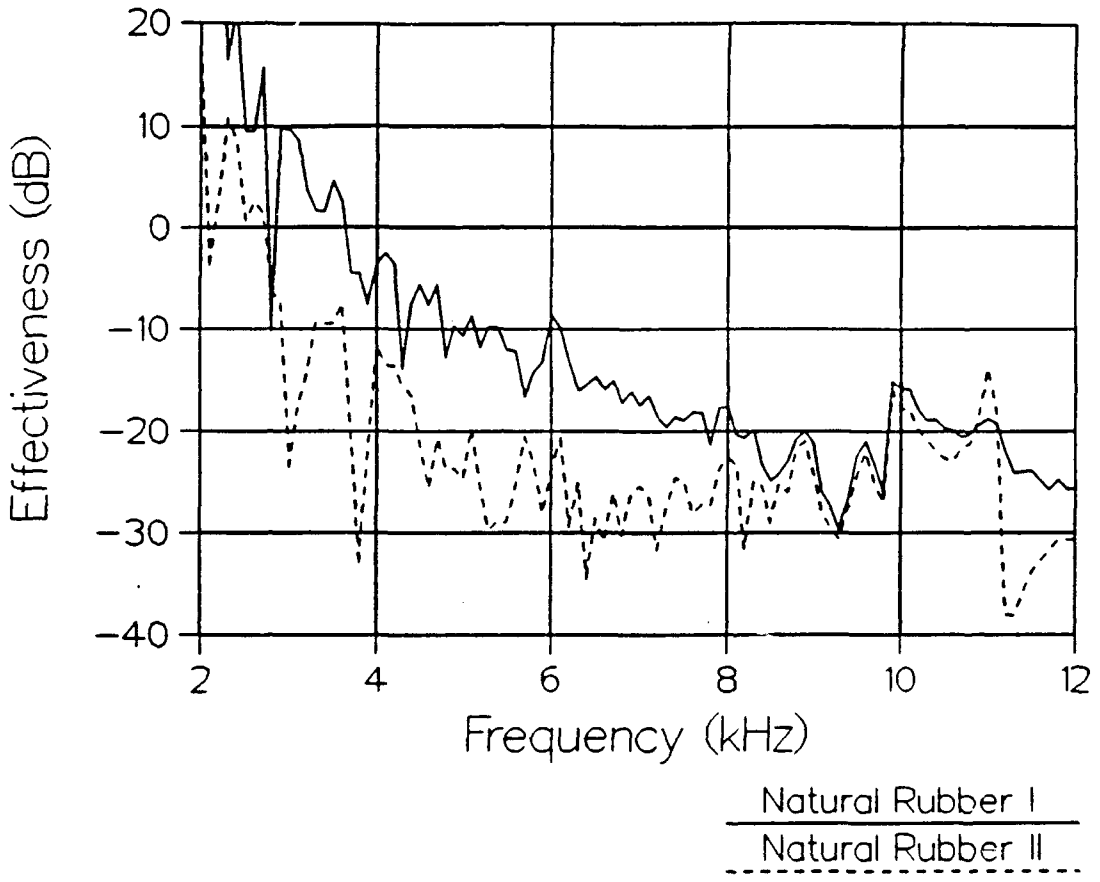

Figure 5.45: Effectiveness of Natural Rubber I and II at $k_d = \pi/4$ cm^{-1}.

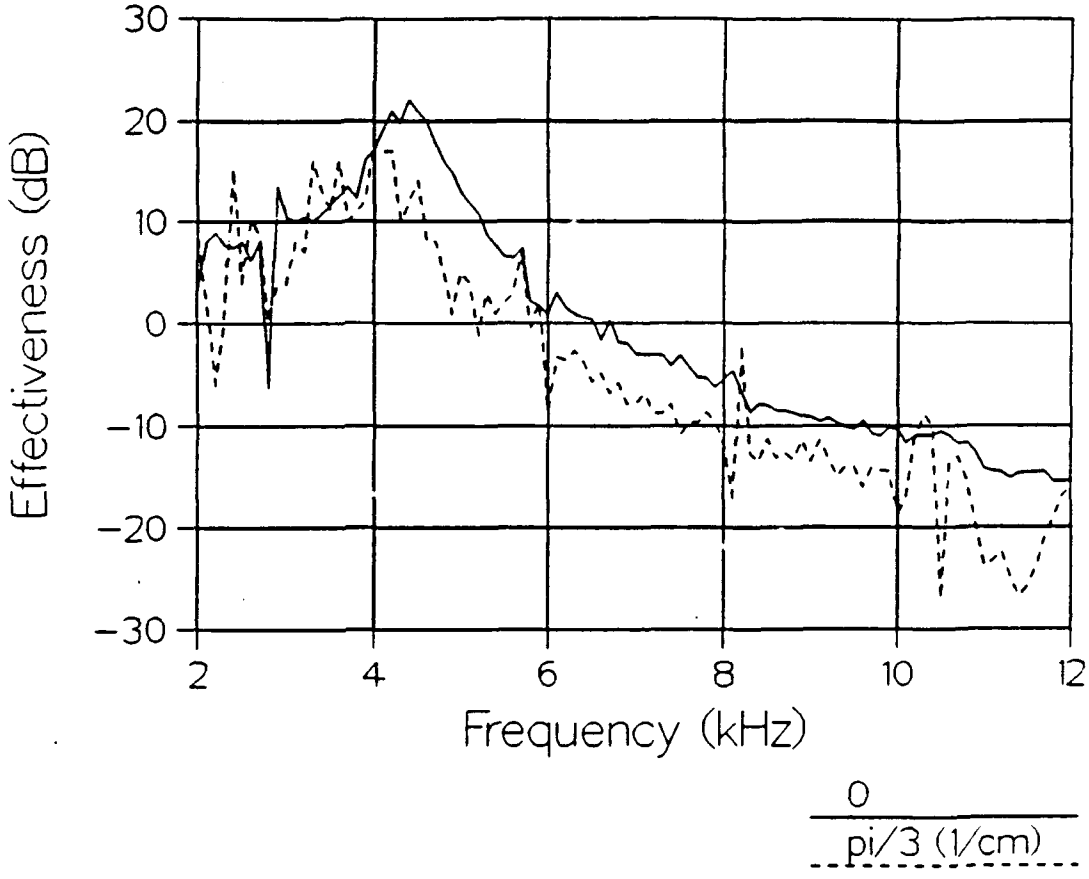

Figure 5.46: Polyurethane effectiveness at $k_d = 0$ and $k_d = \pi/3$ cm^{-1}.

Driving the array at a wavenumber of $\pi/4$ cm^{-1}, the shaker force gauge outputs and the accelerometer were used to obtain the spectra shown in Figures 5.47–5.49. Using the data from the force and velocity spectra of the new layer (Polyurethane II), the effectiveness at the driven wavenumber $\pi/4$ cm^{-1} was calculated and is compared in Figure 5.50 to the effectiveness of the previous layer, Polyurethane I. The resonance peak of Polyurethane II is at approximately 2.7 kHz which is significantly lower than the resonance frequency of Polyurethane I. According to the trends observed in the effectiveness comparisons of different layers, the lower resonance frequency should indicate a lower stiffness for the new layer which may be possible since the two polyurethane layers were made separately.

Figures 5.51 and 5.52 show the force spectrum obtained by the top PVDF array with Polyurethane II. This measurement resembles those obtained by the force gauges in the shakers. The spectrum has the same smooth surface and has the same main lobe, grating lobe, and free bending wavenumber ridge as seen before.

The force spectrum obtained by the PVDF array at the bottom of the layer is shown in Figures 5.53 and 5.54. There exist strong forces at the driven wavenumber *and at the wavenumber of the grating lobe.* Because of the strong forces at the grating lobe, it is possible to determine the transmission loss at two wavenumbers (driven and grating) from only one measurement.

Another experiment was run at a drive wavenumber of $\pi/2$ cm^{-1}. The obtained force spectra at the top and bottom of the layer are shown in Figures 5.55 and 5.56, respectively. These spectra also show a strong response at the driven wavenumber. There is no visible grating lobe for this experiment because

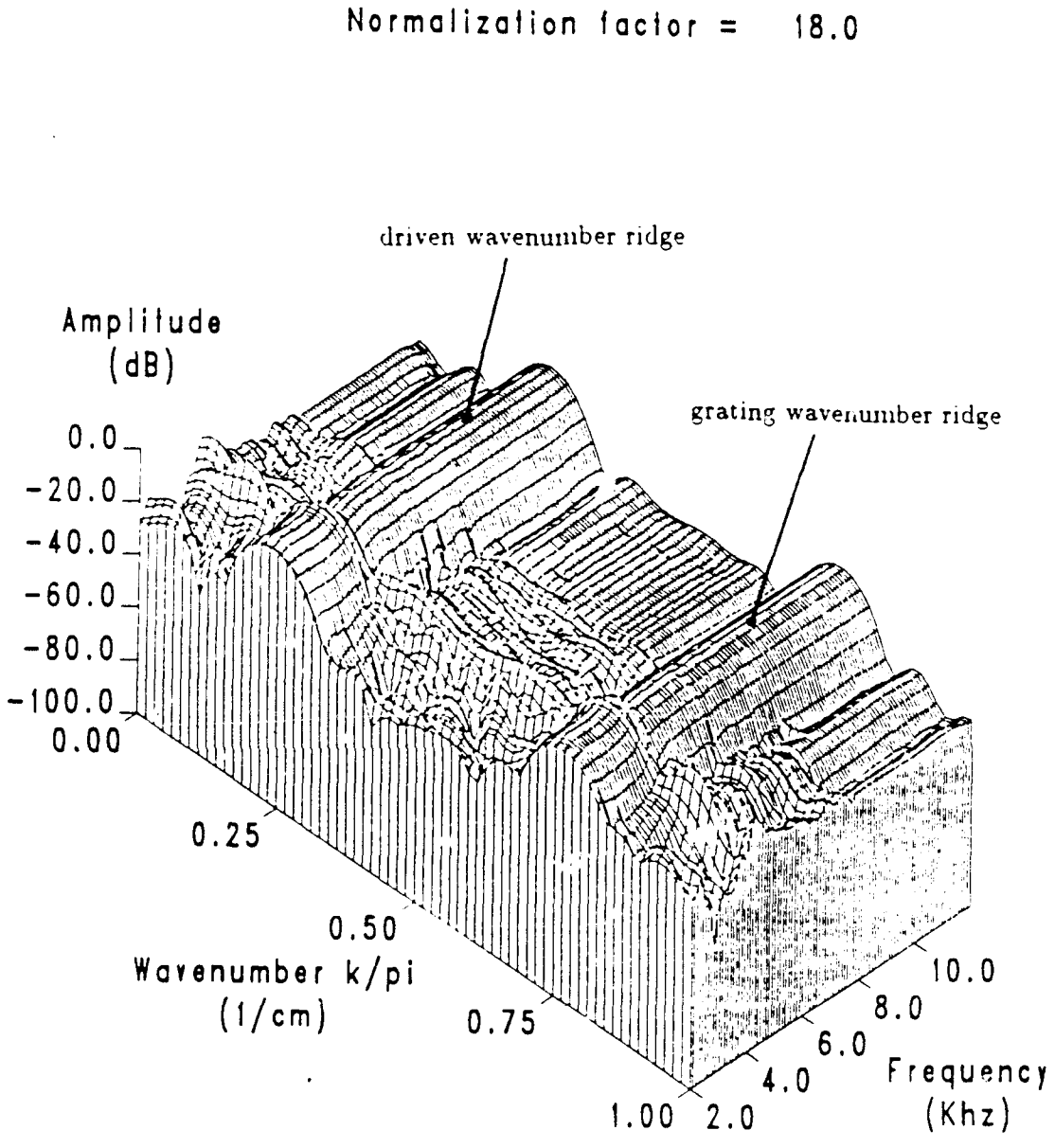

Figure 5.47: Surface plot of the force spectrum for polyurethane layer with PVDF arrays at $k_d = \pi/4$ cm^{-1}.

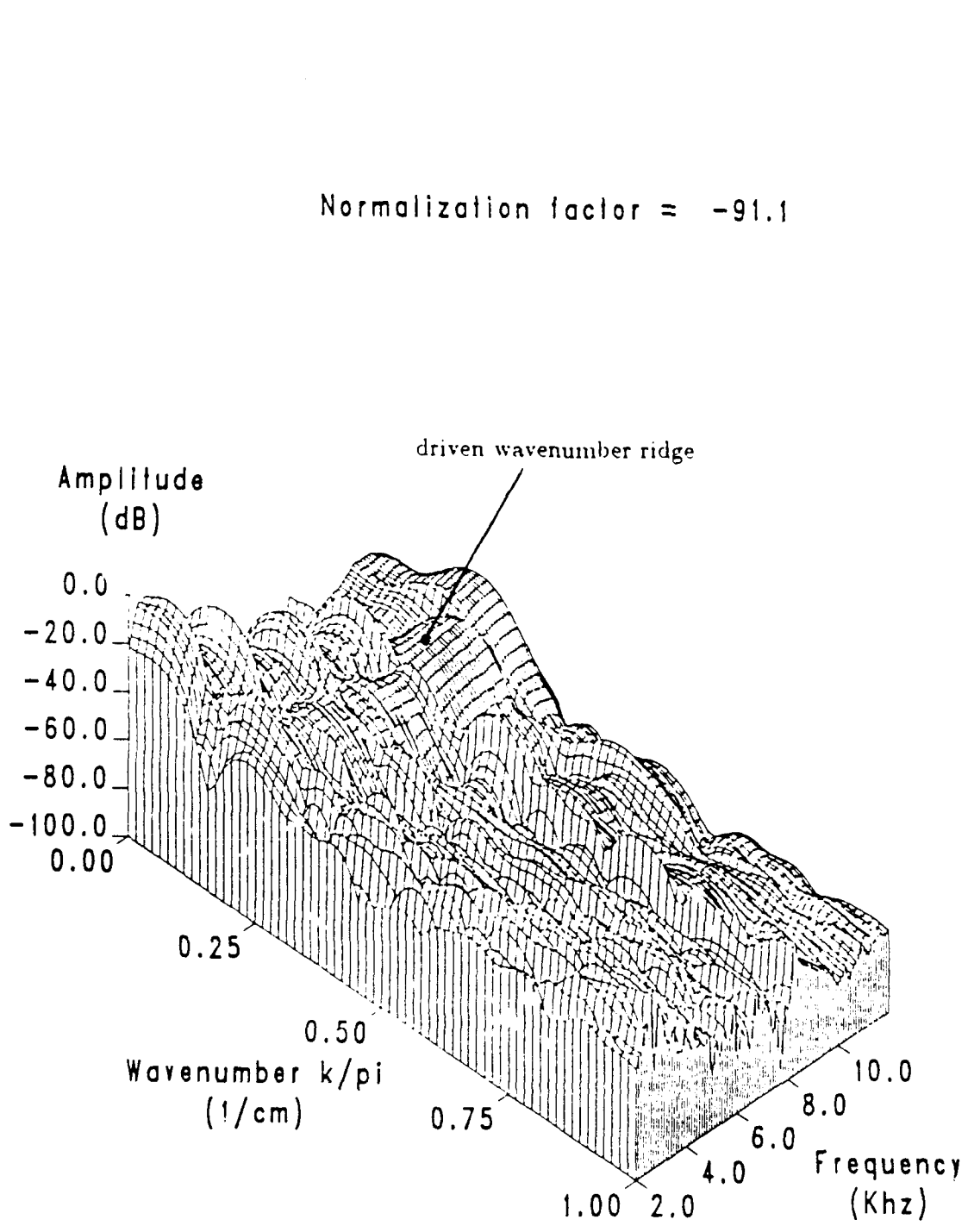

Figure 5.48: Surface plot of the velocity spectrum for polyurethane with PVDF arrays at $k_d = \pi/4$ cm^{-1}.

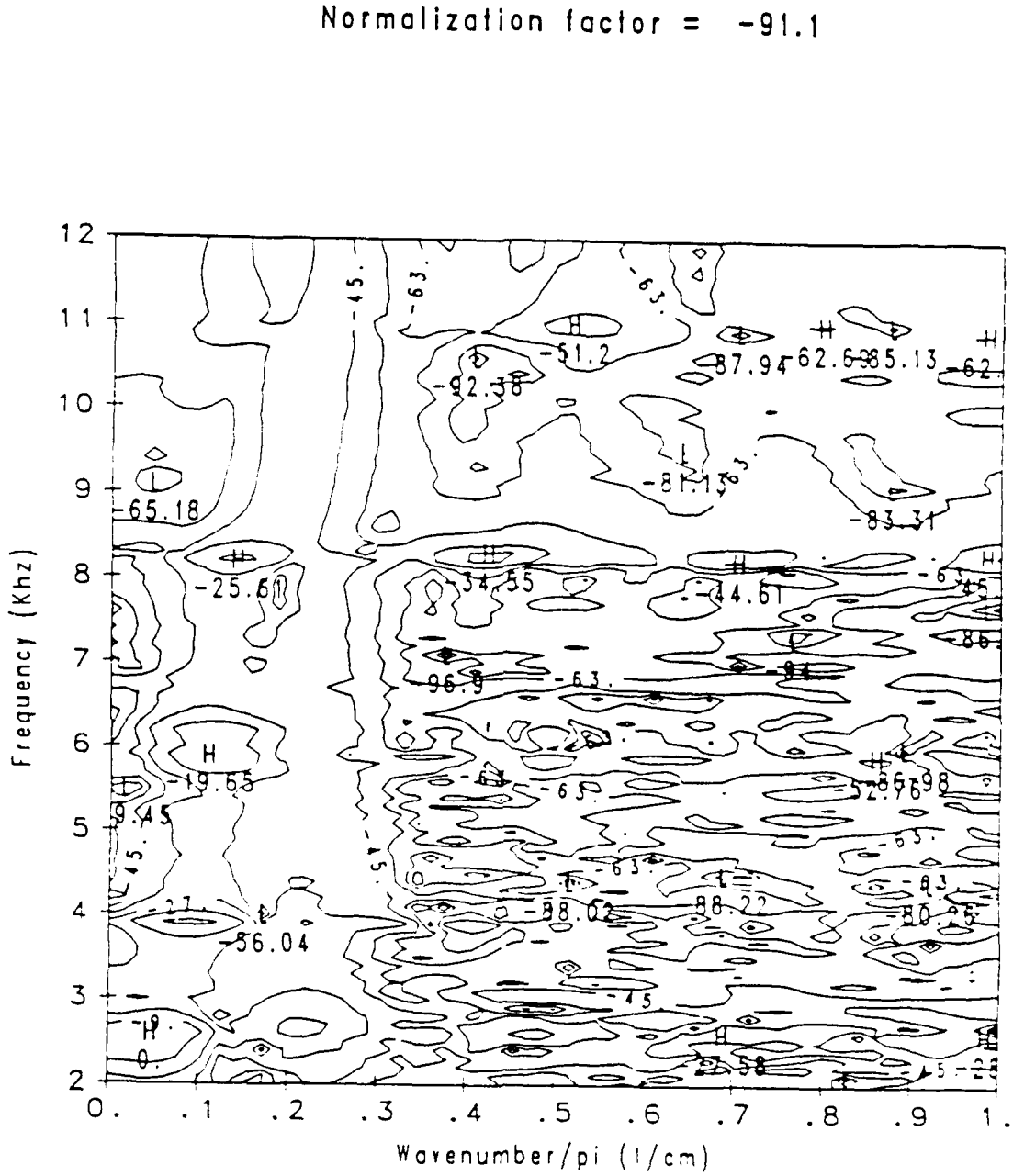

Figure 5.49: Contour plot of the velocity spectrum for polyurethane with PVDF arrays at $k_d = \pi/4$ cm^{-1}.

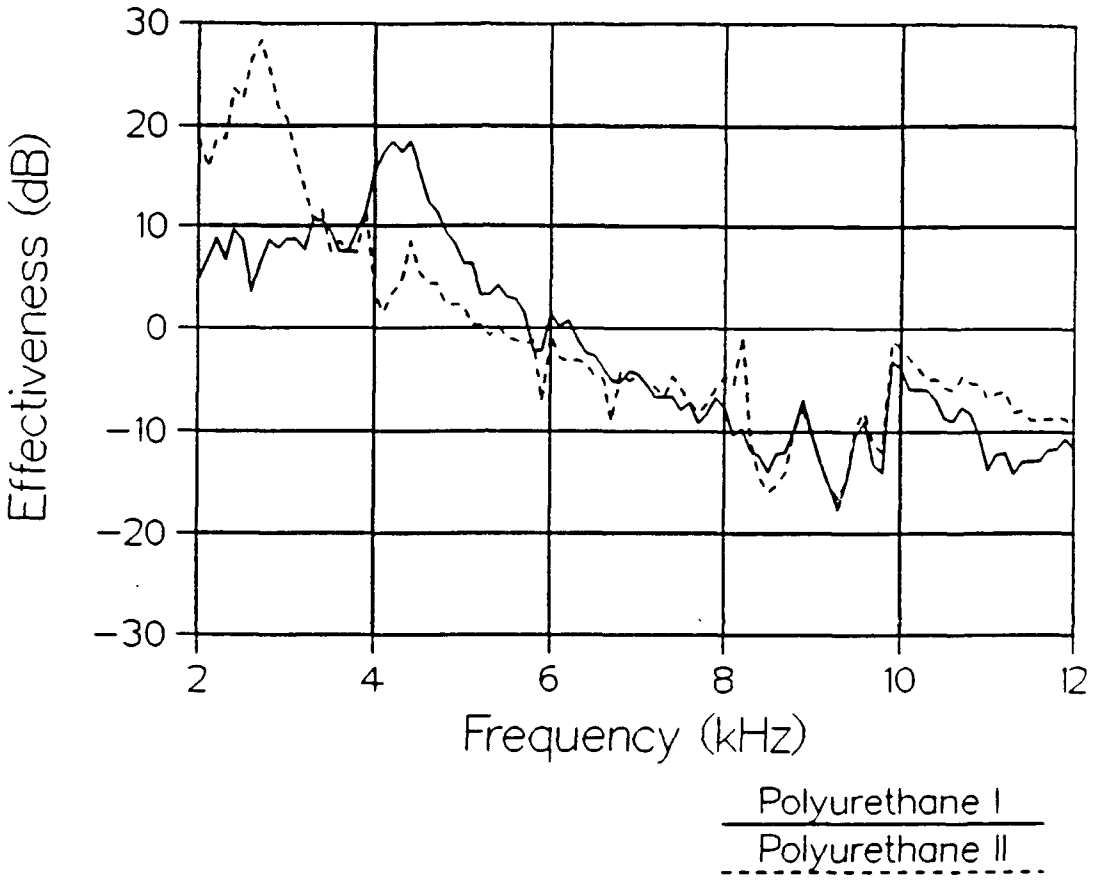

Figure 5.50: Effectiveness of polyurethane layers at $k_d = \pi/4$ cm^{-1}

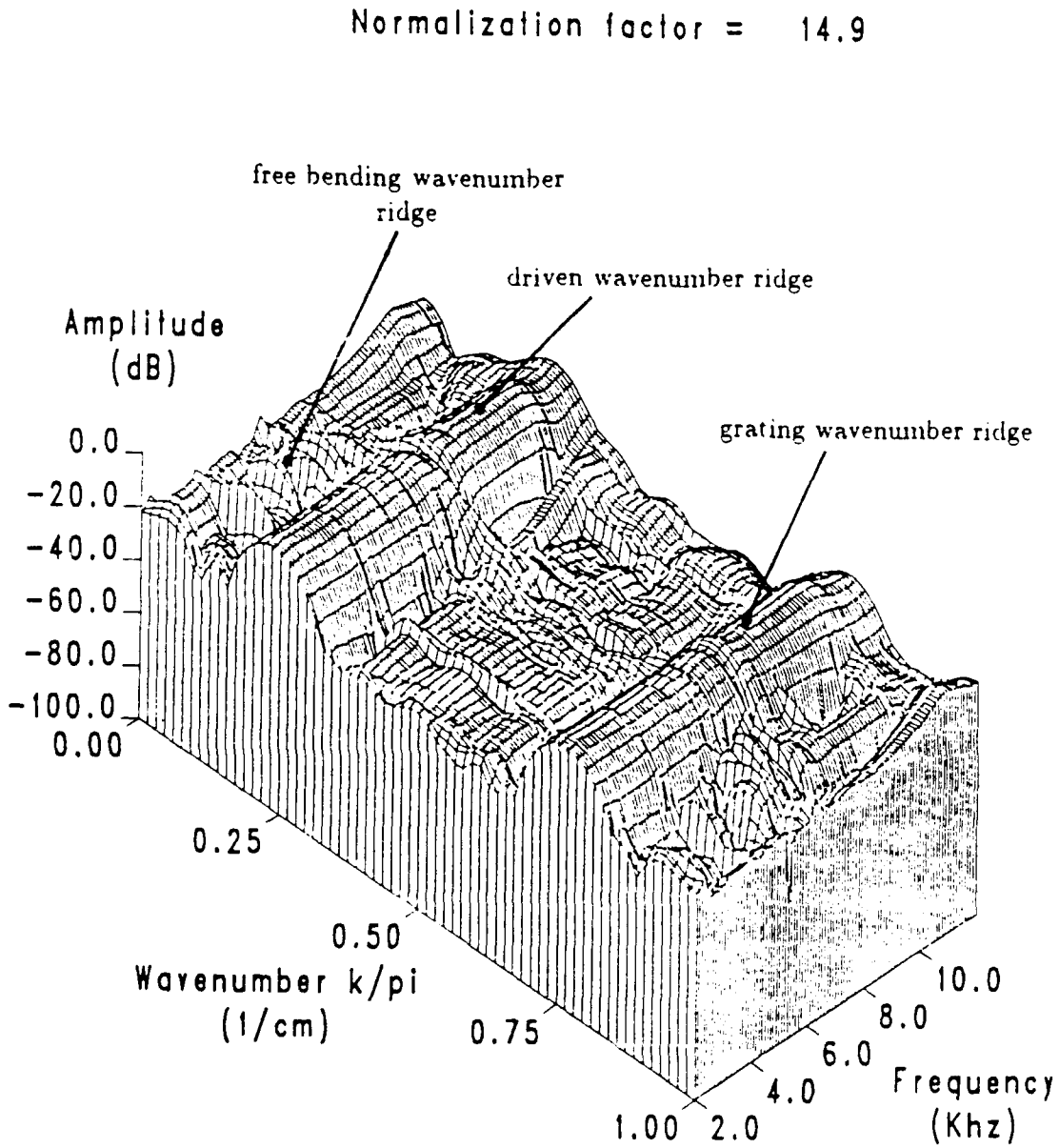

Figure 5.51: Surface plot of the force spectrum measured by the top PVDF array with $k_d = \pi/4$ cm^{-1}.

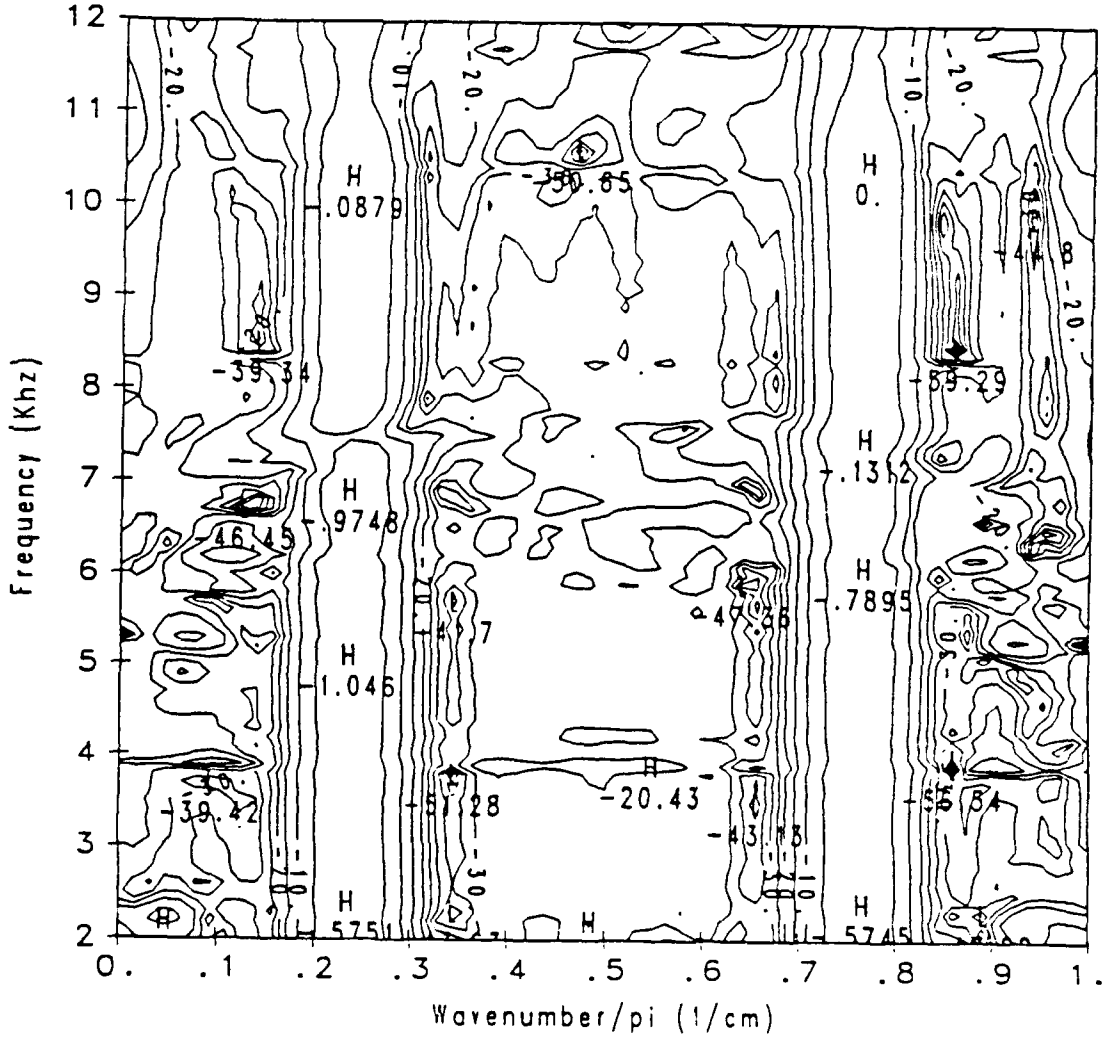

Figure 5.52: Contour plot of the force spectrum measured by the top PVDF array with $k_d = \pi/4$ cm^{-1}.

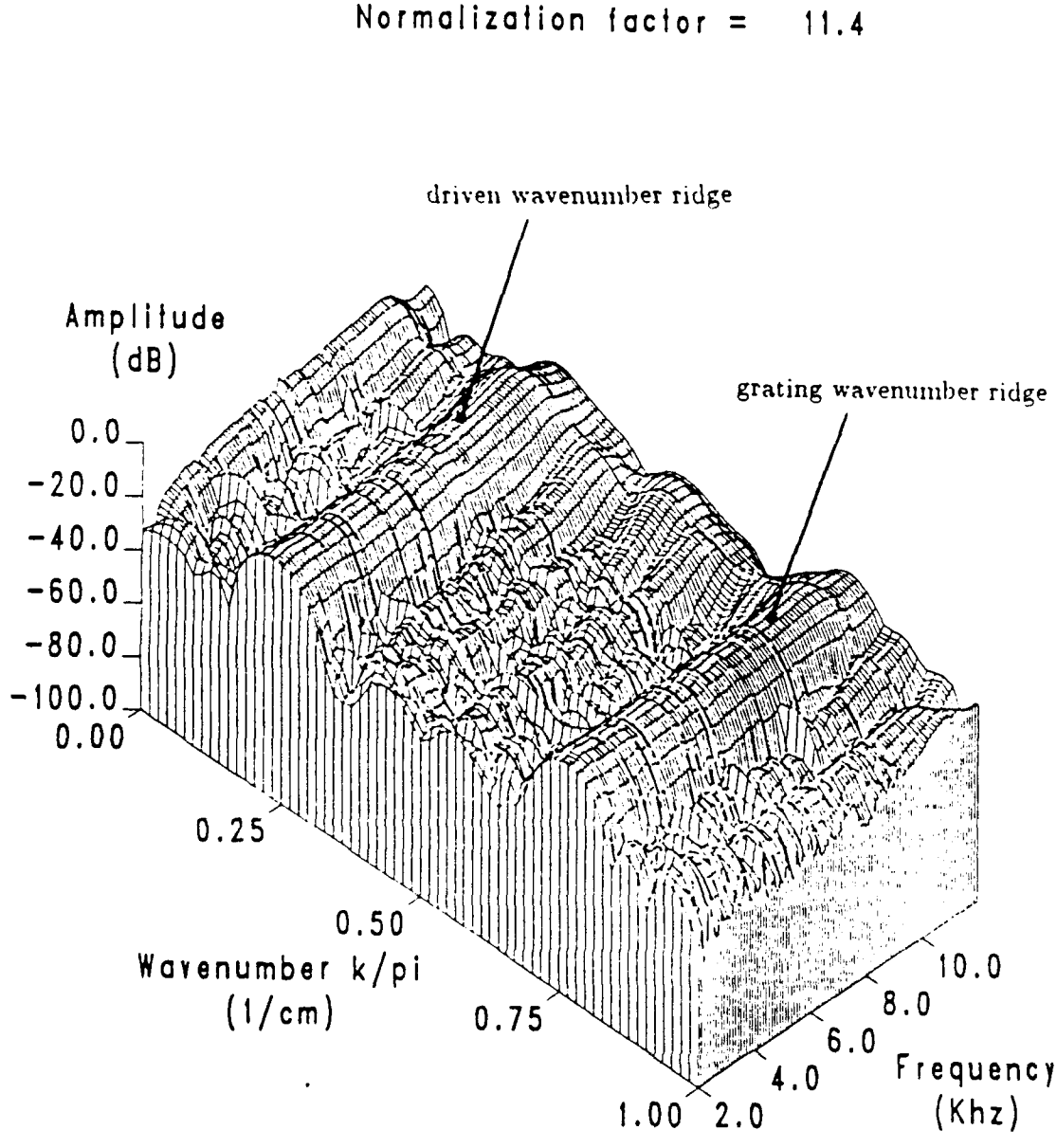

Figure 5.53: Surface plot of the force spectrum measured by the bottom PVDF array with $k_d = \pi/4$ cm^{-1}.

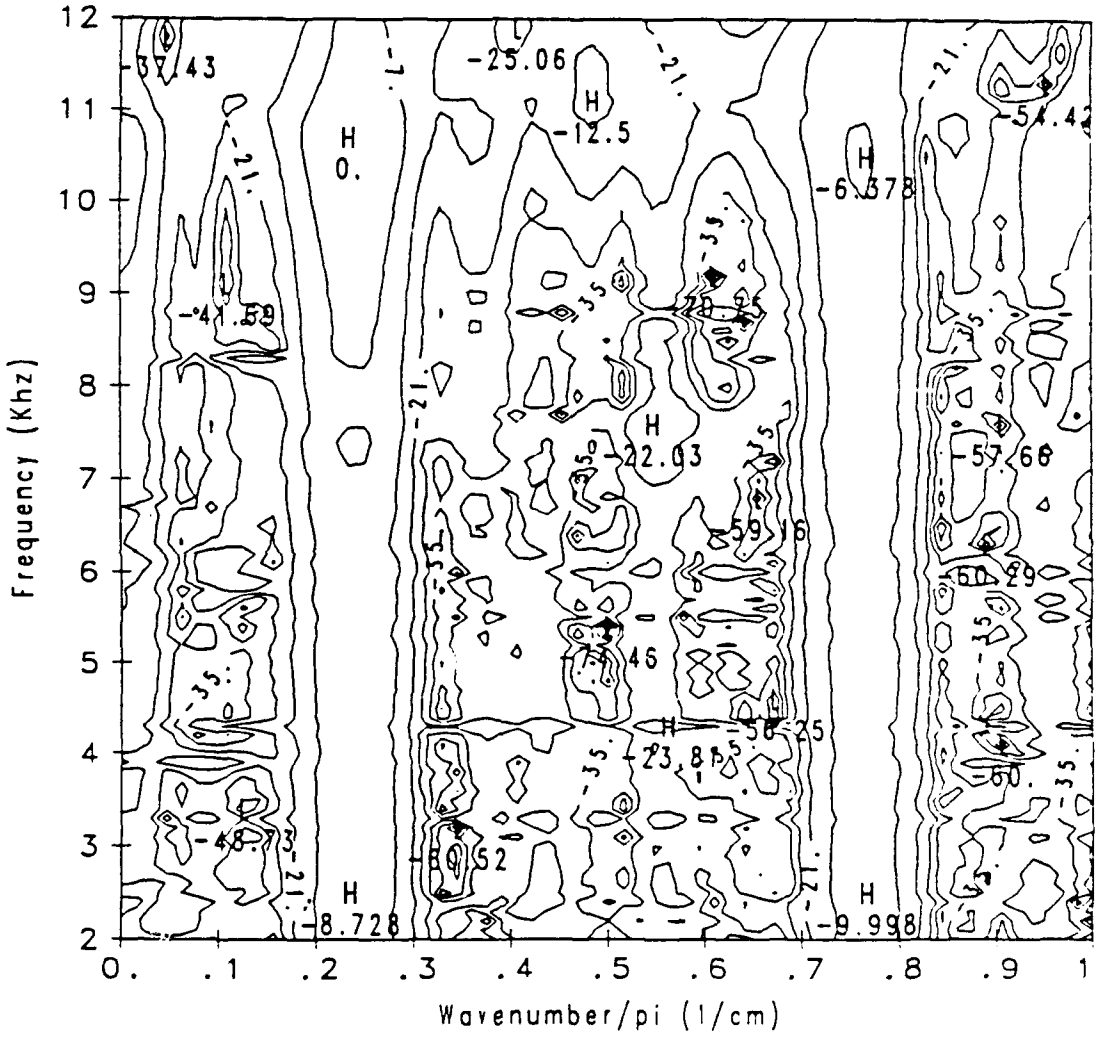

Figure 5.54: Contour plot of the force spectrum measured by the bottom PVDF array with $k_d = \pi/4$ cm^{-1}.

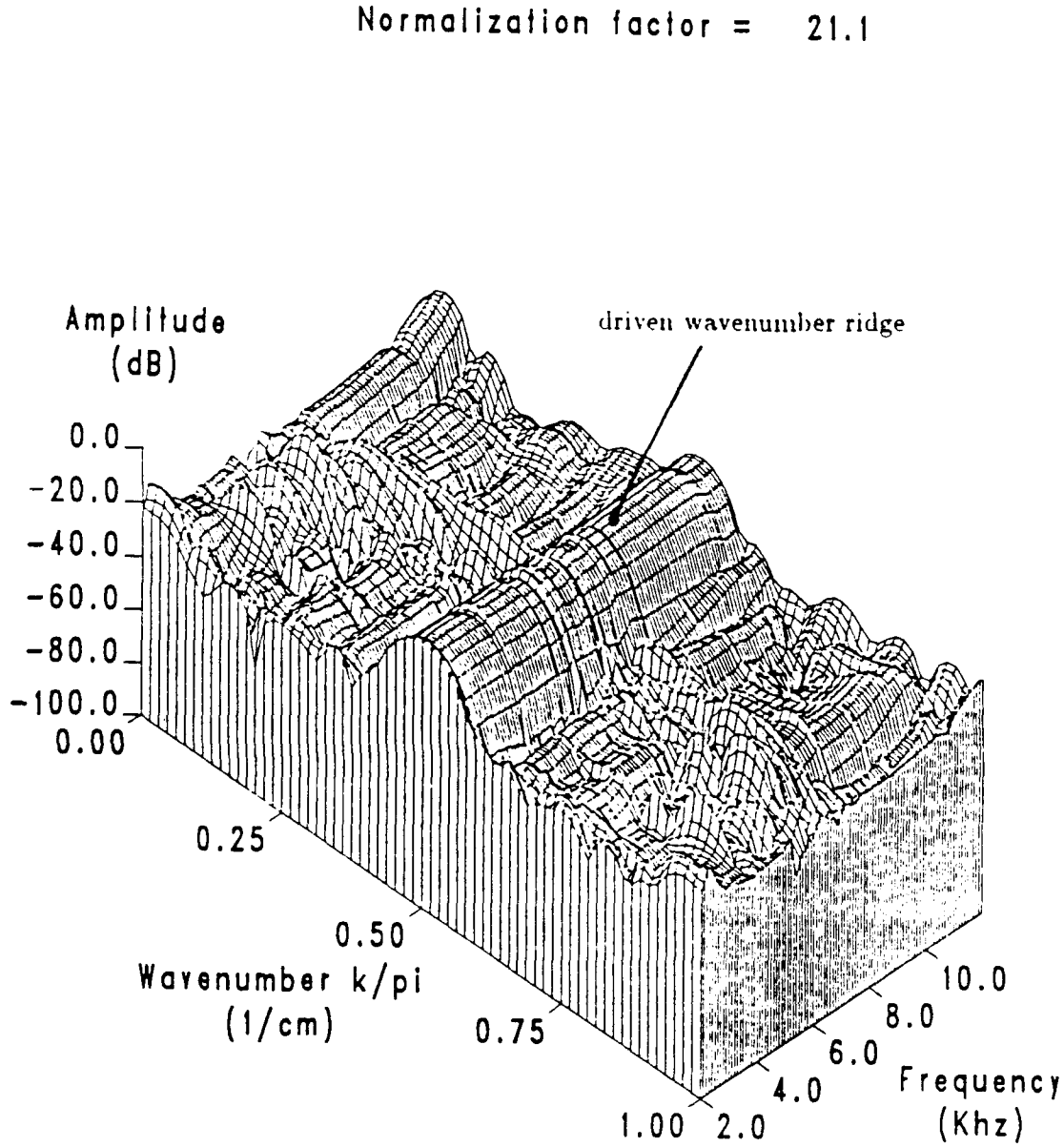

Figure 5.55: Surface plot of the force spectrum measured by the top PVDF array with $k_d = \pi/2$ cm^{-1}.

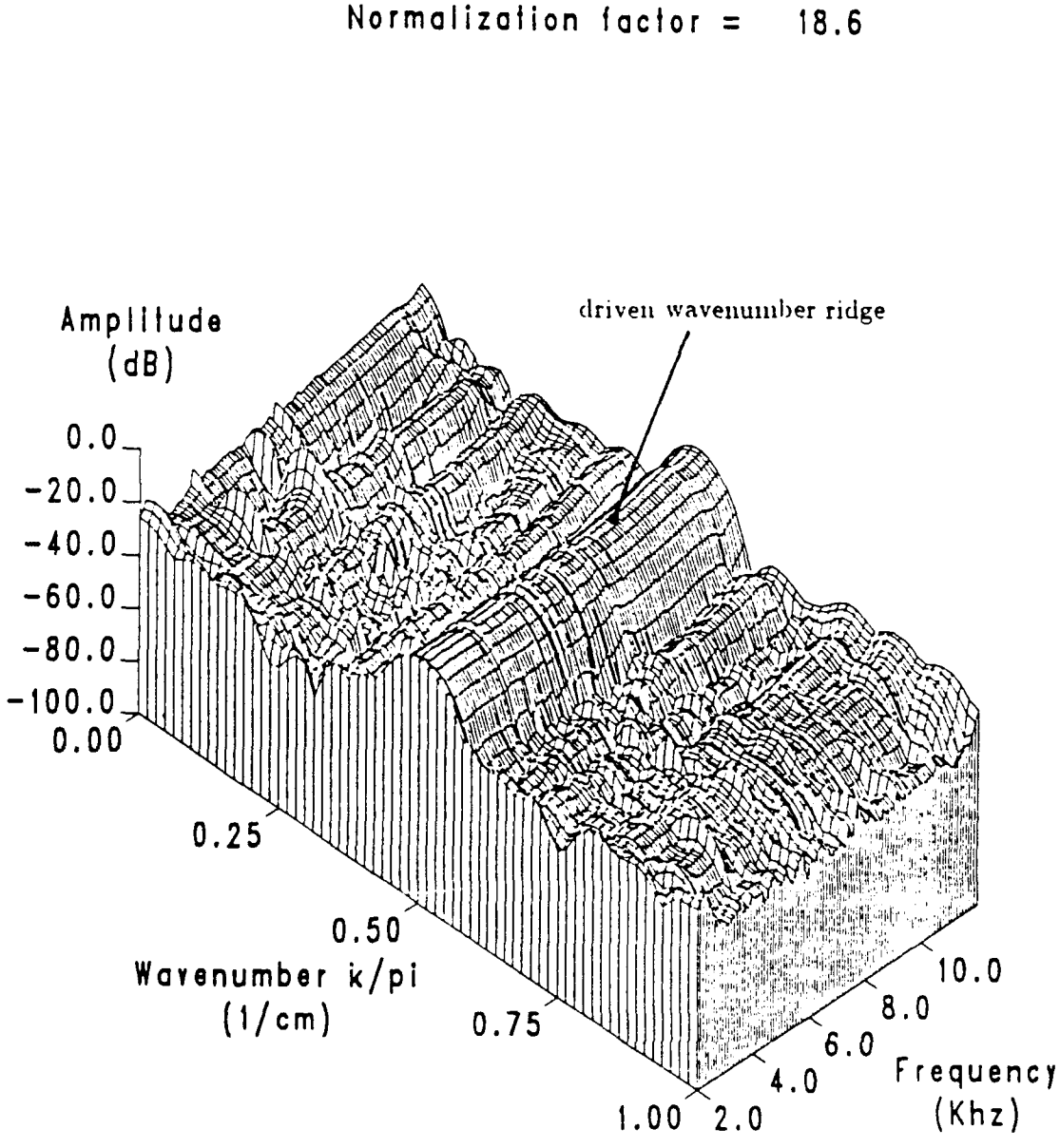

Figure 5.56: Surface plot of the force spectrum measured by the bottom PVDF array with $k_d = \pi/4$ cm^{-1}.

the grating wavenumber is outside the wavenumber measurement band.

The transmission losses at drive wavenumbers of $\pi/4$, $\pi/2$ and $3\pi/4$ cm^{-1} are shown in Figure 5.57. The transmission losses are all around 10 dB at frequencies below 8 kHz, with the largest losses occurring at the highest wavenumber. A peak appears in the transmission loss curve at about 11 kHz for the drive wavenumber of $\pi/4$ cm^{-1}. There may be a similar peak in the curve for the drive wavenumber of $\pi/2$ cm^{-1} just above 12 kHz, outside the measurement frequency range. In general, it appears that a dip in the losses occurred at a lower frequency for the lower drive wavenumbers. The transmission losses shown in Figure 5.57 are similar to the transmission losses measured for the single sample (see Figure 2.3). Resonances in the beam may be responsible for lower losses for the layer than for the single sample. At resonances, the beam admittance is large, which reduces the forces that can be generated under the layer on the beam, which, increases the transmission losses.

At drive wavenumbers of $\pi/4$ and $3\pi/4$ cm^{-1}, the transmission losses measured with Natural Rubber I are plotted as a function of frequency in Figure 5.58. Below 7.5 kHz, the transmission loss for the drive wavenumber of $\pi/4$ cm^{-1} is less than for the drive wavenumber of $3\pi/4$ cm^{-1}. Above 7.5 kHz, the transmission loss for $\pi/4$ cm^{-1} is greater than the transmission loss for $3\pi/4$ cm^{-1}. At the wavenumber of $\pi/4$ cm^{-1}, the transmission losses for natural rubber and polyurethane are compared in Figure 5.59. Above 7.5 kHz, the natural rubber exhibits higher losses than the polyurethane. However, this is not the case at $3\pi/4$ cm^{-1}, as can be seen in Figure 5.60 where the losses for the natural rubber are greater below 7.5 kHz.

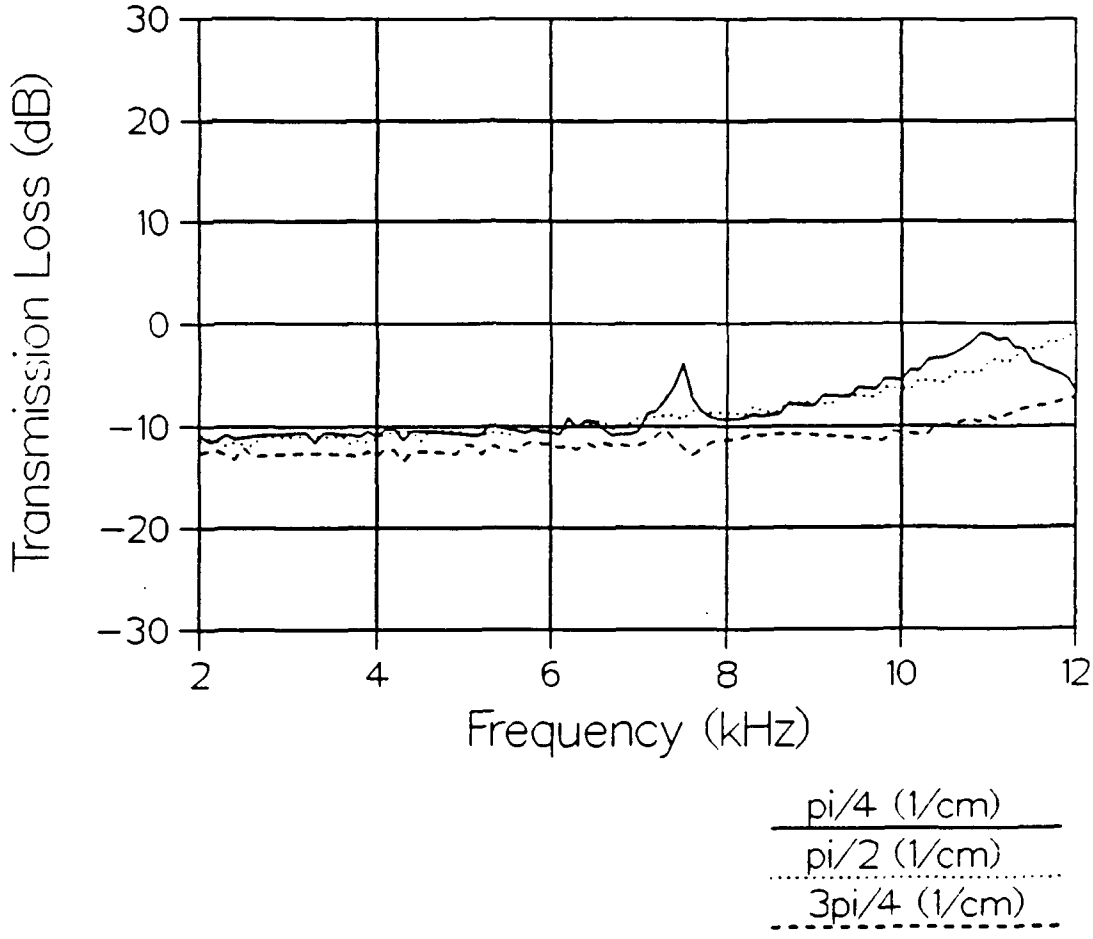

Figure 5.57: Transmission loss for polyurethane layer.

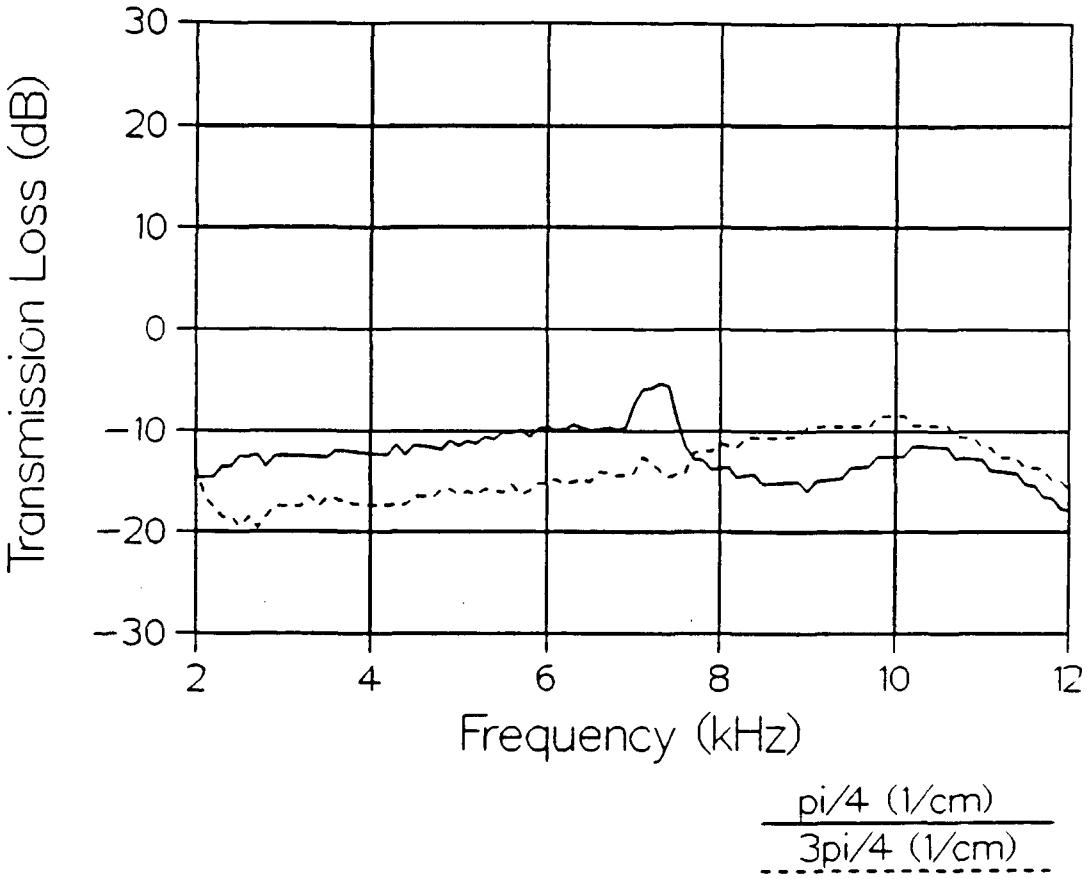

Figure 5.58: Transmission loss for natural rubber layer.

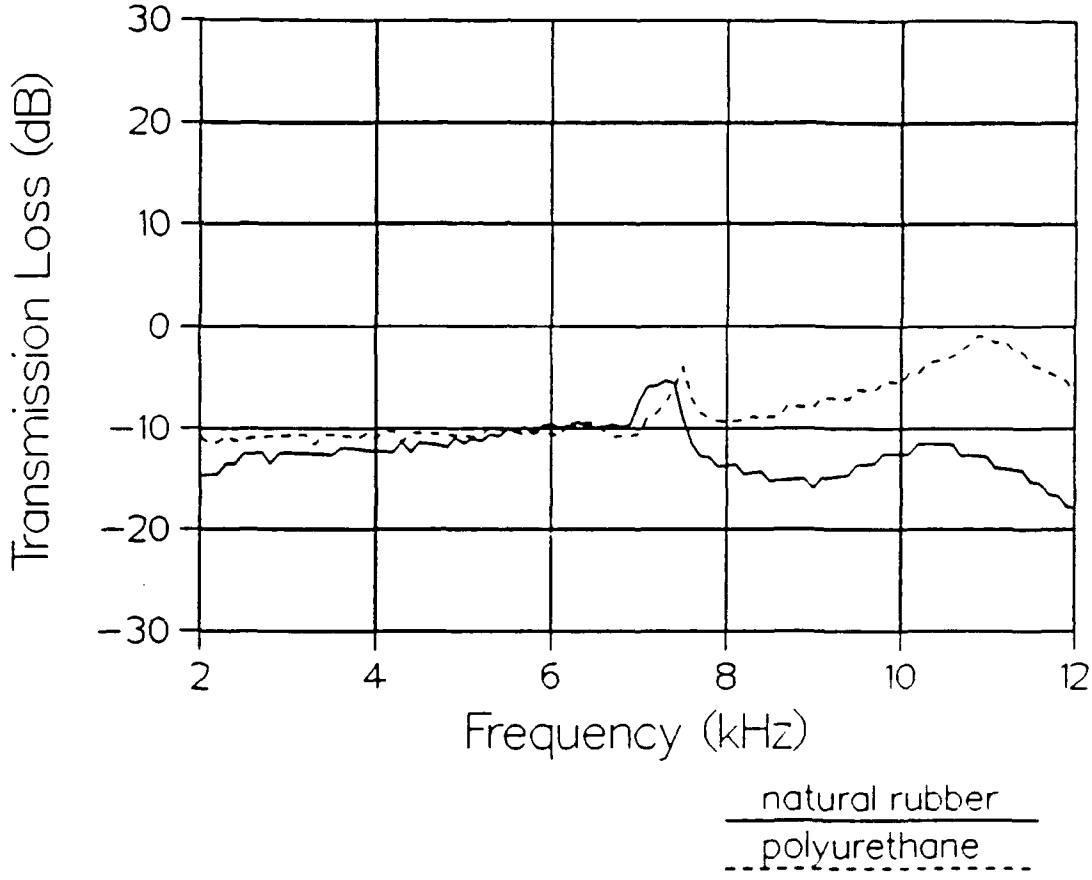

Figure 5.59: Transmission loss for natural rubber and polyurethane layers at $k_d = \pi/4$ cm^{-1}.

At higher frequencies, propagation into the layers is expected as the propagating wavenumbers in the layer increase to greater than the drive wavenumber. The transmission losses should therefore decrease, as shown in Figure 5.60 for the drive wavenumber of $3\pi/4$ cm^{-1}, not increase as shown in Figure 5.59 for natural rubber at $\pi/4$ cm^{-1} drive wavenumber at frequencies above 7.5 kHz. Therefore, the transmission losses for natural rubber with the drive wavenumber of $\pi/4$ cm^{-1} may not be valid for frequencies above 7.5 kHz. Discarding these data, the softer natural rubber shows greater transmission losses than the harder polyurethane and the differences decrease as the propagation wavenumbers in the layer approach the drive wavenumber at increasing frequencies.

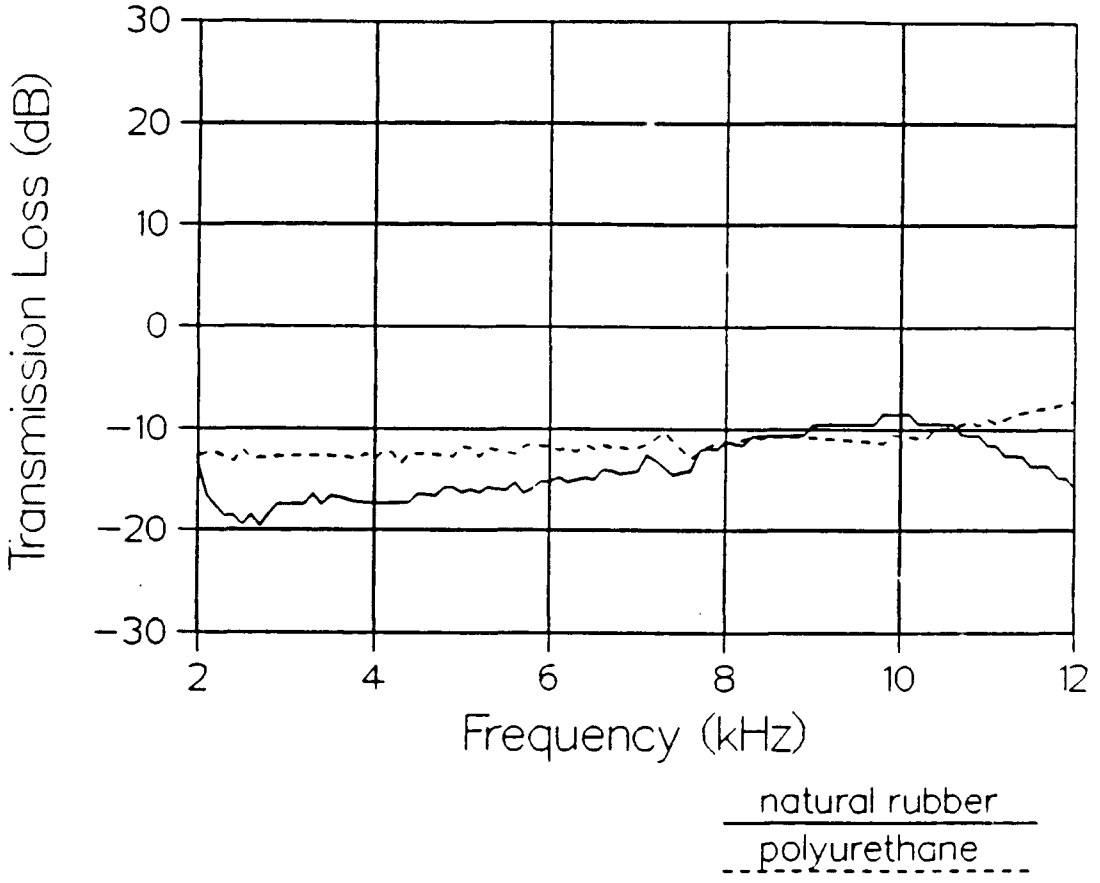

Figure 5.60: Transmission loss for natural rubber and polyurethane layers at $k_d = 3\pi/4$ cm^{-1}.

Chapter 6

CONCLUSIONS AND RECOMMENDATIONS

6.1 Conclusions

Two methods of determining the wavenumber-frequency filtering characteristics of compliant layers have been developed. The first of these methods involved measuring the wavenumber-frequency transfer admittances of the bare beam and the coated beam at the driven wavenumbers. These transfer admittances were then compared to determine the effectiveness of the layer. By determining the effectiveness of each layer, it is possible to characterize and compare the abilities of the layers to reduce the vibration of the beam. By changing the driven wavenumber, it is possible to examine the wavenumber filtering characteristics of a single layer.

However, the effectiveness of each layer was dependent upon the interaction between the layer and the beam as indicated by the spring-masslike resonance evident in the transfer admittance of the coated beam. This dependence indicates that the effectiveness of the layer is not a characteristic of the layer only, but is also a characteristic of the structure to which the layer is mounted. Mounting the layer onto a different structure will change the measured effectiveness.

The second method applied to determine the wavenumber-frequency filtering characteristics of the compliant layer measured the transmission loss of the layer. The transmission loss of the layer is independent of the structure to which

the layer has been mounted provided that the impedance of the structure is high compared to the impedance of the coating. This is usually true for most compliant layer/structure combinations. By changing the driven wavenumber, it was possible to examine the wavenumber filtering characteristics of the layer.

In the transmission loss measurements, strong signals were detected at the driven wavenumber for all wavenumbers and frequencies. Since there is also a strong response at the grating lobes and since it is unnecessary to make any measurements on the bare beam, fewer experiments are needed to determine the wavenumber-filtering characteristics of the layer. Results at two wavenumbers (main and grating lobe) can be obtained from one set of experiments. However, when comparing the transmission loss plots to the plots of the effectiveness of the layers, it can be seen that the transmission loss can be misleading in regard to the actual reduction of the vibration response of the structure. At the resonance frequencies of the layer/beam combination, gains in the vibration response of the beam were detected.

6.2 Recommendations

The purpose of this research was to develop a system to determine the wavenumber filtering characteristics of compliant layers driven by the pressure fluctuations present under a turbulent boundary layer (TBL) by generating pressure fluctuations at arbitrary wavenumbers with an array of point drives.

Most of the energy in the boundary layer is concentrated near the convective

wavenumber of the flow, k_c, given by

$$k_c \approx \frac{\omega}{0.7U_\infty} \tag{6.1}$$

where ω is the angular frequency of the fluctuations and U_∞ is the free stream velocity of the flow [3]. Using $k = 2\pi/\lambda$ and $\omega = 2\pi f$, the wavelength λ_c associated with the convective wavenumber is given by

$$\lambda_c = \frac{0.7U_\infty}{f} \quad . \tag{6.2}$$

Using a typical value for the flow velocity, 280 cm/s, and the low frequency cut off of the shakers, 2 kHz, a wavelength of 0.098 cm is determined. This would require a shaker spacing of 0.049 cm (1/2 millimeter) in order to drive the beam at this wavelength.

It should also be noted that in order to fully observe the wavenumber filtering action of the layer, the spacing of the force drives would have to be comparable in size to the thickness of the layer in order to see any appreciable effects. In all of the experiments, the layer was 0.635 cm thick. The smallest wavelength that was driven was 4 cm. Thus, the layer was less than 1/5 of the smallest driven wavelength.

Therefore, future work should include the development of a driving system that is capable of forcing the beam at higher wavenumbers than the present system. To use the techniques developed in this thesis, smaller shakers will have to be designed and fabricated.

Appendix A

Test Matrix

Table A.1 lists the experiments by their number, description, and the drive wavenumber to which the shakers were weighted. In the first three experiments, there was some trouble with ground loops effecting the force spectra. Experiment #4 was the final one that provided the desired results, so experiments 1-3 were not examined in the text. Experiments #6 and #7 were conducted while the first set of PVDF arrays were in place. Experiment #8 was the first (unsuccessful) attempt at measuring the force distributions using PVDF. It should also be noted that experiment #21 actually involved four experiments: one to measure the force distribution using the shaker force gages, one to measure the velocity distribution, and two more using the PVDF arrays to measure the force distributions on top and below the layer.

Table A.1: Experimental test matrix.

Exp. No.	*Description*	*Drive Wavenumber* cm^{-1}
1	Bare beam	$\pi/4$
2	Bare beam	$\pi/4$
3	Bare beam	$\pi/4$
4	Bare beam	$\pi/4$
5	Bare beam	$\pi/2$
6	Natural Rubber I	$\pi/4$
7	Natural Rubber I	$\pi/2$
8	—	—
9	Natural Rubber I	$\pi/4$
10	Neoprene I	$\pi/4$
11	Polyurethane	$\pi/4$
12	Polyurethane	0
13	Polyurethane	$\pi/3$
14	Polyurethane	$\pi/2$
15	Polyurethane	0.28π
16	Bare beam	0
17	Bare beam	0.28π
18	Bare beam	$\pi/3$
19	Neoprene II	$\pi/4$
20	Natural Rubber II	$\pi/4$
21	Polyurethane w/ PVDF	$\pi/4$
22	Polyurethane w/ PVDF	$\pi/2$
23	Natural Rubber I w/ PVDF	$\pi/4$
24	Natural Rubber I w/ PVDF	$\pi/2$

Appendix B

Experimental Exceptions

It should be noted here that when the text refers to a drive wavenumber of $\pi/4$ cm^{-1}, the actual drive wavenumber was slightly less. The weighted shaker voltages used for this wavenumber throughout the thesis were the same as those used by Grosh [13]. When new, more accurate numbers were generated, it was noticed that this would have required every other shaker to have a zero input voltage. Therefore, the "old" numbers were deemed more desirable.

The reason that two separate neoprene layers were measured for the transfer admittance is that there were some reservations about the validity of the first material. Neoprene I was cut from a piece of material that was beginning to delaminate. Therefore, new material was ordered and this was called Neoprene II.

The spacing of the PVDF force gauges was actually slightly less than 1 cm center to center. This was caused by a slight error in the manufacture of the Kapton pc board used for the positive leads of the PVDF arrays. Apparently, when the copper coating was chemically removed, the exposed Kapton must have shrunk slightly. This was only a slight discrepancy. The total displacement over the whole beam was only approximately 0.25 cm. When the shakers were mounted onto the beam, they were done so in a way such that they were directly over the proper PVDF force gages, ignoring the designed 2 cm spacing. When measuring the velocity with the accelerometer, the probe was also placed in line with the PVDF

force gages. When taking the spatial transforms, these data were then treated as if the spacing were correct. Any error that resulted from this problem appears to have been quite minimal.

Bibliography

[1] G. M. Corcos, **Resolution of Pressure in Turbulence**, J. Acoust. Soc. Am., **35**(2), pp 192–199 (Feb. 1963).

[2] D. M. Chase, **Modeling the Wavevector-Frequency Spectrum of Turbulent Boundary Layer Wall Pressure**, J. Sound Vibr., **70**(1), pp 26–67 (1980).

[3] W. K. Blake. **Mechanics of Flow-Induced Sound and Vibration, Vol. II, Complex Flow Structure Interactions**, Academic Press, New York, 1986.

[4] Mohamed Gad-el-Hak, **Boundary Layer Interaction with Compliant Coatings: An Overview**, Appl. Mech. Rev., **39**(4), pp 511–524 (April 1986).

[5] Cahit A. Evrensel and Arturs Kalnins, **Response of a Compliant Slab to Inviscid Incompressible Fluid Flow**, J. Acoust. Soc. Am., **78**(6), pp 2034–2041 (Dec. 1985).

[6] J. H. Duncan, **The Response of an Incompressible, Viscoelastic Coating to Pressure Fluctuations in a Turbulent Boundary Layer**, J. Fluid Mech., **171**, pp 339–363 (1986).

[7] A. P. Dowling, **Sound Generation by Turbulence near an Elastic Wall.** J. Sound Vibr., **90**(30), pp 309–324 (1983).

[8] H. Haj Hariri and J. R. Akylas, **Mean-Flow Effects on the Low-Wavenumb Wall-Pressure Spectrum of a Turbulent Boundary Layer over a Compliant Surface**, J. Acoust. Soc. Am., **77**(5), pp 1840–1844 (May 1985).

[9] G. Maidanik, R. Biancardi and T. Eisler, **Use of Cecopling to Reduce the Radiated Noise Generated by Panels**, J. Sound Vibr., **81**(2), pp 165–185 (1982).

[10] G. Maidanik and W. T. Reader, **Filtering Action of a Blanket Dome**, J. Acoust. Soc. Am., **44**(2), pp 497–502 (1968).

[11] Sung H. Ko and Howard H. Schloemer, **Calculations of Turbulent Boundary Layer Pressure Fluctuations Transmitted into a Viscoelastic Layer.** J. Acoust. Soc. Am., **85**(4), pp 1469–1477 (April 1989).

[12] F. M. Hutto. **Wavenumber-Frequency Response of Free-Free Timoshenko Beams with Multiple Sources**, Master's Thesis, The Pennsylvania State University (1986).

[13] K. Grosh. **An Experimental System for Measuring the Wavenumber-Frequency Response of Timoshenko Beams**, Master's Thesis, The Pennsylvania State University (1988).

[14] O. E. Brigham. **The Fast Fourier Transform**, Prentice-Hall Book Inc., Englewood Cliffs, NJ (1974).

[15] W. K. Blake and D. M. Chase. **Wavenumber-Frequency Spectra of Turbulent Boundary Layer Pressure Measured by Microphone Arrays**, J. Acoust. Soc. Am., **49**, pp. 862–877 (1971).

[16] M. C. Junger and D. Feit. **Sound, Structures, and Their Interaction**, MIT, Cambridge, MA (1986).

[17] A. V. Oppenheim and R. W. Schafer. **Digital Signal Processing**, Prentice-Hall Book Inc., Englewood Cliffs, NJ (1975).

[18] R. N. Bracewell. **The Fourier Transform and its Applications**, McGraw-Hill Book Company, New York (1978).